UNIVERSITY OF KWAZULU-NATAL ™

INYUVESI YAKWAZULU-NATALI

HIGH-TEMPERATURE PRODUCTION AND DESULPHURISATION OF SYNGAS

Johra Said Ali
[B.Tech (Eng)]

January, 2015

[Examiner's Copy]

High Temperature Production and Desulphurisation of Syngas

Johra Said Ali

A dissertation submitted in the School of Engineering
University of Kwazulu Natal
Durban

In the fulfilment of the requirements of the degree of
Master of Science in Engineering

January, 2015

Declaration

The work presented in this dissertation was undertaken at the School of Chemical Engineering, University of KwaZulu-Natal, Howard College Campus in Durban, South Africa, from February 2013 until December 2014.

The work was supervised by Dr Sammy Lewis Kiambi and Co-supervised by Professor Milan Carsky.

This dissertation represents the full requirement for the degree of Master of Science in Engineering (Chemical).

All work presented is this dissertation is original unless otherwise stated. It has neither in whole nor part been submitted previously to any other University or Institute as part of a degree.

_____

As the candidate's supervisor hereby certify that I find this work to be suitable for submission for the degree of Master of Science in Chemical Engineering.

Supervisor: [redacted] 15/12/2023

Co-supervisor: _____

Acknowledgment

I would like to thank my supervisors Professor Milan Carsky and Dr Sammy Lewis Kiambi for their guidance and assistance throughout my study.

My deepest gratitude to Professor Milan Carsky for the exposure he provided for me through local and international conferences.

I also want to thank Mr Vishal Baruth and Mr Phillip Christopher of the Microscopy Unit and Dr Patrick Ndugu of the School of Chemistry and Physics all in UKZN Westville campus for their help and advice in the characterization process of the sorbent used in this study.

I would like to express my deepest gratitude to the assistance given by the chemical technicians and the workshop team of UKZN throughout my work; Mr Sanjay Addieh, Mr Sadha Naidoo, Miss Xoli Hadebe, Mr Danny Singh, Mr Patrick Mlambo and Mr Elliot Mlambo. Thank you for being patient with me.

I would also like to thank the following postgraduate students; Philani Biyela and Matthew Laisch together with Dr Suren Moodley for their assistance in the modelling part of this study.

I would like to sincerely appreciate the financial support given by ESKOM and the UKZN School of Engineering.

Finally my deepest gratitude to my office mate Presharnthan Arumugam, my friend and Sister Kassa Barakamfitiye, my uncle Mr Omar Osman and my dearest mum Mrs Fatuma Ramadhan for their encouragement and support.

Abstract

Synthetic gas (syngas) produced by the gasification of coal provides a cheap fuel alternative for the production of electricity. However advanced utilization of syngas is limited due to the contaminants which can seriously deactivate the catalysts used in the downstream reactions as well as downstream equipment such as gas turbines. Among the contaminants, sulphur compounds produced in the gasification process, which are mainly H_2S with small amounts of COS must be removed. The method presented here is downstream sulphur capture by a metal oxide at high temperatures. In this study, a laboratory scale unit was used to produce and clean synthetic gas (syngas) containing 1.0-1.15 mole % H_2S from a liquid hydrocarbon fuel consisting of 86 % methanol, 14 % propanethiol by mass, and 18 mole % oxygen gas as the oxidant. The gasifier operates at 830 ^{0}C at atmospheric pressure. Desulphurisation occurs in a fixed bed reactor packed with zinc oxide spherical pellets as the sorbent.

Experiments were performed to determine whether the use of the liquid hydrocarbon mixture as fuel in the laboratory could actually produce H_2S containing syngas, and eventually compare the composition of the gas produced experimentally to the one predicted by a model. Desulphurisation experiments were performed by varying reaction temperatures (350 ^{0}C and 550 ^{0}C) and sorbent particle sizes (1.63-2.03 mm) at atmospheric pressure using sorbent with varying surface areas (average of 5 m^2/g and 25 m^2/g) at high and low gas velocities (average of 3430 $h^{-1}$and 610 h^{-1}). These variations were performed in a 2*2 factorial design to determine the effect of these factors on the desulphurisation process and observe whether there is any interaction between them. Statistical analysis was used to determine the significance of each factor on the sorbent sulphur sorption capacity. A packed bed model using shrinking core model was used to describe the desulphurisation process.

GC analysis specific to sulphur compound detection showed consistent production of H_2S during gasification. In addition to this the composition of the predicted syngas was validated through a GC equipped with a TCD detector and there was a good agreement giving the expected ratio of 2:1 of H_2 and CO respectively. Small particle size sorbent with 5.3 m^2/g surface area and an average space velocity of 610 h^{-1} at 350 ^{0}C reaction temperature had the highest sulphur sorption capacity of 3.71 Wt. % which was a 20% conversion of zinc oxide to zinc sulphide. There was no effect of increase in temperature on the process. The low surface area sorbents were more effective than the increased surface area sorbents. These results were verified by the statistical analysis performed on the sulphur sorption capacity obtained during experimentation. The packed bed model results were not in agreement with the experimental results.

List of Publications and Conference Proceedings

- Ali, J.S., Carsky, M and Kiambi, S.L., "High temperature Production and Desulphurisation of Syngas from Liquid Hydrocarbons and a Metal Oxide", ICCT/SAIChE 2014 conference, 27th July – 1st August, Durban, South Africa.

- Johra, S.A., Milan Carsky, and Sammy, L.K., "High temperature Production and Desulphurisation of Syngas from Liquid Hydrocarbons", 21st International Congress of Chemical and Process Engineering CHISA 2014 and 17th Conference on process Integration, Modelling and Optimisation for Energy saving and Pollution reduction, PRES 2014, 23rd – 27th August 2014, Prague, Czech Republic.

- Ali, J.S., Carsky, M and Kiambi, S.L., "Production of Synthetic Gas from Liquid Hydrocarbons and High Temperature Desulphurisation using Zinc Oxide for Fischer-Tropsch Process", Industrial Fluidisation South Africa conference IFSA 2014, 19th – 20th November 2014, Johannesburg, South Africa.

TABLE OF CONTENTS

List of Figures

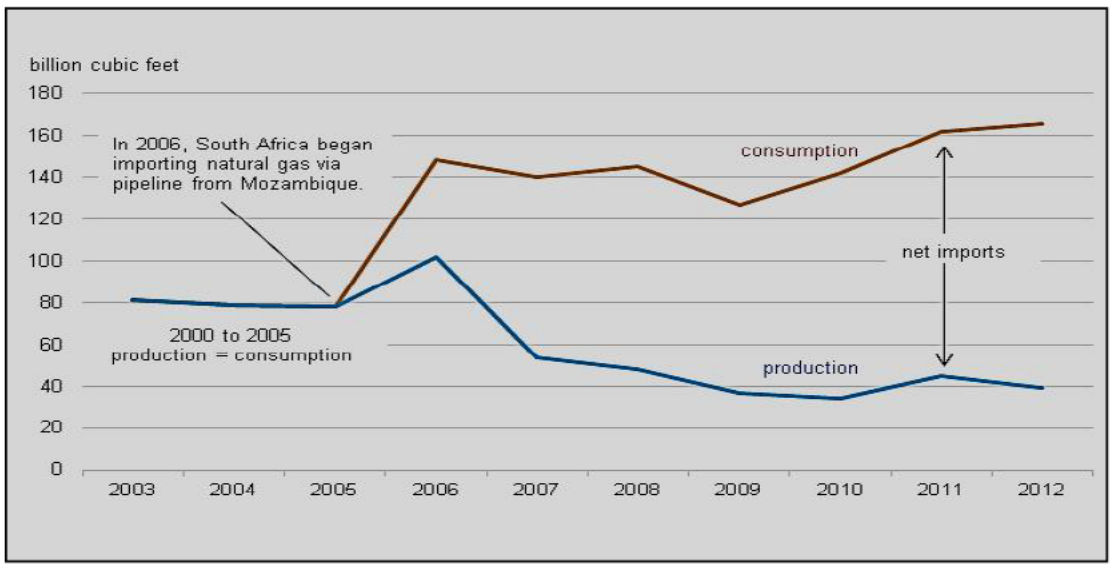

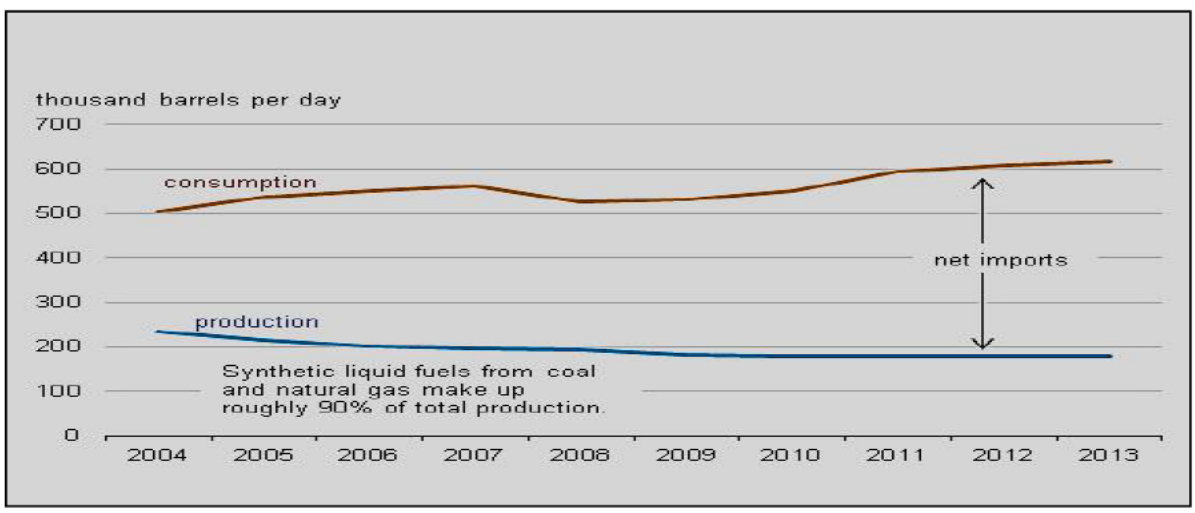

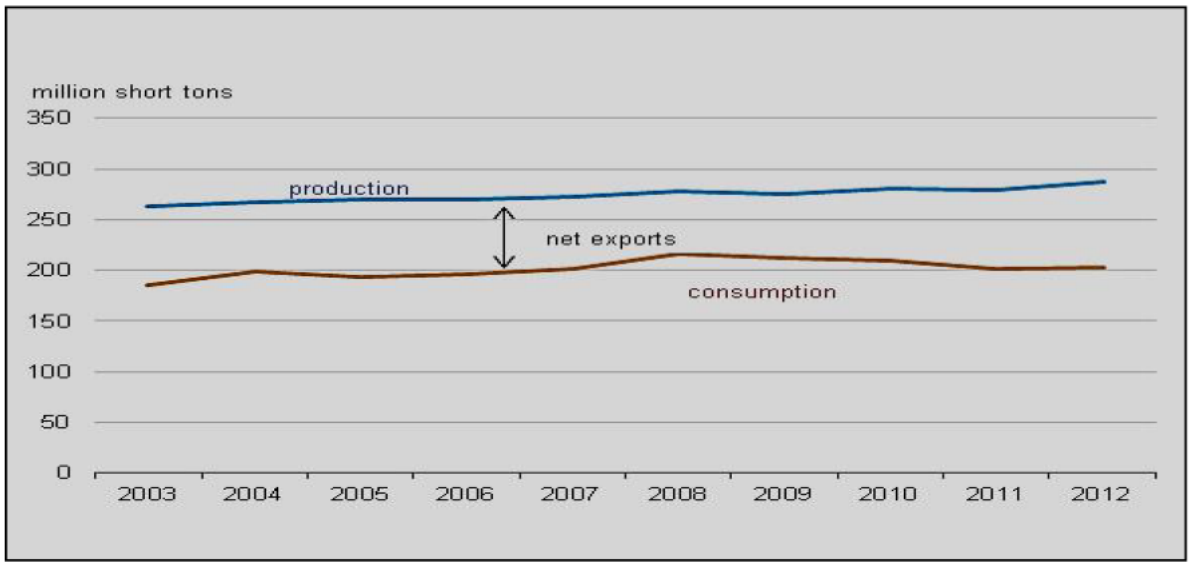

List of Tables

Nomenclature

Dimension	Definition	Units
	Moles of gaseous reactant A	mole
	Moles of solid reactant B	mole
	Overall reaction rate	mol A/min.cm^3
	Radial distance along the product layer	cm
	Radius of the unreacted core	cm
	Radius of particle	cm
	Time	min
t^*	Dimensionless time (t/T_b)	-
	Theoretical breakthrough time	min
	Gaseous reactant (H_2S)	-
	Solid Reactant (ZnO)	-
	Stoichiometric coefficient of solid reactant	-
	Molar concentration of A in the gas phase	mol/cm^3
C^*	Dimensionless concentration of A (C_{Ab}/C_{Ao})	-
	Bulk molar concentration of A in the gas phase	mol/cm^3
0	Molar concentration of A at the reactor inlet	mol/cm^3
	Molar concentration of A in equilibrium at the unreacted core interface	mol/cm^3
	Molar concentration of B in the solid phase	mol/cm^3
0	Initial molar concentration of B in the solid phase	mol/cm^3
	Effective diffusivity of A in the product layer	cm^2/min
	Gas flow rate (STP)	cm^3/min
	Intrinsic reaction rate constant	cm/min
	External mass transfer coefficient	cm/min
	Molar flux of A	mol/cm^2.min
	Length of packed bed	cm
	Superficial gas velocity	cm/min
	Volume of reactor	cm^3
	Volume of particle	cm^3
	Fractional conversion of B	-
	Axial position within reactor	cm
z^*	Dimensionless axial position (z/L)	-
Greek		
	Molar density of B	mol/cm^3
	Bed porosity	-

Chapter 1

INTRODUCTION

1.1 Overview of South Africa's Energy resources and Utilization

A look at South Africa renewable energies, the country most utilized renewable energies are solar, wind, biomass and hydro power. Solar energy has the largest potential because the country experiences approximately 25000 hours of sunshine per year with solar radiations that range between 4.5 to 6.5kwh/m^2 per day (DOE South Africa, 2013). In addition, South Africa has a 24 hour global solar radiation of 220W/m^2 compared to 150W/m^2 and 100W/m^2 in USA and combination of Europe and the UK respectively. Annually 5MW photovoltaic solar panels are assembled and solar water heaters are manufactured (DOE South Africa, 2013). Unfortunately for solar energy to be efficiently utilized large amount of energy needs to be stored during the day and fed to the national grid. This will also require a big area of open land to put up the photovoltaic cells as well as provide maximum radiation and consequently affecting other sectors like agriculture and forestry (Danie, 2011).

There are only two wind energy farms in South Africa. One of the farms is owned by ESKOM the sole electricity utility supplier in an area called Klipheuwel in Malmesbury, Western Cape and it is producing 4GWh of energy annually (DOE South Africa, 2013). Another wind energy producing farm which started operation in 2008 is the Darling wind farm located 70km north of Cape Town. This farm produces about 6-8GWh of energy annually. The electricity generated is fed into ESKOM grid and sold in the city of Cape Town (DOE South Africa, 2013).For wind energy to be also viable vast areas of land are required and this also affects the agriculture sector. The tourism sector is also affected because along the coastal line is where strong winds are experienced and this is where the tourism industry booms.

Hydropower is generally used for small scale generation of electricity. This is because South Africa is limited in water resources therefore majority of hydroelectricity is in fact imported from Mozambique in their Cahora Bassa hydropower station. Despite this, there are still high prospects for hydropower in the Kwazulu Natal province and in the Eastern Cape (DOE South Africa, 2013).

Biomass is another source of renewable energy utilized in South Africa in providing energy. It is a main source of energy at the domestic level and in industries like pulp and paper and sugar processing. In the sugar industry a harvest of about 20 million tons produces 7 million tons of

bagasse with a heating value of 6.7MJ/kg. This bagasse is heated in the boilers and the heat is used to make steam which generate electricity and also used for process heating (Alison and Mary, 2007).In the pulp and paper industry the bark from softwoods and the black liquor are used to fire boilers, generate electricity as well as process steam. The sugar and pulp industries have the capacity of producing about 245MW and 170MWof electricity respectively (Winkler et al., 2006). For domestic purposes, biomass in form of wood, vegetable material and dung is used for heating and cooking. These methods of utilizing biomass are unfortunately hazardous to the environment by pollutant emissions and reckless cutting of trees. Finally biomass can be converted to biofuels such as biodiesel, ethanol, methanol and hydrogen. The only drawback for such kind of conversion is the amount of feedstock required to produce a substantial amount of the biofuels and thus making large scale production very costly (Alison and Mary, 2007).

Fossil fuels make up the primary sources of energy in South Africa. Figure 1.1 clearly shows this. The fossil fuels include natural gas, crude oil and coal. South Africa has very minimal natural gas reserve. The only operational gas field as reported by Winkler et al., (2006) is the F-A field on the south coast. It supplies Mossgas a company that converts the gas to liquid (GTL) fuels (diesel, kerosene, etc.) via Fischer-Tropsch process with approximately 5.4 million m^3 of gas per day. This gas reserves in this field, according to Winkler et al., (2006) was to run out by 2008. Petroleum Oil and Gas Corporation (PetroSA) a state-owned company and other stake holders are developing two natural gas fields; F-O field and Ibhubesi field which are to continue feeding gas to the GTL plant starting 2016 (EIA, 2014). According to EIA, (2014) reports, in 2012, South Africa consumption of natural gas exceeded its supply by 360 million m^3. The deficit was imported from Mozambique via a pipeline. Figure 1.2 shows the country's natural gas production and consumption from 2003 to 2012. The government is confident that new two gas production fields coupled with imports from Mozambique and Namibia will reduce the country reliance on coal as primary source of energy in the production of electricity. This will have a tremendous advantage since natural gas is a source of clean energy. About 11 trillion m^3 of technically recoverable shale gas resources were discovered in the Karoo basin. This makes South Africa the eighth country worldwide to have such large amounts of technically recoverable shale gas resources. A technically recoverable resource simply means the volumes of oil and gas resources that can be produced with the current technology regardless of their market prices and production cost (EIA, 2014). Despite this, exploration of shale gas is dragging because of environmental concerns regarding the effects of the extraction process to aquatic life (EIA, 2014).

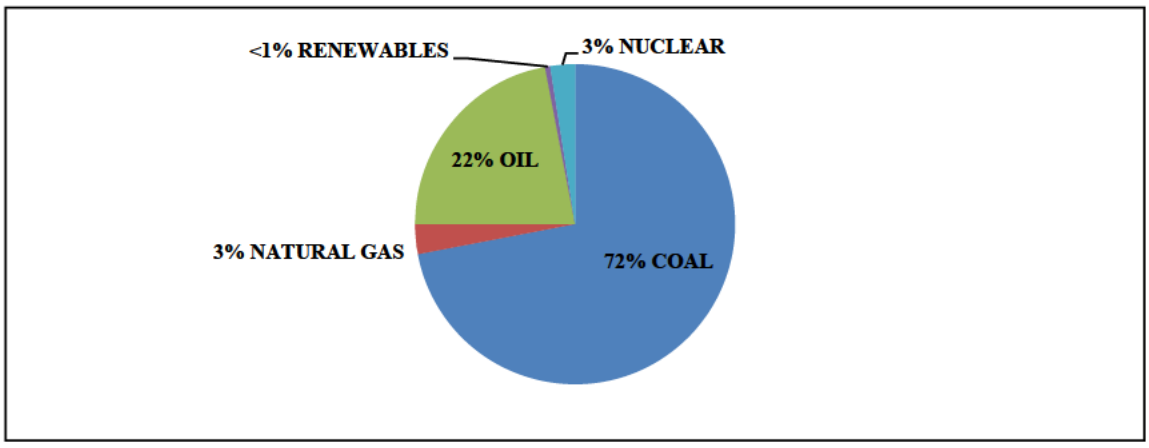

Figure 1.1 Primary Energy resources consumption in South Africa (EIA, 2014)

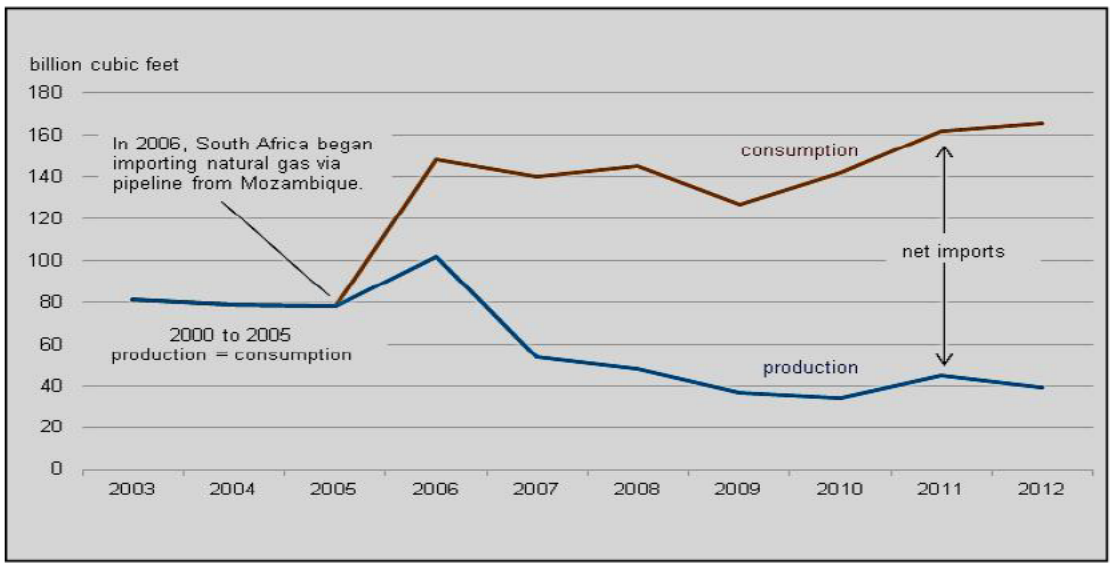

Figure 1.2 South Africa's Natural gas production and Consumption between 2003-2012 (EIA, 2014)

South Africa's crude oil reserves are minimal. By the end of 2013, 15 million barrels of crude oil reserves were proved (EIA, 2014). Managed by PetroSA, the Oryz and Oribi fields are currently producing crude oil and lease condensate. A newer field, the Sable field in Bredasdorp basin is postulated to produce 30000 to 40000 barrels per day (Winkler et al., 2006). If this happens, South Africa will save up to 10% of its crude oil imports from Middle East and West African countries, Saudi Arabia making up its biggest supplier (EIA, 2014). South Africa's total oil production mainly comes from the coal to liquid (CTL) and GTL plants and from the locally refined, imported crude oil. CTL and GTL plants contributing to 90 % of the total oil produced in the country.

Coal is the number one primary energy resource in South Africa. Statistics show that South Africa has an estimated 30.2 tons of coal reserves (EIA, 2014). The country has the 9th World's largest

amount of recoverable coal reserves and holds 95 % of Africa's total coal reserves (EIA, 2014). According to Alison and Mary, (2007), 80% of coal produced in South Africa comes from Mpumalanga, 11% from Limpopo, 7% from the Free State and 1% from Kwazulu Natal. The type of coal extracted is bituminious with high ash and low sulphur content(Winkler et al., 2006). More than half of the coal is converted to electricity by the state owned company ESKOM followed by the production of synthetic fuels and chemicals by SASOL and the rest by Metallurgical industry and domestic heating and cooking (DOE South Africa, 2013). Approximately 28% of the coal produced is exported to China and India via the Richards Bay Coal Terminal and about 22% discarded (Prevost & Msibi, 2005). As seen in Figure 1.4, South Africa's coal production and consumption has been very constant in the past years. Research has shown that in the few decades to come coal will still be the major source of energy in South Africa compared to the other primary energy resource (EIA, 2014).

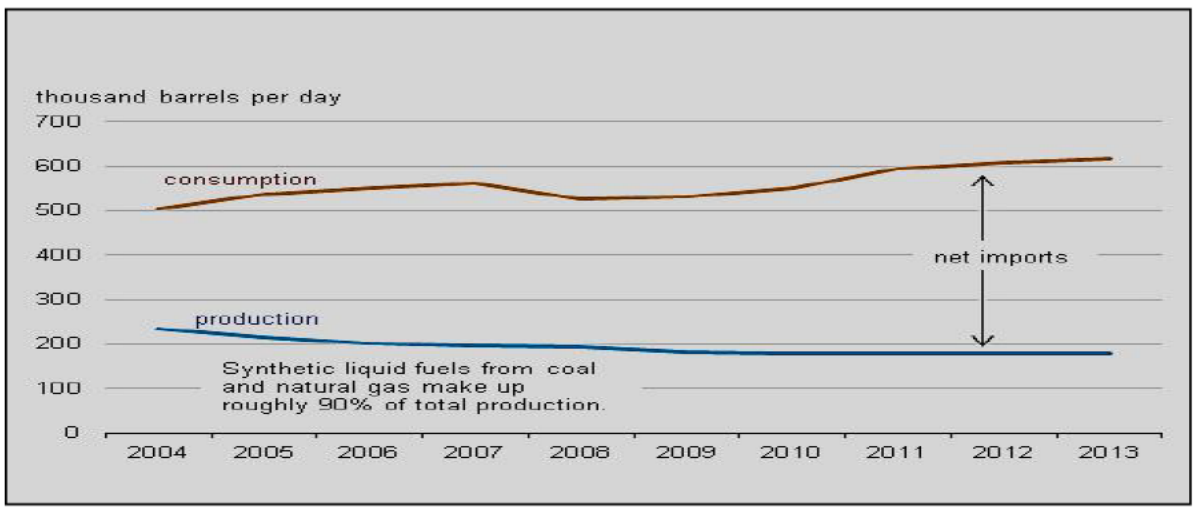

Figure 1.3 South Africa's production and Consumption of Oil in the period 200 - 2013 (EIA, 2014)

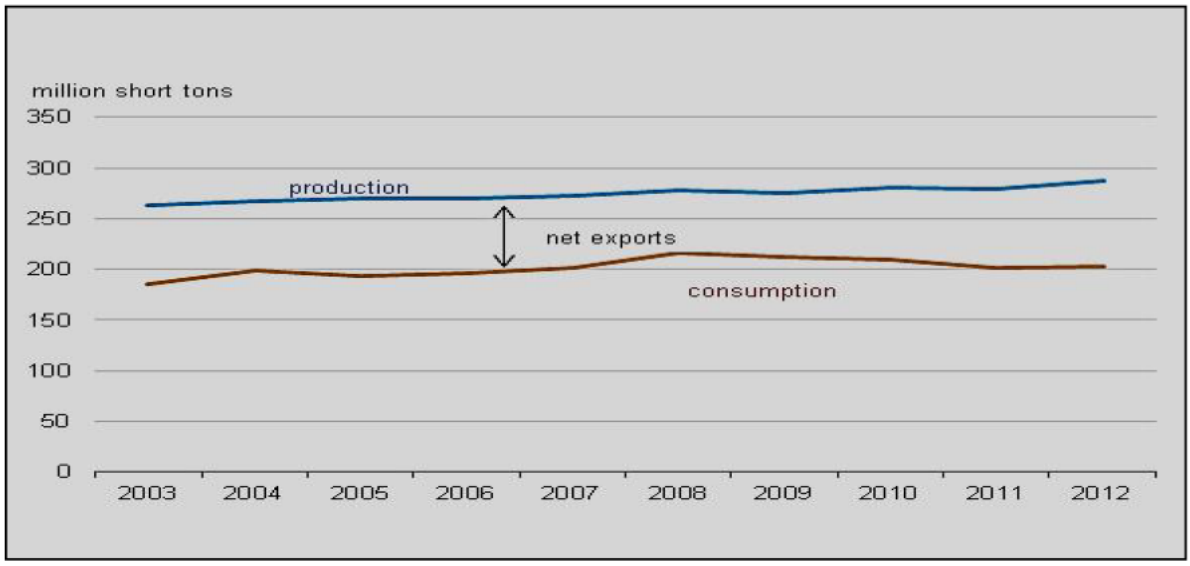

Figure 1.4 South Africa's Coal production and Consumption between 2003 - 2012 (EIA, 2014)

1.2 Area of research and its significance

Clean and alternative energy sources and technologies have become a key area of study globally. This is because of the increase in demand brought by economic and human development growth. One of the tools that measure a country's development is technological advancement which increases the demand for energy to supply the industries. Energy sources vary from renewable to non-renewable. Many nations are looking forward to renewable energy sources like solar, wind, biomass and hydro as being their main sources of energy. This is because these types of energy sources do not pollute the environment and can provide remote areas with cheap sources of energy. Despite their benefits, these resources will take ages to supply the current and ever growing energy demands due to their economic and technical limitations. In addition much of the renewable energy sources can only be utilized in generation of electricity unlike the non-renewable sources which apart from electricity generation they are converted to liquid fuels and other valuable materials. For these reasons much reliance is put on non-renewable resources which include natural gas, oil and coal. These are precious gifts from nature and must be effectively and efficiently utilized for sustainable development. In that sense, to get the most out of them, new technological developments must be put in place.

In the production of electricity using coal, South Africa uses the conventional pulverized fuel combustion (PFC) technology in majority of its coal fired power plants. The coal is finely ground into tiny particles, transported to a boiler via conveyor belts and combusted to produce heat (Osman et al., 2013). The heat produced is used to heat up water in the tubes which make up the wall of the boiler producing high pressure steam. The steam passes through a steam turbine which runs a generator and electricity is produced. This method of electricity generation wastes a lot of energy because of the thermodynamic restrictions of the heat engine governed by the maximum efficiency

of the Carnot cycle (Chunshan, 2009). This efficiency could be improved by co-generation of the heat but this is not the case in the South African power plants whose configuration is to generate electricity only. The design of the South Africa PFC plants also contributes to the low efficiency. The plants use sub-critical boilers which produce steam with pressures below the critical pressure of water (approximately 218 atmospheres). Using supercritical boilers design has been proven to raise the pressures above the critical pressure of water and consequently increase efficiency (Alison and Mary, 2007). In addition to the low efficiencies of the PFC plants, all of the flue gases (CO_2, H_2O, NOx, SO_2 and particulate matter) from coal combustion are emitted to the atmosphere. This has made environmental groups to raise concerns to coal industries due to air, land and water pollution making South Africa the number 1 emitter of CO_2 in Africa and 14th largest in the world (EIA, 2014). These emissions cause global warming, acid rains and urban smug resulting to severe damage to the environment. On the 23rd of November 2007 the minister of Environmental Affairs declared Highveld region (parts of Mpumalanga and Gauteng provinces) as a priority area due to poor air quality (DEA, 2011). This area contains more than 90 % of South Africa coal fired power plants for electricity generation, of which five are the largest in the world.

From the above statistics of the primary sources of energy in South Africa and their utilization, we can conclude that coal is the number one primary energy resource provider and will remain in that position for decades to come. Therefore maximum utilization of this resource must be observed while ensuring less emission to the environment. Among the ways of effectively utilizing this resource are:

- Improving on the current technologies to increase efficiency for example the co-generation configuration where the steam produced can be utilised to provide both electric power and heat.
- Adopt new technologies that will utilize it effectively for example by using the gasification technology instead of combustion.
- Integrate the power plant with flue gas treatment technologies.

Fossil fuels in general constitute from conventional elements (H, C, O, S, and N) to light and heavy hydrocarbons. When they are reacted under a controlled environment of oxygen, air or steam, they produce synthesis gas (Syngas).This syngas production process is called gasification. The process extracts more of the energy contained in the fuel than direct combustion. In addition, it can entirely convert any carbonaceous material i.e. wood, biomass or even plastic waste into syngas becoming a renewable energy technology. By using oxygen gas as the oxidant in the gasifiers the CO_2 produced is in a concentrated stream making it easier and less expensive to separate and capture (Speight, 2011). Syngas constitutes mainly of H_2, CO, H_2O, CH_4, CO_2 and other impurities depending on the source composition. Apart from the advantages obtained from adopting the gasification process, the syngas produced can be a huge breakthrough to the challenges facing the

energy sector. It can be used as fuel to generate electricity. It can as well be converted to methane through the Sabatier reaction and synthetic liquid fuels like diesel through the Fischer- Tropsch process (Speight, 2011). This in summary efficiently utilizes the fossil fuels.

Depending on the chemical composition of the fossil fuel, Hydrogen sulphide (H_2S) is a by-product of the gasification process from sulphur element present in the fuel as well as minute amounts of Carbonyl sulphide (COS). Before processing raw syngas, these sulphurous impurities must be removed as they poison catalysts in downstream gas reactors, leads to corrosion of process equipment and for environmental compliance. The mostly used approach to H_2S removal is by chemical or physical absorption but removal by hot gas desulphurisation (HGD) process using metal oxides has significant advantages. It lowers the plant capital and operational costs. Details of these different purification processes will be discussed in the literature review section.

1.3 Objectives of the Study

Although computational fluid dynamics (CFD) has developed tremendously in the recent years to simulate most chemical engineering processes in fluid mechanics, mass and heat transfer, experimental data is still indispensable. First of all, complex systems are difficult to simulate and secondly experimental data is needed to validate the simulation results.

This study presents a lab scale production of syngas which contains H_2S by gasification of a liquid mixture of methanol and 2-propanethiol using oxygen as the oxidant in a fixed bed gasifier. From literature this method of syngas containing H_2S production is limited to a series of gas cylinders controlled by flow meters which is very expensive compared to production using liquids. The syngas produced is further analysed by a gas chromatograph to identify its composition at fixed operating conditions. The data is then later used to validate the simulation work done prior to the designing of the equipment.

The syngas produced which contains H_2S is then purified using zinc oxide spherical pellets in a packed bed reactor. This arrangement of gasification preceding desulphurisation represents an industrial scale unit for production of syngas and HGD process. Experiments were performed to investigate the interaction between different reaction temperatures of the process as well as varying sorbent size in a 2*2 factorial design. The effects of space velocity and sorbent surface area on the desulphurisation process were also investigated. The main aim of these variations was to get the optimum conditions for desulphurisation based on the conversion of zinc oxide to zinc sulphide. This contradicts the many research done on HGD where a single solid particle is used to study individual factors affecting HGD process in a thermogravimetric apparatus using a simulated syngas containing H_2S. This work only focuses on the desulphurisation part and not on the regeneration of the sorbent. Finally since it is not based on controlled single particle experiments,

accurate data of rate constant, mass transfer coefficients and effective diffusivity cannot be directly measured.

Mastering of the gas chromatography (GC) was imperative. This is because it was the method used to analyse the concentration and composition of syngas produced as well as the drop in concentration during HGD.

Finally a more insight into the HGD process was done. The reaction is of the gas-solid type and therefore a model into gas-solid reactions was created to predict the effect of operating conditions on the desulphurisation performance of the sorbent in a fixed bed reactor. The model results were later compared to the experimental data.

1.4 Outline of the Dissertation

This study was divided into three stages:

- A background research on the subject: This is covered in Chapters 2 to 4.
- Experimental work and commissioning of the unit are covered in Chapter 5.
- Discussion of the results obtained and the final recommendation are covered in Chapters 6 and 7.

The main objective of reviewing the literature was to compare the current technologies being used in the industries to the one proposed in this study as well as find ways of modifying the equipment together with the experimental design.

The experimental work and commissioning of the unit included the experimental procedure under different conditions to achieve the optimum conditions for the production and purification processes.

Chapter 2

LITERATURE SURVEY: GASIFICATION TECHNOLOGIES

2.1 Introduction

Gasification has undergone a series of transformations since the early 1800s to date. From the production of "town gas" specifically used for heating and lighting, to production of synthetic fuels, high value chemicals and production of electricity through the integrated gasification combined cycle (IGCC). In Africa, South Africa leads in the production of synthetic fuel and chemicals from coal gasification since 1955 (NETL, 2013). In Asia, countries like Japan, India and China use gasification in generation of electricity, production of ammonia fertilizer and production of chemicals respectively. In Europe, most of the projects focus on generation of electricity through IGCC. These include countries like Italy, Spain and the Netherlands, similarly to North America where gasification is used in generation of electricity as well as production of chemicals and fertilizers (NETL, 2013). This technology has gained a lot of attention because of its versatility (Figure 2.1) and consequently more research and development for its improvement is going on. The striking characteristics of gasification process which outlines its advantages over combustion process include (Jeffrey, 2006):

- In the oxygen limited environment of the gasifier, carbon and hydrogen atoms in the fuel are converted to CO and H_2 instead of CO_2 and H_2O in the case of combustion. CO and H_2 are excellent fuels when used in the combustion turbines to generate electricity and also as raw materials in the production of synthetic fuels through Fischer-Tropsch process.
- In combustion process the fuels chemical energy is converted to heat whereas in gasification process most of the fuels chemical energy is retained in the produced syngas. The fraction of the fuels chemical energy retained in the syngas is in fact the measure of the gasification process efficiency referred to as cold gas efficiency consequently utilising fossil fuels efficiently.
- Gasification accommodates almost any carbonaceous substance i.e. coal, biomass, oil, refinery waste, black liquor, municipal solid waste and plastics.
- It acts as a renewable energy technology by converting low value products like wastes into high value products.
- The sulphur and nitrogen atoms in the fuel are converted to H_2S and COS for sulphur and HCN, NH_3 and N_2 for nitrogen instead of SO_3, SO_2, NO and NO_2 during combustion. The latter products

are easily removed to very low concentration with the syngas and consequently lowering emissions to the environment as well as protecting downstream equipment and catalyst.

2.2 Gasification Methods

Gasification is a partial oxidation process, meaning that less oxidant (either pure oxygen, air, steam or a mixture of these) is used in the process as would be required for complete combustion when burning the same amount of fuel. Reizayan and Cheremisinoff (2005) reported that it generally consumes about 20-70% of the amount of oxidant theoretically required for complete combustion. These results in a complete different composition of gases compared to products of combustion as shown in Table 2.1. Figure 2.2 indicates that the products of gasification depend on the ratio of the available oxygen in the gasifier to the amount of carbon in the feed. The higher the ratio goes the more the process tends to combustion therefore depending on the intended use of the syngas an optimum of this ratio can be established.

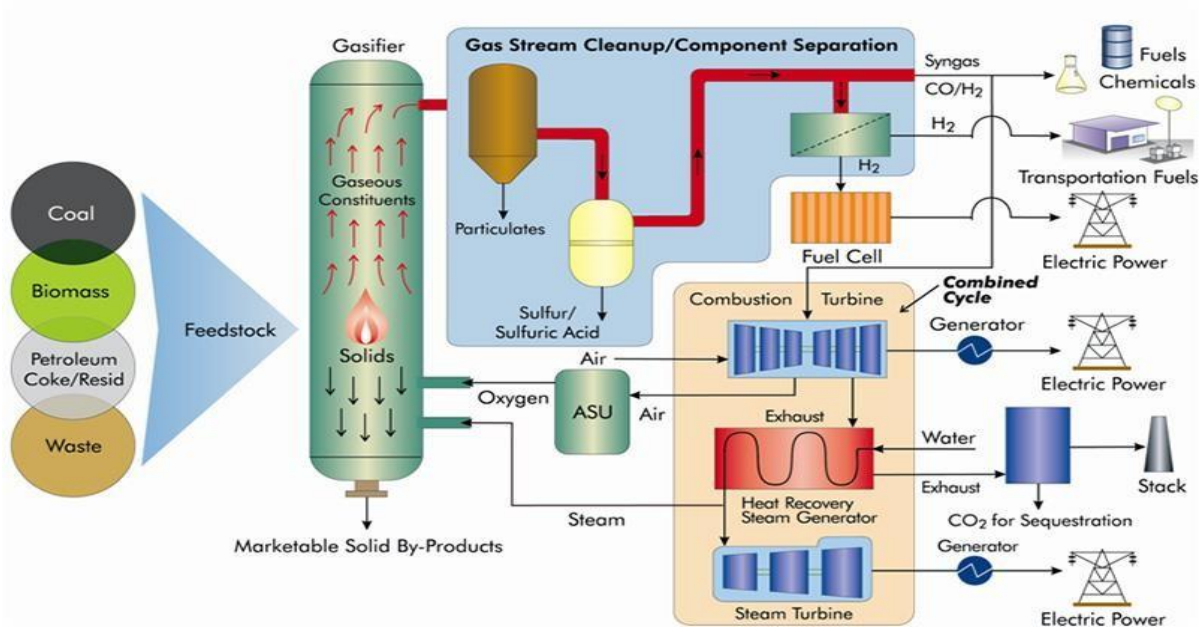

Figure 2.1 Gasification process from different feedstock and the final use of the syngas produced (NETL, 2013)

Table 2.1 Comparison between products of combustion and gasification processes (Jeffery, 2006).

Gasification		Versus		Combustion
CO	←	C	→	CO_2
H_2	←	H	→	H_2O
N_2	←	N	→	NO,NO_2
H_2S	←	S	→	SO_3, SO_2
	←	O	→	O_2

Mole %

O_2/C

Figure 2.2 Gasification reaction products as a function of Oxygen to Carbon in the feed (Jeffery, 2006)

Other engineering factors that differentiate the gasification technologies include(Reizayan and Cheremisinoff, 2005):

- Level and type of oxidant used
- Reactor configuration
- Source of heat
- Operating temperature

These factors define three main ways of syngas production namely; steam reforming (SR), partial oxidation (POX) and gasification. It will be imperative to mention that all these processes are literally gasification processes but they differ according to the factors mentioned above. In addition, gasification process is always related to partial oxidation of solid feed stocks like coal, biomass, pet coke and solid waste whereas the reforming processes are related to partial oxidation of gaseous and liquid hydrocarbon fuels like natural gas, alcohols and crude oil . Discussions of the three ways of syngas production will follow with the aim of describing the four factors stated above. The objective of this discussion will show the applicability of using a mixture of methanol and 2-propanethiol as fuel in production of syngas in this study. It will also explain the choice of operating conditions adapted in this study as well as the reactor design. For SR and POX discussion will be limited to gasification of methanol which is the main fuel in the mixture of fuel used in this study having the below advantages as a fuel (Keith and Yu-Chuan, 2009):

- Has a high hydrogen/carbon ratio than other liquid hydrocarbons (Figure 2.3).
- Can be produced from biomass resources
- Reactions involving methanol are of high rates
- The reactions are exothermic
- Methanol is easy to handle

Coal gasification will as well be discussed under gasification of solid feedstock with the objective of elaborating the four engineering factors that differentiate the technologies.

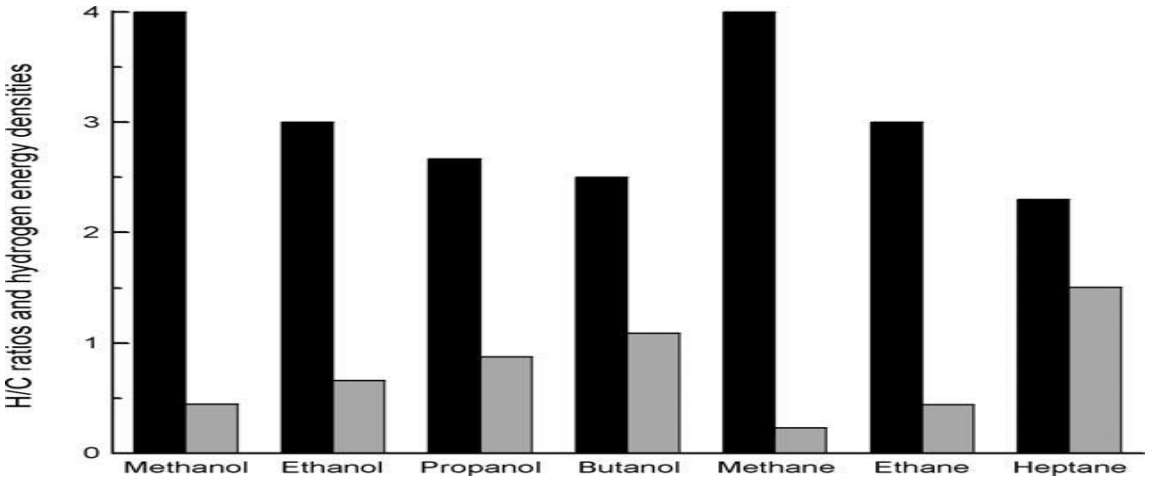

Figure 2.3 Comparison of Methanol Hydrogen/Carbon ratio (black) and Hydrogen energy density (grey) with other hydrocarbons (Keith and Yu- Chuan, 2009)

2.2.1 Steam Reforming

Steam reforming (SR) process occurs when a hydrocarbon fuel and steam are passed through a bed of catalyst to produce syngas. In SR the reforming catalyst are packed in inside tubes of the reactor and on the outside tube the fuel is burnt to supply heat required for the endothermic reactions (Ke at al 2010). Equations 2.1, 2.2 and 2.3 show the main gasification reactions using natural gas, liquid hydrocarbons and methanol as fuel in SR process respectively.

$$CH_4 + H_2O \rightarrow CO + 3H_2 \qquad (\Delta H^o_{298} = +205.9\, kj/mol) \qquad (2.1)$$

$$C_mH_n + \frac{}{2}O_2 \rightarrow mCO + \frac{}{2}H_2 \qquad (2.2)$$

$$CH_3OH + H_2O \rightarrow CO_2 + 3H_2 \qquad (\Delta H^o_{298} = +49.3\, kj/mol) \qquad (2.3)$$

Steam reforming of methanol (SRM) is a well-developed process and widely used in oil refineries where large amounts of H_2 are required in refineries to upgrade the crude oil through hydrocracking and hydrotreating to produce gasoline and diesel (Ke et al., 2010). It has also gained popularity as a source of H_2 for fuel cell applications (Trim and Onsan, 2001). SRM is a chosen process because of the high H_2: CO ratio obtained. This is made possible because part of the H_2 comes from steam and the fuel used in the process. The catalyst used are Cu- based or noble metal-based catalyst. The widely used copper based catalyst is Cu-ZnO-Al_2O_3 because of its high H_2 selectivity at steam to carbon ratio of 1 but deactivates at temperatures above 330 ^{0}C through sintering (Ghencio, 2002). This limits the operating temperatures between 200 ^{0}C and 300 ^{0}C at atmospheric pressure. The low temperatures have the advantage of reducing CO equilibrium selectivity via the water gas shift (WGS) reaction and thus producing a methane free hydrogen at low temperatures and high pressures (Holladay et al., 2004). Therefore the optimum operating conditions for SRM is around a methanol (carbon) steam ratio of 1.5 at temperatures in the range of 250 to 300 ^{0}C for 99% conversions using Cu-ZnO-Al2O3 (Nielsen and Christiansen, 2011). An alternative for the catalyst was suggested by Chao et al., (2003). They proposed a Pd/Zn catalyst which is thermally stable and non-pyrophoric.

External heat supply is required because of the endothermic nature of the process which can be evaded by adding stoichiometric amounts of O_2. Presence of O_2 aids in the exothermic partial oxidation reaction consequently supplying the heat required for endothermic reaction (Ke et al., 2010). This process is called oxidative steam reforming of methanol as shown in equation 2.4 (based on the high heating value of methanol) and its gaining popularity over SRM especially for fuel cells application (Palo et al., 2007).

$$CH_3OH(l) + (1 - 2\partial)H_2O(l) + \partial O_2(g) \rightarrow CO_2(g) + (3 - 2\partial)H_2(g) \quad (if\ \partial = 0.23, \Delta H^o_{298} = -0.5\, kj/mol \qquad (2.4)$$

The kinetics of SRM over Cu- based catalyst has been proposed from literature. It is shown to either occur through methanol decomposition as shown by equation 2.5 or by methanol dehydrogenation to formaldehyde or methylformate route to formic acid then finally decompose to CO_2 and H_2 as shown by equation 2.6 (Ke et al., 2010). More evidence of the latter kinetics has been shown and supported by Frank et al. (2007).

$$CH_3OH \xrightarrow{-H_2} CO \xrightarrow{+H_2O} CO_2 + H_2 \quad (2.5)$$

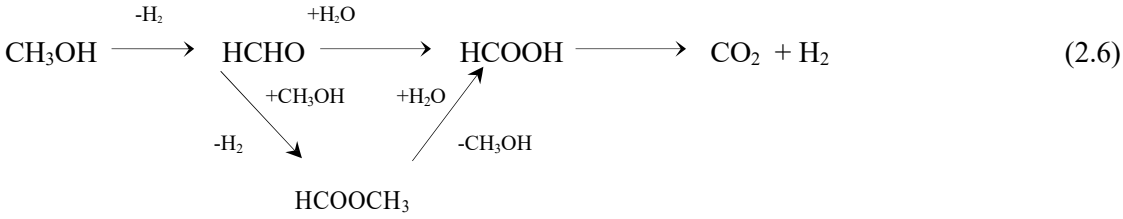

(2.6)

With the rise in interest for methanol as fuel source for fuel cells in automotive, compact units for methanol reforming have been studied. These include micro-channel, plate, plasma and membrane reformers (Ke et al., 2010). Plasma reforming (PR) technology processes a wide range of feedstock from alcohols to natural gas and biomass. It uses the enhanced reactivity of chemical species in the excited states present in plasma (Ke et al., 2010). The disadvantage of this process is the need of electricity to generate the plasma. Massachusetts Institute of technology (MIT) is doing research on PR technology (Siddle et al., 2003).

Membrane reactors combine reaction and separation steps either physically or catalytically. Physical separation occurs in packed bed membrane reactor where the membrane offers a physical barrier through which one product (hydrogen) can diffuse through. Alternatively a catalyst is deposited on the membrane itself and hydrogen is selectively removed as it is produced on the catalyst. This method produces pure hydrogen and saves in downstream CO clean-up for use in Proton exchange membrane fuel cells (PEMFC) (Dushyant et al., 2011).

In plate reformers, plates separate stacks of combustion and reforming chambers filled with catalyst. Combustion process releases heat which is used to run the reforming process. This heat is efficiently transferred across the plate which provides high surface area. Companies in the UK and U.S are currently developing this technology (Ke et al., 2010).

Micro reactors consist of channel gaps in the order of micro scale (Ke et al., 2010). They are characterized by high heat and mass transfer rate. This is because of the high surface area to volume ratios as well as short transfer distances in the reactor. Combining the metallic structure of the unit with the high surface area to volume ratios, micro reactors portray isothermal operations and efficient use of the catalyst bed. This is done by dampening of the local temperature elevations by fast heat transfer rates at macro scales. In the U.S, Pacific Northwest National Laboratory is developing a micro reactor using methanol fuel to supply sub watt to above 100 W powers (Holladay et al., 2004).

2.2.2 Partial Oxidation (POX)

This process involves partial oxidation of the hydrocarbon fuel with pure O_2 either catalytically or non-catalytic in the absence of steam. With addition of steam and presence of a catalyst it results in auto thermal reforming (ATR) process. The process typically results in a H_2/CO = 1.7-1.8 (Nielsen and Christiansen, 2011). Partial oxidation processes are highly exothermic and thus do not require supply of heat to the reactor. Other by-products like olefins and soot maybe produced through cracking of the hydrocarbons during partial oxidation (Nielsen and Christiansen, 2011). In general the main factors to consider when designing a POX reactor are the heat balance and by-products formation. Figure 2.4 (HEX-Heat Exchanger) shows a schematic representation of catalytic partial oxidation (CPO), non-catalytic partial oxidation (NCPO) and ATR systems. Equation 2.7, 2.8 and 2.9 shows the reactions for syngas production during partial oxidation of natural gas, liquid hydrocarbons and methanol:

$$CH_4 + O_2 \rightarrow CO + 2H_2 \quad (2.7)$$

$$+ \frac{}{2} O_2 \rightarrow mCO + \frac{}{2} H_2 \quad (2.8)$$

$$+ \frac{1}{2} \rightarrow CO_2 + 2H_2 \quad (\Delta H^o_{298} = -192.5\, kj/mol) \quad (2.9)$$

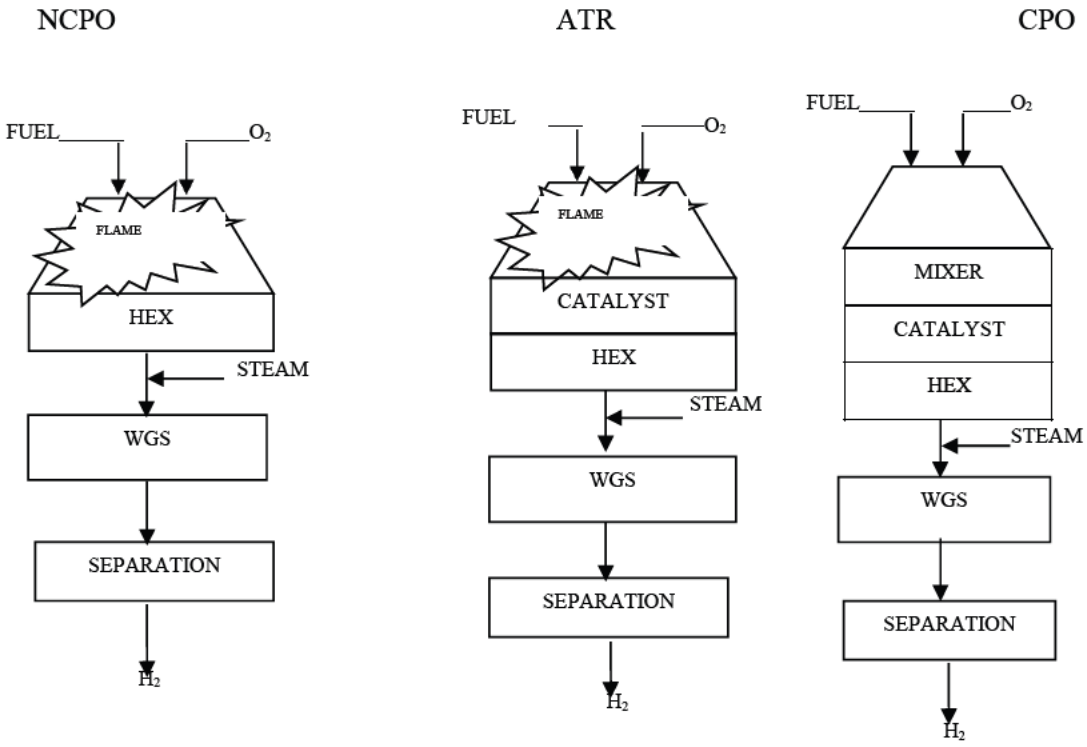

Figure 2.4 Block diagram of non-catalytic partial oxidation, autothermal reforming and catalytic partial oxidation processes (Ke et al., 2010)

2.2.2.1 Non-catalytic Partial oxidation

NCPO process is still undergoing research and not much literature of the process is available. This exothermic process does not require catalyst because of the high temperatures (1150-1500 ^{0}C) in the diffusion flame area of the reactor capable of driving the reactions (Ke et al., 2010). The high temperature in the burner favours the thermodynamic production of H_2 and CO and limits the production of CH_4 and CO_2. The use of O_2 as the source oxidant has the advantage of a compact system and saves in downstream gas clean up unit. As shown in Figure 2.4 for the purpose of hydrogen production, a NCPO plant consists of the partial oxidation reactor, a shift reactor then finally a hydrogen purification unit. The most outstanding feature of the reactor is the burner/feed injector. It allows proper mixing of the fuel with oxidant which prevents coke formation, hot spots in the reactor and consequently explosions.

Despite the fact that the process efficiency is lower than in steam reformers due to the high temperatures required, NCPO reactors are more compact and can accommodate virtually any hydrocarbon fuel from coal, methanol, and ethanol to natural gas. Another advantage of this process is the production of incomplete combustion products that means the chances of NOx and SOx formation are very low. This is because of the fuel-rich burner. Most of the large scale NCPO (Shell and Texaco gasification processes) reactors are used in refineries to produce hydrogen for other refinery operations (Ke et al., 2010). This technology was used in our study because of the simplicity in the reactor design and operation.

2.2.2.2 Catalytic Partial Oxidation

In CPO the hydrocarbon fuel reacts with O_2 at high space velocity in the presence of a catalyst. The reactants are first premixed in the mixing section before sent to the catalytic reactor without a burner for conversion as shown in Figure 2.4 (Christien and Nielsein, 2011). The absence of a burner in the reactor brings out the design difference between CPO and ATR. CPO is characterized by complete and near complete conversion of oxygen and fuel respectively in the catalytic reactor (Ke et al., 2010). Schmidt et al., (2006) did experiments to clarify the speculations made on the mechanism of CPO which also agreed with the results of Lyubovisky et al., (2005). It was speculated that partial oxidation reactions occurred in the beginning 20 % length of the catalyst bed where almost all oxygen is consumed. That means the temperature profile in the reactor rose to approximately 1200 ^{0}C at the top of the catalyst bed. Then the remaining part of the bed experienced steam reforming and water gas shift reactions which use up the heat from exothermic POX reactions and consequently lowering the temperature in the remaining part of the catalyst bed. Schmidt et al., (2006) performed POX of CH_4 on Rhodium coated α-Al_2O_3 foam monoliths. They inserted a capillary tube inside the catalyst bed and monitored the *in situ* concentration profile along the bed by moving the capillary tube using a stepper motor and the gas samples sent to a mass spectrometer which was connected on the capillary tube. Temperature was monitored by K- type thermocouples as well as an optical pyrometer. Their results revealed complete oxygen conversion within 2 mm of the catalyst bed. H_2 and CO were partly

formed in the POX zone and more in the endothermic SR zone. Small amounts of CO_2 was formed in the POX zone and remained constant thereafter. The whole process of syngas production in this experiment was done within milliseconds. This makes CPO an attractive technology in compact systems. The rise in temperature in the first part of the catalyst before the other endothermic zone allows the reactions to be close to equilibrium and thus producing a favourable product distribution. In addition the CPO process produces a H_2: CO ratio of 2 thus making it favourable for Fischer-Tropsch reaction.

Apart from methane, research has shown the feasibility of other fuels for CPO which includes ethanol, methanol and biodiesel. By varying the O_2/C, steam/C ratio and type of catalyst the products from CPO can be syngas or olefins. For example Schimdt et al., (2005) used ethanol to produce syngas over noble metal catalyst. Velu et al., (2006), used methanol as fuel over derived CuZnAl- layered catalyst to produce a gas with high H_2 and CO_2 concentrations at 200 ^{0}C. Krumpelt and his research team designed a CPO fuel cell system for use in vehicles using methanol as fuel at Argonne National Laboratory. They used Cu/ZnO and other proprietary catalysts to generate a H_2 rich and CO- free product (Yu-Chuan Lin., 2006). Johan et al., (2003) performed investigation of conversion of methanol to hydrogen over Cu/ZnO binary catalyst derived from precursors synthesised through oxalates formed in microemulsion and hydroxyl carbonates formed in aqueous solution. The microemulsion formed catalyst showed higher activity in low temperature region than the other catalyst. Both the catalyst had high H_2 selectivity but CO formation was more in the micro emulsion catalyst.

Catalysts play a major role in CPO process which include (Ke et al., 2010);

- Increase reactions rates and permit high gas velocities.
- Prevent formation of soot by scavenging radicals
- Prevent formation of HCN and NH_3 which are toxic compounds as well as consume hydrogen.

Most of the 1st row transition metals (Ni, Co, and Fe) and noble metals (Ru, Rh,Pd, and Ir) have been extensively researched (Ke et al., 2010). One of the main characteristics of the catalysts is to maintain long term activity. Ni based catalyst are at a disadvantage because of carbon deposition thus deactivating them despite being cost effective.

2.2.2.3 Autothermal Reforming

By adding steam to the feed and a burner to the catalytic partial oxidation process as shown in Figure 2.4, the process operates in an autothermal mode and consequently increases the reaction rate and hydrogen yield (Xin et al., 2009).

$$4\ \ _{3}\ +\ 3\ \ _{2}+\ \ \frac{1}{2}\ _{2}\ \rightarrow\ 4CO_{2}+\ 11H_{2}\ \ (\Delta H^{o}_{573}=0\,kj/mol) \qquad (2.11)$$

Autothermal reforming (Equation 2.11) operates at very high temperatures ranging from 900-1150^{0}C and high pressures of 1-80 bar (Ke et al., 2010). The mode of operation produces high H_2: CO ratio suitable for downstream methanol and synthetic fuel processing. Because of the autothermal mode of operation, ATR does not require external heat source resulting in compact system than steam reformers and consequently low capital cost. In addition, recent research in catalysis has resulted in synthesis of catalyst which integrates both SR and POX processes within a single catalyst bed. This makes the ATR systems even more compact than the other processes.

Xin et al., (2009) studied the ATR of methanol in a miniature reactor. He used two stage monolithic catalyst; Pt/Al_2O_3 for catalytic combustion and $ZnO.Cr_2O_3/CeO_2.ZrO_2$ for ATR. The reformed gas at optimum conditions composed of 51.04% H_2, 26.68% N_2, 2.12% CO, and 20.16% CO_2 with a 96.4 % methanol conversion. He also reported that water/methanol and oxygen/methanol ratios greatly affect the conversion process. His optimum water/methanol and oxygen/methanol ratios were 1.4 and 0.27 respectively.

Hirotaka et al., (2006) in their study synthesized a Cu/ZnO catalyst/ceramic fibre composite using a paper making technique. This paper catalyst was used in the ATR of methanol for production of hydrogen in fuel cell applications. They observed that the catalyst hydrogen selectivity at 250 ^{0}C was twice as high as the commercial catalyst pellets and the process was stable. For additional stability of the process and high hydrogen yields they combined a ZSM-5 zeolite with the paper catalyst.

James & Michael, (2006) performed ATR of methanol studies under near adiabatic condition over copper-based catalyst. They observed that using copper-based catalyst with a maximum bed temperature of 300 ^{0}C resulted in high activity and low selectivity of CO at high steam/carbon ratio starting with a low feed temperature (oxidation zone) and high air rates.

2.2.3 Gasification of Solid Feedstock

Solid feedstock gasification process is achieved through physical alterations of the feedstock and chemical reactions in the gasifier (Reizayan and Cheremisinoff, 2005). The solid feedstock is heated and any moisture content in it is evaporated yielding a dry material and water vapour which is used in the preceding reactions. As the temperature in the gasifier rises it devolatilises the carbonaceous material producing char and volatile gases which generally depends on the feedstock composition. The volatiles may include H_2O, H_2, N_2, O_2, CO_2, CO, CH_4, H_2S, NH_3, and C_2H_6, acetylenes, olefins, aromatics and tars. The volatile materials and some of the char react with the limited oxidant to form carbon dioxide and carbon monoxide and in doing so produce heat energy required for the gasification reactions. Combustion of char also produces ash.

Equations 2.12, 2.13, 2.14 and 2.15 are the main combustion reactions (Reizayan and Cheremisinoff, 2005 and Christopher and Maarten, 2008).

$$C + \frac{1}{2}O_2 \rightarrow CO \qquad (\Delta H_{rxn} = -111\, MJ/kmol) \qquad (2.12)$$

$$CO + \frac{1}{2}O_2 \rightarrow CO_2 \qquad (\Delta H_{rxn} = -283\, MJ/kmol) \qquad (2.13)$$

$$H_2 + \frac{1}{2}O_2 \rightarrow H_2O \quad (\Delta H_{rxn} = -242\, MJ/kmol) \qquad (2.14)$$

$$Char + Heat \rightarrow Slag\ (liquid\ ash) \qquad (2.15)$$

Gasification step follows. This step involves the chemical reactions between the carbon in the char with steam, carbon dioxide and hydrogen in the gasifier as well as the other reactions between the resulting gases. Equations 2.16, 2.17 and 2.18 are the main gasification reactions namely water gas shift reaction, boudouard reaction and methanation reaction respectively.

$$C + H_2O \leftrightarrow CO + H_2 \quad (\Delta H_{rxn} = -131\, MJ/kmol) \qquad (2.16)$$

$$C + CO_2 \leftrightarrow 2CO \qquad (\Delta H_{rxn} = +172\, MJ/kmol) \qquad (2.17)$$

$$C + 2H_2 \leftrightarrow CH_4 \qquad (\Delta H_{rxn} = -75\, MJ/kmol) \qquad (2.18)$$

At high carbon conversions equations 2.16, 2.17, and 2.18 can be reduced to two homogenous reactions namely water gas shift (equation 2.19) and steam reforming of methane equation 2.1 respectively. These reactions determine the final composition of syngas at equilibrium.

$$CO + H_2O \leftrightarrow CO_2 + H_2 \qquad (\Delta H_{rxn} = -41\, MJ/kmol) \qquad (2.19)$$

$$CH_4 + H_2O \leftrightarrow CO_2 + 3H_2 \qquad (\Delta H_{rxn} = +206\, MJ/kmol) \qquad (2.1)$$

From the gasification reactions above it can be deduced that as temperature increases formation of CO and H_2 increases and formation of CO_2 and CH_4 decreases. In addition, as pressure increases formation of CO_2 and CH_4 increases although this phenomenon is limited with temperature. At much higher temperatures the effect of pressure is cancelled. This is shown in Figures 2.5 and 2.6. The oxygen/steam ratio also affects the composition of syngas. That is, as the ratio reduces H_2 and CH_4 formation increases and as the ratio increases CO and CO_2 increases.

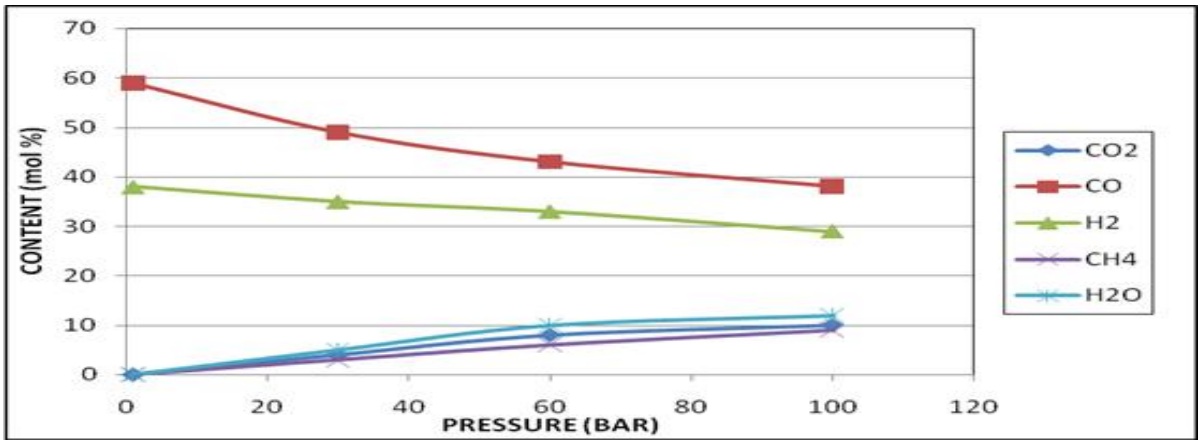

Figure 2.5 Effect of Pressure on syngas composition at 1000 ^{0}C (Christopher and Maarten, 2008)

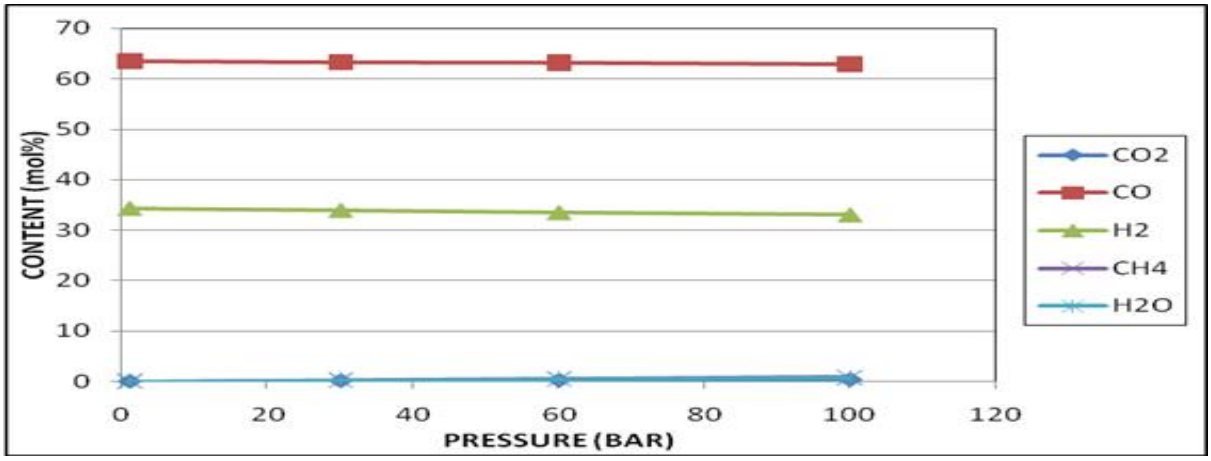

Figure 2.6 Effect of Pressure on syngas composition at 1500 ^{0}C (Christopher and Maarten, 2008)

Depending on the source of the solid fuel, elements like sulphur, nitrogen and chlorine may be present in minute quantities. Because of the low-oxygen reducing environment of the gasifier, most of the sulphur coverts to hydrogen sulphide (H_2S), with a small amount forming carbonyl sulphide (COS). Nitrogen converts to gaseous nitrogen (N_2), with some ammonia (NH_3), and a small amount forming hydrogen cyanide (HCN). Chlorine is converted to hydrogen chloride (HCl). Other components like mercury, arsenic and heavy metals are deposited in the ash and slag. All these by-products must be removed or their concentration lowered prior to further use of the syngas.

2.2.3.1 Solid Feedstock Gasifier Designs

There are three main flow gasifier configurations which are commercially used in the production of syngas using solid feedstock. These designs are described on how the solid feed comes into contact with the reactive gases producing syngas of different composition (Ronald, 2010 and Reizayan and Cheremisinoff, 2005).

- Fixed (Moving) bed
- Entrained-flow
- Fluidized bed

In **Fixed- or moving-bed** (Also referred to as down-draft and up-draft gasifier) gasifier the flow of fuel and the oxygen rich stream is counter current. The flow across the bed is divided into different process zone depending on temperature. From the top of the reactor going down these zones include drying, devolatilization, gasification and combustion. Figure 2.7 shows a moving bed reactor and reactants temperature as they navigate the height of the reactor. Operation in this configuration is of two types;dry-ash mode (e.g., Lurgi dry ash gasifier) and slagging mode (e.g., British Gas Lurgi gasifier). In the dry-ash mode of operation excess steam is fed into the reactor to lower the temperature to below ash melting point consequently producing dry ash. In the slagging mode of operation the opposite happens and the ash exiting the reactor is in form of a viscous liquid.

Advantages of moving bed gasifier include:

- Simple gasification arrangement and process
- Equipment is highly efficient
- Requires less oxidant (oxygen or air)
- Simple feedstock preparation and utilizes coarse coal particles.
- No heat recovery equipment required because of low exit temperatures (420-650 ^{0}C).
- Can handle coals with high reactivity and moisture
- High "cold-gas" thermal efficiency

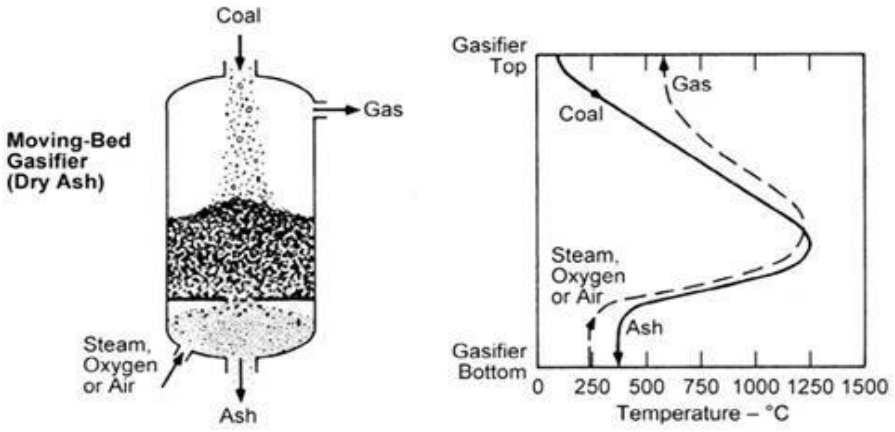

Figure 2.7 Flow of reactants in a fixed bed configuration (Jeffrey, 2006)

Disadvantages of fixed bed gasifiers include:

- Cannot handle coal chunks
- Long residence time
- Slag flow characteristics require carefully controlled feed size distribution for proper operation
- Tars and oils are produced. This intensifies the purification of syngas depending on the intended use.
- High chances of explosions in case of poor process monitoring due to the different reaction zones.
- Limited ability to handle coal fines.

Entrained-flow gasifiers utilize fine coal of about 100 mesh which together with the oxidant (air or oxygen) and/or steam are fed co-currently to the gasifier as shown in Figure 2.8. It operates at high temperatures 1200-1500 ^{0}C and pressure and at high turbulent flow resulting into high carbon conversion efficiencies. Exit temperatures are between 350-700 ^{0}C with ash exiting as a vitreous inert slag. The fine coal feed is fed in either a dry or slurry form. Most commercially used entrained-flow gasification technology include Hitachi, Shell Coal Gasification Process (SCGP), Mitsubishi Heavy Industries (MHI), Texaco (now GE), Babcock Borsig Power (BBP), E-Gas and Prenflo.

Advantages of Entrained-flow gasifiers include:

- Can accept a variety of solid feedstock
- Uniform temperature within the reactor
- Short reactor residence time
- High carbon conversion
- High level of sensible heat in product gas
- Environmentally friendly; produces syngas consists of mainly H_2, CO and carbon dioxide (CO_2) with trace amount of other contaminates due to its operating conditions.

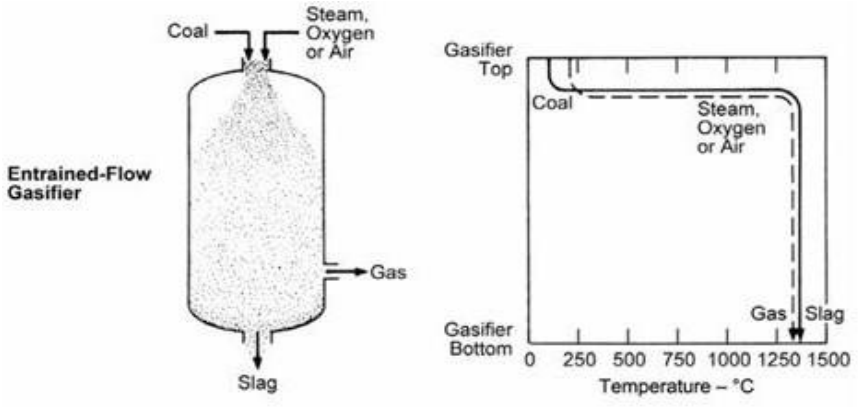

Figure 2.8 Flow of material in an Entrained-flow gasifier (Jeffrey, 2006)

Disadvantages of Entrained-flow gasifier include:

- Large oxidant requirements
- Low cold gas efficiency,
- Heat recovery is required to improve efficiency

Fluidized-bed gasifier operate at high temperatures of about 815-1040 ^{0}C and the feeds as shown in Figure 2.9 enter at very high velocity to fluidize the bed. For proper fluidization, coal particles of normally <6mm are used. Fluidized-bed gasifiers differ in ash conditions (dry or agglomerated/slagging) and in design configurations to improve char utilization. In addition depending on the degree of fluidization and bed height, results in two types of fluidized beds; circulating fluidized bed reactors, and transport reactors. Most commercially used fluidized bed gasification technology include; High Temperature Winkler (HTW), Integrated Drying Gasification Combined Cycle (IDGCC), KRW, Air-Blown Gasification Cycle (ABGC), BHEL, Kellog Transport reactor.

Advantages of Fluidized-bed gasifiers include:

- Has high heat transfer rates
- Can gasify a wide range of feedstock
- Has adequate oxidant and steam requirements
- The high temperature in gasifier is uniformly distributed
- Has a high cold gas efficiency as compared to entrained-bed gasifiers

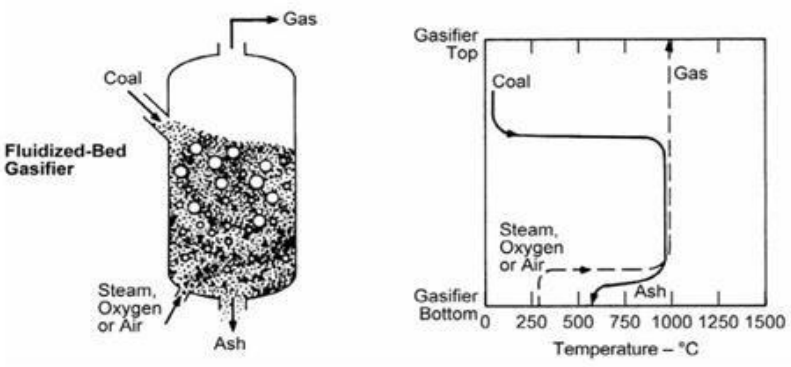

Figure 2.9 Flow of material in a Fluidized-bed gasifier (Jeffrey, 2006)

Disadvantages of fluidized bed gasifier include:

- Has low carbon conversion
- Requires extensive char recycling

2.3 Modelling of Gasification Processes

In the gasifier many reactions as shown above are occurring. These reactions may occur simultaneously. In addition, the feed stock varies in composition and consequently different process conditions. For these reasons most studies prefer using thermodynamic equilibrium models over kinetic based models. Kinetic-based models give more precise and comprehensive results of the process. The limitation of these kind of models are that they are specific to a particular reactor, reaction mechanism must be defined and kinetic rates for each reaction occurring must be given. This becomes cumbersome because of the complexity of the gasification reactions. On the other hand, thermodynamic equilibrium models are found to be useful for preliminary evaluation of the gasification process. They predict equilibrium composition of the syngas as well as effect of operating conditions on the gasifier performance (Maria et al., 2010 and Samson et al., 2011). However, studies have shown that thermodynamic models fail to agree with experimental results by either overestimating or under estimating some components. Zainal et al. (2001) used an equilibrium model in a downdraft gasifier using wood as a fuel to predict the composition of syngas. Their prediction compared well with the experimental data with a 6 mole % overestimate of H_2. Altafini et al. (2003) applied the equilibrium model in fixed bed downdraft gasifier with sawdust as fuel. The model as well over estimated H_2 by 6 mole % and under estimated CH_4 by 2.5 mole %. Other researchers have tried to modify this model by using the quasi equilibrium temperature (QET) approach. This approach assumes that the system undergoes through a sequence of states that are infinitesimally close to equilibrium and the equilibrium reactions occur at lower temperatures than the actual process temperature. Li et al. (2001) used the equilibrium model to predict the syngas composition of a circulating fluidized bed coal gasifier. They observed that real gasification process deviates from the chemical equilibrium. They modified their model

by factoring in non-equilibrium factors. They also observed that the kinetic carbon conversion for pressurized gasification of sub-bituminous coal in the temperature range 747-877 ^{0}C is comparable to the equilibrium predictions for a temperature 250 ^{0}C lower when using QET approach.

The principle of the thermodynamic equilibrium model is the minimisation of Gibbs free energy at equilibrium. The thermodynamic basis of this criterion is shown below.

The Gibbs free energy of a reaction at any given time is defined as:

$$\Delta G = \Delta G^o + RTlnQ \qquad (2.21)$$

Where

ΔG Change in Gibbs Free energy at temperature T (J)

ΔG^o Standard state Gibbs free energy (J)

R Ideal gas constant (J/mole. K)

T Temperature (K)

Reaction quotient (Ratio of the concentration of products and reactants)

At Equilibrium:

$$\Delta G = 0 \; and \; lnQ = K_E \qquad (2.22)$$

Where :

K_E Equilibrium constant

Therefore rearranging Equation 2.21 at equilibrium it becomes:

$$\Delta G^o = -RTlnQ \qquad (2.23)$$

And ΔG^o is defined as: $\Delta G^o = \Delta H^o + T\Delta S^o$ (2.24)

Where:

ΔH^o Standard state enthalpy (J/mole)

ΔS^o Standard entropy (J/mole. K)

These standard thermodynamic data can be obtained from chemical engineering reference books. The standard state is given at 1 bar pressure and at a temperature of 298 K. By obtaining ΔG^o the equilibrium constant can be calculated and therefore equilibrium composition obtained. For a system with many and unknown reactions the Gibbs free energy minimization is combined with atomic balances for each element in the system and species are added and removed as the minimization takes place. Smith et al. (2001) and Buragohain et al. (2010) used the minimization of Gibbs free energy and they used Lagrange undetermined multipliers with constraint of mass balance to get the solution through subsequent iteration. Botha (2010), also used a similar approach with fuel mixture similar to the one used in this study.

Advanced System for Process Engineering (ASPEN) software package can be used to predict the equilibrium composition of the gasification process using its unit operation model, the Gibbs reactor. By specifying the feed, the expected product, the operating conditions and the property method thermodynamic calculations based on Gibbs energy minimisation can be performed. This yields the equilibrium composition of the specified products. For this study, ASPEN was used to predict the equilibrium composition of the syngas to be produced.

Chapter 3

LITERATURE SURVEY: DESULPHURISATION OF SYNGAS

3.1 Introduction

Most hydrocarbon fuels like petroleum, natural gas and coal contain other elements in small quantities which after gasification are transformed to impure compounds. These impurities include compounds of sulphur, nitrogen, chlorine, alkali metals, and some heavy metals like mercury, particulates and tar. A lot of attention has been given to sulphur compounds and therefore this study is focussed on its removal. At high temperature gasification process, sulphur is converted to mainly H_2S and some minute quantities of COS (Ke et al., 2010). Other sulphur compounds like CS_2, thiopenes and mercaptans may also be found in low quantities depending on the process conditions. Desulphurisation either before reforming or after gasification is imperative for the below reasons:

- Corrosion of downstream equipment like turbines when used in IGCC
- Pollution of environment
- Deactivation of downstream process catalyst used in Fischer-Tropsch (FT) process, Sabatier process and water gas shift reaction

Depending on the intended use of syngas, each process has contaminant specification which must be met for proper and efficient running of the downstream processes. Bambang (2013) studied the utilization of syngas for FT process using Co/SiO_2 catalyst in a slurry- bed reactor with syngas contaminant limits shown in Table 3.1. Spath et al. (2003) gave contaminant limits for Sabatier process (methanol synthesis) as shown in Table 3.2. Horazak et al. (2005) gave contaminant limits of syngas to be used in IGCC in Table 3.3 and finally Ke et al. (2010) gave the contaminant limits of syngas to be used in IGCC and fuel cells operating at high temperatures as shown in Table 3.4.

Table 3.1 Syngas impurity limits as feedstock in FT processes (Bambang et al., 2013)

Contaminant	**Limit**
Total Sulphur (H_2S,COS,CS_2)	**< 1ppmv**
NH_3 +HCN	< 1ppmv
Total halides (HBr, HCL,HF)	< 10ppbv
Alkaly metal	< 10ppbv
Solids (soot, ash, dust)	Essentially complete
Organic compounds(Tar)	< dew point
Hetero-atoms (Class 2)	< 1ppmv

Table 3.2 Syngas impurity limits as feedstock for methanol processing (Spath et al., 2003)

Contaminant	**Limit**
Tars	<0.1 mg/ Nm3
CH4	< 3%
NH3	10ppmv
HCN	0.01ppm
Total Sulfur	**0.5ppm**
Halides	0.001ppm

Table 3.3 Syngas impurity limits for use in IGCC (Horazak et al., 2005)

Contaminant	**Limit***
Total Sulphur (H2S, COS)	**750ppmv**
Halides	5ppmv
Particulate	0.7ppmw
Fuel Nitrogen (HCN + NH3)	40ppmv

* Contaminant content in moisture free syngas prior to humidification or nitrogen dilution for typical oxygen-blown gasification syngas.

Table 3.4 Syngas impurity limits for use in IGCC and fuel cells (Ke et al., 2010)

Contaminant	**Solid Oxide Fuel Cell**	**PEMFC**	**Gas Turbine(IGCC)**
Total Sulphur (H2S, COS, etc.)	**60ppbv** -	**10ppbv** -	**760ppmv fuel gas** **20ppmv for selective catalytic reduction (SCR)**
Total Halides (Ci, F, Br)	100ppbv	Not available	5ppmv fuel gas
Total fuel nitrogen (NH3, HCN)	Not available -	1ppmv NH3 -	Fuel-bound Nitrogen 200-400ppmv
Total Alkali metals (Na, K, Li vapour, and solid phases	Not available	Not available	100ppbv fuel gas
Volatile metals (V, Ni, Fe, Pb, Ca, Ba, Mn, P)	5ppbv As 0.2ppmv Se 30ppbv Cd -	Not available - - -	20ppbwPb 10ppbw V 40ppbwCa 40ppbw Mg
Particulates	Not Available	Not available	0.1-0.5 ppm fuel gas

The H_2S in the raw syngas is conventionally removed through the 'wet' processes which will be detailed in section 3.1. Research has shown that by adopting 'dry' desulphurisation methods at temperatures similar to the raw syngas have advantages in the overall plant thermal efficiency. This will also be

discussed under hot gas desulphurisation technology in section 3.3. Table 3.5 gives a summary of all the processes, their conditions and advantages and disadvantages when used in desulphurisation. The sulphur removed from this processes either as H_2S or Sulphur dioxide (SO_2) is sent to the Claus process reactor where they are converted to elemental sulphur.

In this study 2-propanethiol (C_3H_7SH) was in cooperated in the mixture of fuel as a source of sulphur. It was assumed that it will be converted to H_2S during the partial oxidation process. Verification of this assumption will be detailed in Chapter 6.

Table 3.5 Summary of the different methods of desulphurisation (Ke et al., 2010)

Process	Amine	Rectisol	Selexol	Metal Oxides
Absorbent	Amine Solution	Cold Methanol	DEPE	Fe>Mn>Co>Zn>Cu>Ce
Pressure(MPa)	<7	5.8	1.6 – 7.0	70
Temp. (^{0}C)	25 – 60	-70 to -30	-5 to 25	250 -900
Outlet S (ppm)	MEA<1,MDEA< 0.1	< 0.1	< 5	< 0.1
Advantages	Solvent regeneration Low solvent cost CO_2 coabsorption	High sulphur removal efficiency Complete CO_2 CO_2 coabsorption	CO_2 coabsorption Moderate cost	High sulphur removal efficiency High thermal efficiency Sorbent regeneration
Disadvantages	Corrosion Foaming Solution degradation	High cost Loss of thermal efficiency Coabsorption of hydrocarbons	High sulphur outlet content	Requires huge space for reactor set up

3.2 Conventional Desulphurisation Technologies

Conventional methods of desulphurisation involve absorption of the acid gases (H_2S, COS and CO_2) using regenerative solvents moving counter currently with the syngas in an absorber column. The syngas is normally termed as sour gas because of the acidic nature of the gases and after purification it is referred to as sweet gas. The choice of solvent to be used in the absorption process is what differentiates the technologies. It varies according to the degree of acid gas removal required for different end user applications. Other factors include the concentration of the acid gas present in the feed, temperature and pressure which will affect the interaction of the gas and liquid phase, the size of the unit, process economics, consistency, flexibility and environmental limitations (Mahin, 2000). For efficient removal the ideal solvent should possess the following characteristics (Ke et al., 2010):

- High sulphur absorption capacity
- Higher selectivity for sulphur compounds
- Minimal heat of reaction
- Stable under the operating conditions
- Minimal vapour pressure
- No to minimal corrosion
- Easily separable from water
- Appropriate viscosity
- Easy recovery process

The absorption process according to the above mentioned factors are classified into three main processes. They include Chemical solvent process, Physical solvent process and Hydride solvent process (Mixture of Chemical and physical solvents). Details of these processes will be discussed in the next section.

3.2.1 Chemical solvent process

When using chemical solvents, the process of absorption involves a chemical reaction between the acid gases and the solvent to form a loosely bonded reaction product (Kohl and Reisenfield, 1997). The most widely used solvents for this process are predominantly the amine based solvents. The structure of amines consists of at least one hydroxyl group and one amino group. The hydroxyl group serves to reduce the vapour pressure and increase water solubility, while the amino group provides the alkalinity in the water solution for acid gas absorption (Kohl and Reisenfield, 1997). Amines are of three classes; primary, secondary and tertiary. Primary amines consist of Monoethanolamine (MEA) and Diethyleneglycolamine (DGA). They have two hydrogen atoms attached to one nitrogen atom. They form the most stable bond with the acid gases followed by the secondary amines (Kohl and Reisenfield, 1997). Secondary amines consist of Diethanolamine (DEA) and Diisopropanolamine (DIPA). They are composed of one hydrogen atom directly attached to the nitrogen atom. Both primary and secondary amines are degraded by the presence of COS in the acid gas and because of their high basicity, they evolve a high heat of reaction which results to high consumption of energy during regeneration. This makes the tertiary amines favourites for absorption especially in IGCC plants. Tertiary amines consist of Triethanolamine (TEA) and Methyldiethanolamine (MDEA). These types of amines are completely substituted ammonia molecules with no hydrogen atom attached to the nitrogen. They form the weakest bond with the acid gas and have very high H_2S/CO_2 selectivity (Ke et al., 2010). They are less degraded and less corrosive. For applications where both CO_2 and H_2S are to be lowered, the MDEA solvent is combined with activators like MEA, DEA and DGA. MDEA has also a high H_2S content from the regenerator (Figure 3.1) making sulphur recovery possible through Claus process. Most amine based

absorption units are small in size because of their high reaction rates and thus high gas-liquid contact times (DOE/NETL (b), 2013).

Figure 3.1 Flow of diagram of a typical amine gas removal process (Kohl and Reisenfield, 1997)

3.2.2 Physical solvent process

Treating raw syngas which contains high concentration of the acid gases becomes very costly when using the heat re-generable (chemical) solvents. For this reason the need to use non-reactive organic solvents as the treating agents becomes necessary. Physical solvents performance depends on the solubility of the individual gaseous components into the solvent which follows Henry's law (Kohl and Reisenfield, 1997). That is the solubility of the individual component into the solvent is directly proportional to its partial pressure in the gas phase. The process is not reactive which makes the regeneration process very easy and cost effective since one needs to only lower the pressure and consequently strip the acid gases from the solvent. Many organic solvents can be used for this process but for them to be practical they must satisfy the below criteria (Ke et al., 2010):

- Have low vapour pressure to avoid loss of solvent
- Have a high capacity for acid gases and low capacity for the main constituents of the syngas like hydrogen and methane.
- Have low viscosity
- Thermal stability

- Have low hygroscopic nature
- Not reactive with all the syngas components
- Non-corrosive to metals
- Commercially available at minimal cost

Some of the few solvents which have met these criteria and have been used commercially include; N-methyl-2-pyrrolidone (Purisol process), tributylphosphate (Estasolvan process), propylene carbonate (Fluor Solvent process), methanol (Rectisol and IFPEXOL processes), polyethylene glycol dialkyl ethers (Selexol, Sepasolv MPE, and Genosorb processes) (Ke et al., 2010). Among these physical solvent processes, the most widely used are Selexol and Rectisol for acid gas removal in gasification plants.

The solvent for Selexol process is a mixture of dimethyl ethers of polyethylene glycol ($CH_3(CH_2CH_2O)_nCH_3$), where n is between 3 and 10 (Kohl and Reisenfield, 1997). The process is not just limited to dimethyl ether, other dialkyl ether of polyethylene glycol can be used. Genosorb, a process brand name, uses dimethyl ether as well as dibutyl ether of polyethylene glycol as a solvent. The Selexol process apart from being highly selective to H_2S and COS over CO_2 it can also remove NH_3, HCN, CS_2, mercaptans, chlorinated hydrocarbons and BTEX (Benzene, toluene, ethyl benzene and xylene)because of their high solubility in the solvent as shown in Table 3.6. From Table 3.6 it can also be seen that the solvent is at a disadvantage because it is capable of absorbing hydrocarbons present in the gasification gas due to their high solubility consequently high loss of hydrocarbons in the gas (Ke et al., 2010). In addition, refrigeration of the lean solution and high pressure absorption for efficient desulphurisation add complexity and cost of the overall system. Selexol solvent process can be designed subject to the level of H_2S/CO_2 selectivity, bulk CO_2 and H_2S removal and the need for the gas to be dehydrated. Figure 3.2 shows a configuration for bulk removal of both CO_2 and H_2S. The two stage configuration consists of two absorbers for CO_2 and H_2S removal followed by flash drums and stripping column for CO_2 and H_2S solvent regeneration units respectively.

Rectisol process developed by Lurgi GmbH is the most widely used physical solvent process for acid gas treatment in the world. Mostly used in deep sulphur removal, the process can lower the sulphur content to <0.1ppmv and is able to remove HCN, NH_3 and iron and Nickel Carbonyls (Ke et al., 2010). The solvent used in Rectisol process is chilled Methanol at temperatures between -40^oC to -62^oC .It is highly selective to H_2S and COS but less selective to CO_2 as compared to Selexol process at typical process operating temperatures.

Table 3.6 Relative solubility of various gases in the Selexol solvent process (Ke et al., 2010)

Component	R = K'CH_4/K' component
H_2	0.2
CO	0.43
CH_4	1
CO_2	15.2
H_2S	134
COS	35
CS_2	360
SO_2	1400
H_20	11000
HCN	19000
CH_3SH	340
C_4H_4S	8200
CH_2Cl_2	5000
NH_3	73
C_6H_6	3800

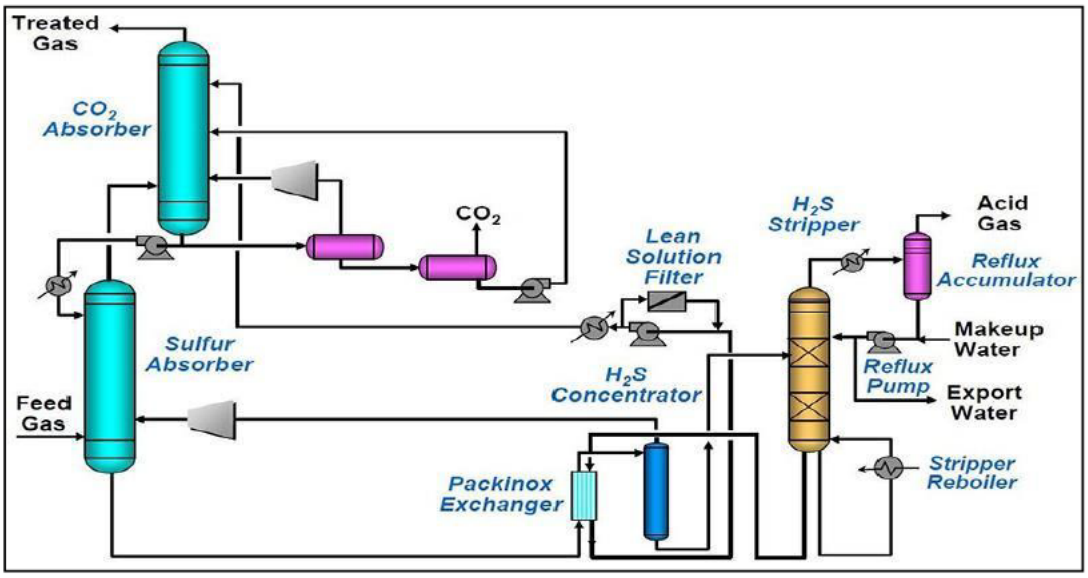

Figure 3.2 Selexol process showing a two stage configuration (DOE/NETL, 2013)

Despite its flexibility to accommodate different configurations (Figure 3.3) depending on the final products desired, the Rectisol process requires high capital due to high operating cost resulting from the complex scheme and the need to refrigerate the solvent due to its low boiling point. In addition it requires high vapour pressure resulting in solvent losses.

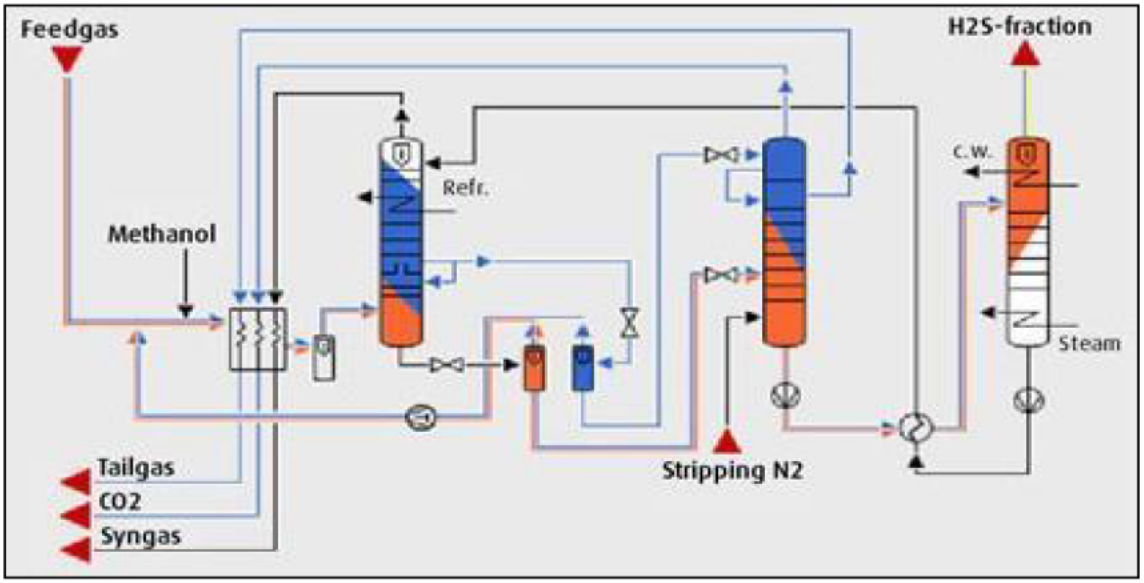

Figure 3.3 Rectisol solvent process for dual removal of sulphur gases and CO_2 (DOE/NETL, 2013)

3.2.3 Hydride solvent processes

A mixture of chemical solvents (amines) and physical solvents (sulfolane) results in a solvent that takes advantage of the best characteristics of the two. Among the main advantages include better solvent loadings at high acid gas partial pressures and higher solubility of COS and other organic sulphur compounds. The two most commercially used hydride solvent processes are Sulfinol (Shell) and Flexsorb (Exxonmobil) (Ke et al., 2010).

Sulfinol process, developed by Shell in the early 1960s, is a hydride solvent process that uses a mixture of water, sulfonale (Tetrahydrothiopene dioxide) and one or more alkanolamine to remove acid gases. The Sulfinol process can adapt different names depending on the type of amine mixed with water and sulfonale. For example, Sulfinol-D uses Diisopropylamine (DIPA). Sulfinol-D is used in the natural gas and petroleum industry to partially remove organic sulphur compounds. It is not highly selective to H_2S.Sulfinol-M uses Methyldiethanolamine (MDEA), and it is highly selective to H_2S. Finally there is Sulfinol-X which uses either DIPA or MDEA and an accelerator. Shell considers Sulfinol-X using DIPA as the best choice in applications of removing H_2S, CO_2, COS, mercaptans and organic sulphides from gas streams. In addition, it is highly suitable when refurbishing deep CO_2 removal plants from the claims that because of the high loadings, small absorbers with fewer trays can be effectively used in the cleaning process. The solvents are also re-generable.

FLEXSORB was developed by ExxonMobil in 1983. The process was mainly designed for selective removal of H_2S in the presence of CO_2. It has broad application in natural gas and petroleum refining industries. The process uses steric hindered amines as the solvent. Hindered amines are chemical compounds containing an amine functional group surrounded by a crowded -CH_2- group that brings about a change in the shape and reactivity of the overall compound (Nick et al., 2002). This hindered form of amines have advantages over the tertiary amines and this makes them more suitable to use. The hindered amines are more basic, which increases the rate of the reaction and consequently absorbs more H_2S. They react slowly with CO_2 because of the bulky -CH2- group as compared to its reaction towards H_2S thus selectively removing H_2S. ExxonMobil has three types of technology each having a function towards removal of H_2S. FLEXSORB SE selectively removes H_2S while FLEXSORB SE Plus selectively removes H_2S to less than 10ppm and finally FLEXSORB SE Hybrid removes H_2S, CO_2 and other sulphur compounds. It is a very reliable, robust and simple to operate process. Low flow rates of the solvent are experienced with less corrosion and foaming.

3.3 Hot Gas Desulphurisation Technology

Raw syngas exits the gasifier at temperatures between 900-1600 ^{0}C (Ke et al., 2010). When using the conventional desulphurisation processes this syngas has to be cooled to near ambient or even lower than ambient (Table 3.5) prior the absorption column then reheated back again depending on the intended use. For example the methanol synthesis and Fischer-Tropsch process requires a syngas feed of 220-350 ^{0}C and IGCC turbines requires a syngas feed of 500-1000 ^{0}C. The lowering and heating of the gas requires additional equipment (heat exchangers, condensate handling systems etc.) and lowers the overall thermal efficiency of the system. For this reasons research on hot gas desulphurisation (HGD) systems has been on since 1970s especially in the U.S, Europe and Japan (Nick et al., 2002). The main motivation for HGD especially in IGCC is increasing the overall efficiency of the system. Gupta and Gasper-Galvin (1992) and Furimsky and Yumura (1986) report that conventional pulverized coal systems have efficiencies between 35-36 % whereas IGCC using the cold gas desulphurisation process has efficiencies between 43-46 %. Adopting HGD into the IGCC process has the capability of improving the efficiency by about 6 %. Yunhan et al. (2012) performed thermodynamic studies on how IGCC can benefit from HGD process and removal of particulates in the dry hot conditions. They studied IGCC systems using full cold gas clean up system and hot gas clean up system using ASPEN simulation software and zinc oxide as the sorbent for HGD. Their results showed that IGCC with full hot gas clean up system efficiency improved by 1.77 % compared to cold gas clean up system. 1 % of the efficiency was contributed by dry particulate cleaning and the remaining from HGD. They also reported that the HGD will only be beneficial at temperatures not exceeding 350 ^{0}C. This indicates a limitation on HGD which will further be discussed below. Apart from increasing the process efficiency and saving on the plants cost HGD being a dry process as opposed to the wet process of using solvents has the following additional advantages (Ke et al., 2010):

- Solid sorbents are less toxic and corrosive than amine solvents used in cold gas desulphurisation
- There is no formation of sour water which forms when syngas is cooled below the dew point of water and thus save on its treatment.
- No formation of black mud (mixture of ash, char and water) formed during wet scrubbing of particulates in the syngas.

3.3.1 Principle of HGD and Choice of Sorbent

HGD process involves a gas-solid reaction between H_2S and metal oxides sorbents at temperatures >250 ^{0}C to form a solid metal sulphide and steam in an equilibrium limited sulphidation reaction shown in equation 3.1. The metal sulphides can be regenerated back to the original metal oxide as shown

in equation 3.2 through oxidation using air (oxygen) a process analogous to ore roasting. Studies in this work will focus on sulphidation and not regeneration part of the process.

$$MeO_{(s)} + H_2S_{(g)} \leftrightarrow MeS_{(s)} + H_2O_{(g)} \quad (3.1)$$

$$\text{( )} + \frac{3}{2}\ \text{2( )} \leftrightarrow MeO\ \text{( )} + \text{2( )} \quad (3.2)$$

Westmoreland and Harrison (1976) performed thermodynamic screening on 28 metal oxides based on the minimization of free energy to establish their ability to remove equilibrium sulphur and the sorbent stability in HGD for low-Btu gas at temperatures up to 1500 ^{0}C. The oxides of iron, zinc, molybdenum, manganese, vanadium, calcium, strontium, barium, cobalt, copper and tungsten were the eleven feasible metal oxides. They came up with a diagram (Figure 3.4) showing the states of the metal oxides as a function of temperatures on which they can be sulphided, regenerated and become inactive in desulphurisation process. Using Figure 3.4 the sorbents were grouped into 2 categories; high temperature sorbents >600 ^{0}C and medium temperature 300-500 ^{0}C. High temperature included the oxides of Ba, Ca, Sr, Cu, Mn, Mo and W and the middle temperature included oxides of V, Zn, Co and Fe.

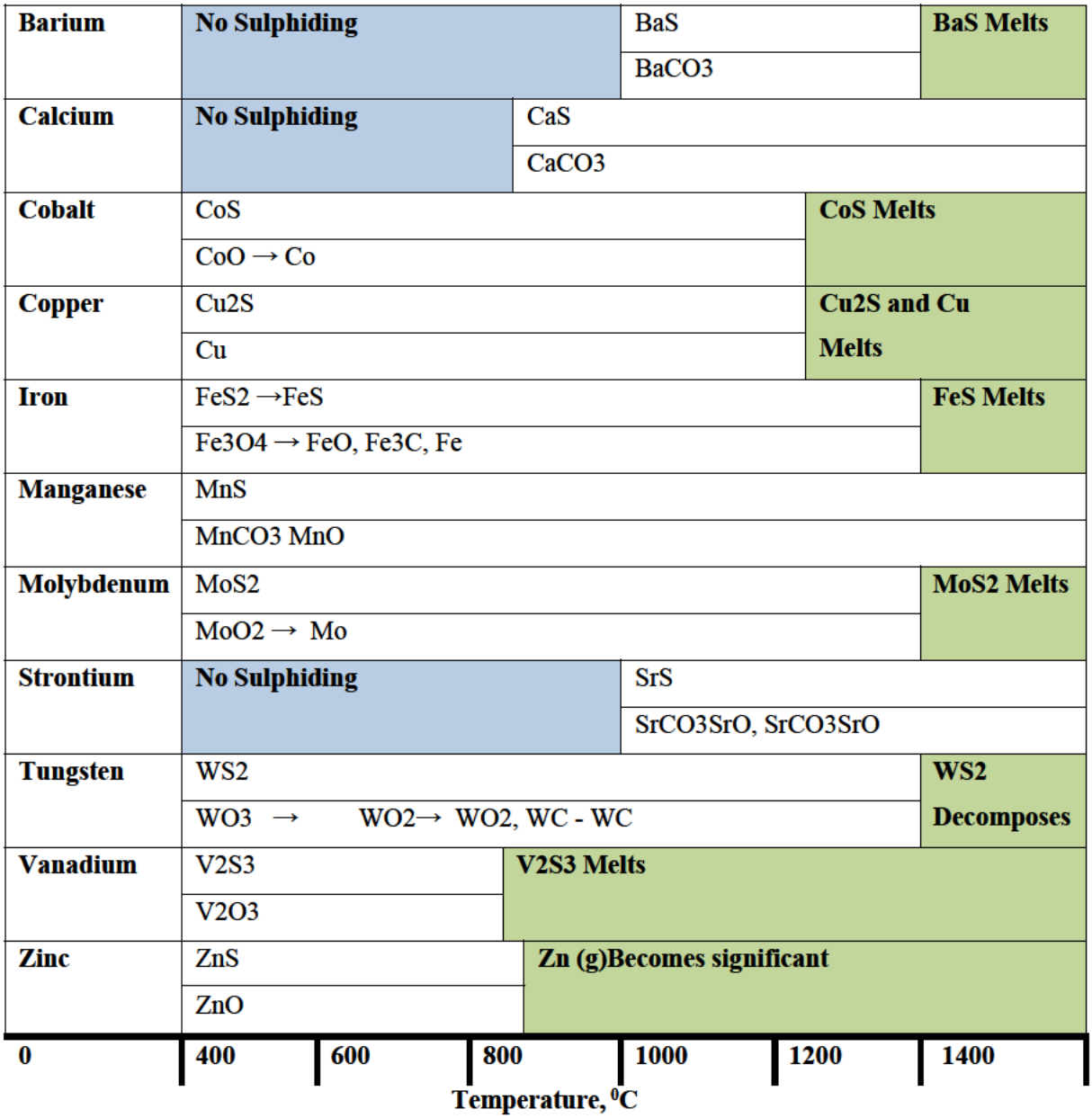

Figure 3.4 Metal Oxides stability as a function of Temperature in HGD (Westmoreland and Harrison, 1976)

The high temperature sorbents could work well in in-situ desulphurisation process especially in coal gasification process. This is where the sorbent is introduced into the gasifier and desulphurisation proceeds simultaneously with the gasification process. Most of these sorbents are non-regenerable. The most widely used sorbents for in-situ desulphurisation are limestone and dolomite. These sorbents despite being commercially available and cheap, they do not lower the sulphur levels below 100ppm. This then requires a polishing desulphurisation bed prior the use of syngas in many applications. In addition, the form of metal sulphide formed (CaS) requires an expensive treatment to transform it to a more stable and disposable form as $CaSO_4$ and they are only limited to fluidised bed gasifier configurations (Artos et al., 1995).

All of the other categories of sorbents can be used as regenerable sorbents in an external bed for either intensive desulphurisation or as polishing bed (Figure 3.5). Unfortunately, each and every sorbent have limitations. In intensive desulphurisation raw syngas is sent to reactors which can either be a fluidized, moving or fixed bed reactor loaded with sorbent. In the case of a fixed bed reactor (Figure 3.6), two reactors packed with sorbents operate in series. One operates as the front bed and the other the trail bed by changing the flow of the raw syngas. This arrangement saves on the usage of the sorbent. Once the front bed is exhausted it can either be regenerated by passing through air or it can be replaced by a fresh lot. Gupta et al. (1992) used Zinc Ferrite as a sorbent for HGD in a fixed bed. He concluded that fixed bed reactors require high temperature pressure valves because of the operating conditions of HGD, there is difficulty in handling the heat released during regeneration and that the off-gas released after regeneration has a non-uniform composition. Because of the fixed bed limitations other researchers in the Department of Energy in the U.S and the Research Triangle Institute have redirected their focus in developing sorbents that would work best in moving and fluidized bed (Ke et al., 2010). For this study though we chose to use a fixed bed reactor despite its limitations, the sorbent available could only work well in that reactor configuration.

An ideal sorbent must possess the below characteristics (Ke et al., 2010):

- High activity towards sulphur compounds and be able to lower them to <0.1ppmv before breakthrough.
- High sulphur capacity (1-3.5g S/100g sorbent before breakthrough).
- Non-pyrophoric
- Regenerable
- Be able to maintain its desulphurisation ability for a minimum of 100 recycles and withstand attrition.
- Be able to be easily prepared for scale up in commercially available equipment
- Disposable as a non-hazardous waste upon being spent
- Suitable morphology for high desulphurisation capabilities
- Minimize undesired reactions in adsorption and regeneration conditions.
- Operate with a sharp reaction front in order to attain high conversions at breakthrough.
- Have apparent physical changes like colour change to provide visual indication of process progress.

The ability of a sorbent to lower H_2S to very low levels is determined by the thermodynamic equilibrium of the reaction of H_2S with the stable form of the metal oxide in the reducing environment created by the syngas constituents CO, H_2, CO_2 and H_2O. The process involves simultaneous sulphidation and reduction of the metal oxide (equation 3.3) as opposed to the general equation 3.1 above (Gangwal, 2011):

$$Me_xO_{y(s)} + zH_2S_{(g)} + (y-z)H_{2(g)} \leftrightarrow Me_xS_{z(s)} + yH_2O_{(g)} \quad (3.3)$$

Performance of Iron and Copper oxides despite their high thermodynamic efficiencies are highly affected by the composition of syngas because of their reduction to metallic state. On the other hand compounds like Fe_2O_3 and CeO_2 needs to be partially reduced for sulphidation to occur kinetically to Fe_3O_4 and Ce_2O_3 respectively (Gangwal, 2011). ZnO has attracted a lot of attention in HGD and a lot of work has been done using it. ZnO has a very high thermodynamics efficiency thus capable of lowering H_2S to <1ppmv far much lower than MnO, and CuO. It also has a high theoretical sulphur capacity of about 25 wt. % and it is non-pyrophoric once sulfided making it suitable sorbent for use in fuel cells. ZnO sulphidation reaction does not have many side reactions as compared to the other metal oxides and it is a cheap sorbent (Chiche et al., 2013). For this reasons ZnO was chosen as the sorbent for the HGD studies in this work.

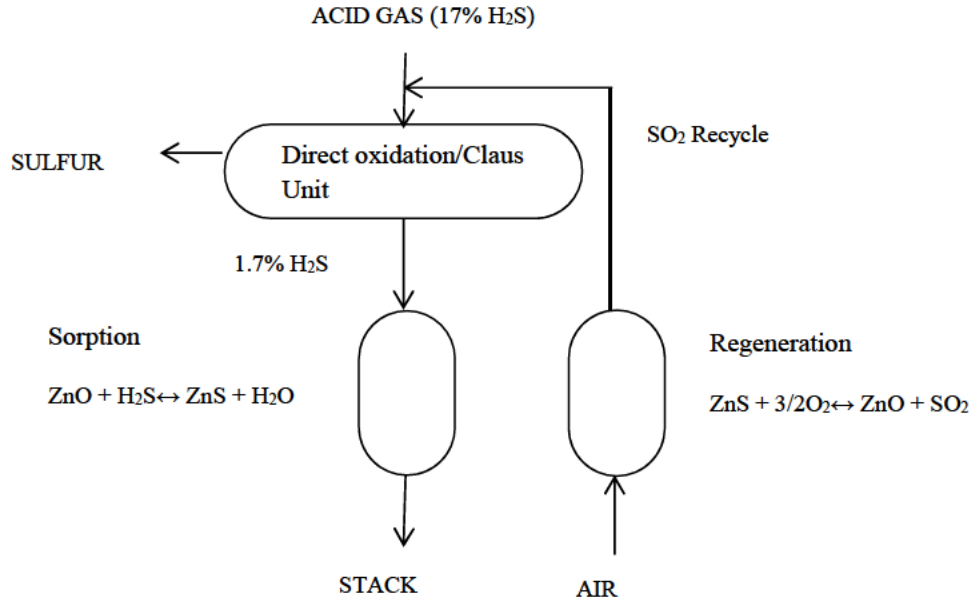

Figure 3.5 HGD used as a polishing bed (Kohl and Reisenfield, 1997)

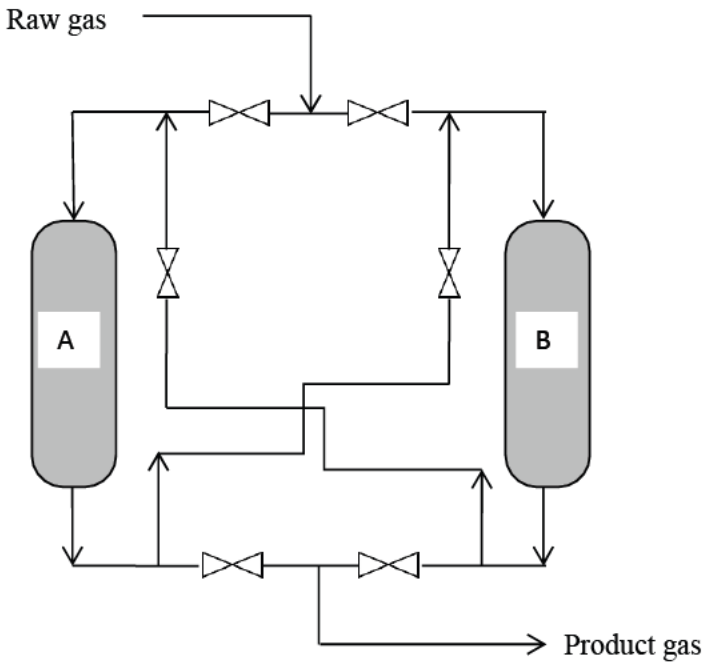

Figure 3.6 Intensive use of HGD

3.3.2 ZnO Sulphidation studies in HGD

The sulphidation reaction between ZnO and H_2S is given by equation 3.4. The reaction is very exothermic and can even occur at room temperature. However, it is carried out at high temperatures to increase the reaction rate.

$$ZnO_{(s)} + H_2S_{(g)} \leftrightarrow ZnS_{(s)} + H_2O_{(g)} \qquad \Delta H_{rxn} = -78.9kj/mol \qquad (3.4)$$

Studies have however shown that ZnO get reduced to its metallic form at temperatures < 500 - 600 ^{0}C (Westmoreland et al., 1976, Lew et al., 1992 b and Chiche et al., 2013). This resulted in development of more resistant Zn- based sorbent like zinc titanate (which is formed by reacting ZnO and titanium oxide (TiO2). Lew et al. (1992 b) studied the kinetics of ZnO and ZnO-TiO_2 at temperatures between 400-700 ^{0}C with varying stoichiometric ratios of ZnO and TiO_2. They concluded that both sorbents have the same intrinsic sulphidation kinetics only that ZnO-TiO_2 serves to inhibit sintering of ZnO. They also observed that an increase in the stoichiometric ratio of TiO_2 and ZnO of about 2/3 the sulphur loading of zinc titanate reduces.

The kinetics of the sulphidation reaction of ZnO follows the rate law given in equation 3.5 and an Arrhenius relationship given in equation 3.6. Most researchers have reported a first order kinetics with

respect to H_2S (Westmoreland et al., 1976, Lew et al., 1992 a and Turton et al., 2004). They varied sorbent particle size and gas flow rates to eliminate external mass transfer and pore diffusion limitations. The summary of the work done on intrinsic kinetics by different researchers is summarised in Table 3.7 all the experiments being done at atmospheric pressure.

$$= \quad _2 \qquad (3.5)$$

$$= \quad exp\,(\frac{-E_a}{}) \qquad (3.6)$$

Where:

Initial molar rate of ZnS formation per unit surface area of the solid reactant (mole/cm^2.s)

2 Molar concentration of H_2S in gas (mole/cm^3)

Molar concentration of ZnO solid (mole/cm^3)

Activation energy (kJ/mole)

Gas constant (kJ/mole.K)

Reaction absolute temperature (K)

Frequency factor (cm/s)

Reaction order with respect to H_2S (-)

Reaction order with respect to ZnO (-)

Table 3.7 Summary of research done on the kinetics of the sulphidation of ZnO (Botha 2010)

Researchers	Temperature Range	Activation Energy,	Frequency factor,	Conditions	Comment
	°C	kJ.mol-1	cm.s-1		
Westmoreland *et al.* (1977)	300-750	30.3	1.22		H_2S: 1-9 mol %. H_2 at 5 times the H_2S mol %. Balance N_2.
Lew *et al.* (1992 a)	400-800	43.1	1.31		H_2S: 2 mol %, H_2 1 mol %, balance N_2
Turton *et al.* (2004)	482-593	31.4	0.333	H_2S: 0.5-2 mol %, balance N_2	24.5-38.2 kJ.mol-1 95% confidence interval for *Ea*.
Li *et al.* (1997)	200-400	11.84	0.0044	H_2S: 5.41-19.25 g.Nm^{-3}, balance N_2. 4 mm pellet	(ZnO-MnO ratio 9:1) Apparent kinetics
Huiling *et al.* (2002)	200-320	15.85	0.21	H_2S: 8.73-16.4 g. Nm^{-3}, H_2 20 mol %, balance N_2. 3-3.5 mm sphere	Apparent kinetics in presence of H2.
Huiling *et al.* (2002)	200-320	19.32	0.08	H_2S: 8.73-16.4 g. Nm^{-3}, balance N_2. 3-3.5 mm sphere	Apparent kinetics.

ZnO sulphidation process is affected by several factors which many researchers vary in their experiments to observe their effect on HGD using ZnO and finally optimize the process. They include:

- Syngas composition
- Sorbent surface characteristics (porosity and specific surface area)
- Sorbent morphology
- Reaction temperature
- Reaction pressure
- Sorbent particle size
- Gas flow rate

Novochinskii et al. (2004) did an investigation on the effect of H_2O present in the syngas composed of 1.2ppmv H_2S, 34.4 vol % H_2, 20 vol % H_2O and the balance N_2 to ZnO desulphurization at temperatures between 100 to 700 ^{0}C. They observed that the presence of water limited sulphur removal by shifting the equilibrium of equation 3.4 towards the reactants. Similar observations were reported by Chiche et

al. (2013).Yang et al. (2008) performed studies on the effect of CO, CO_2 and steam on reformate desulphurization using ZnO. The reformate was composed of 10 % CO, 20 % CO_2, 40 % H_2, 20 % steam and 4000ppmv H_2S. The experiment was performed at atmospheric pressure and at 400 ^{0}C with a space velocity of about 14000h^{-1}. They observed a sorbent utilization of 30 %. They removed CO, CO_2 and steam and studied only a gas composed of H_2 and H_2S and with this they observed a sorbent utilization of close to 90 %. Chiche et al. (2013) reported that there is competitive adsorption between CO_2 and H_2S as well as reaction of CO, CO_2 with H_2S (equations 3.7 and 3.8 respectively) to form COS which cannot be absorbed by ZnO.

$$CO_{(g)} + H_2S_{(g)} \leftrightarrow COS_{(s)} + H_{2(g)} \qquad \Delta H_{rxn} = -10.9kj/mol \qquad (3.7)$$

$$CO_{2(g)} + H_2S_{(g)} \leftrightarrow COS_{(s)} + H_2O_{(g)} \qquad \Delta H_{rxn} = 30.3kj/mol \qquad (3.8)$$

The reactivity of a solid in catalysis is a function of the chemical composition of the solid, its structure and morphology (Bolis et al., 1989). Zinc oxide of low purity has a disadvantage in that the inactive impurities will occupy a reactor volume in direct proportion to their percentage in the overall sorbent. In addition, ZnO of low bulk density is at a stoichiometric disadvantage since the weight charged into the reactor is directly proportional to its bulk density. The specific surface area of a sorbent as well affects reactivity. Finer particles exhibit high reactivity because of the high surface area available for reaction unlike large particles. Westmoreland et al. (1977) reported that ZnO in pellet form in HGD are at a disadvantage because of mass and diffusion limitations. To correct this Jain et al. (2014) proposed a change in the morphology of ZnO that will increase the surface area and shorten the diffusion distance. Change in morphology can be achieved by different preparation techniques like decomposition of salts (carbonates and oxalates) as well as adding additives to the zinc oxide to increase its reactivity. Currently a lot of work has been focussed in production of ZnO Nano particles for both high and low desulphurisation reactions (Corrie and Kenneth, 2001, Jain et al., 2014). Shangguan et al. (2011) added graphite, Al_2O_3 and K_2CO_3 into the composition of a ZnO sorbent. The Al_2O_3 improved the pore structure of the sorbent consequently increasing the diffusion of H_2S through the sorbent. K_2CO_3 increased the basicity of the overall sorbent and raised the COS catalytic hydrolysis rate on the sorbent reducing the concentration of COS in the outlet gas.

Research done on the effect of temperature and pressure by different researchers is summarised in Table 3.8 and effect of particle size, gas space velocity and H_2S inlet concentration is summarised in Table 3.9

Table 3.8 Effect of temperature and pressure on HGD using Zn- based sorbents (Botha, 2010)

Researcher	Sorbent	Reactor Type	Temperature	Pressure
Yumura and Furimsky (1985)	ZnO	TGA	Increasing the temperature from 600-800 °C had little effect on sulphur removal capacity of the sorbent.	-
Woods *et al.* (1990)	Zinc titanate	TGA	For low temperatures (< 400 °C), the reaction rate was very slow. As the temperature increased to 650 °C, the reaction rate increased considerably. However, from 650-750 °C, there was almost no dependence of the reaction rate upon temperature.	An increase in pressure from 1-10 atm at 705 °C caused a decrease in reaction rate, attributed to a decrease in the transfer coefficients with the increase in pressure. This was at constant H_2S concentration.
Lew *et al.* (1992 b)	ZnO	TGA	The reaction rate for zinc oxide increased significantly from 400-600 °C and then only slightly to 700 °C.	-
Turton *et al.* (2004)	ZnO	TGA	The reaction rate increases from 482-593 °C	-
Sánchez *et al.* (2005)	Z-Sorb III	fixed bed	There was little influence in solid adsorption capacity in 400-650 °C and minor differences in breakthrough time. However, at 250 °C, breakthrough occurred at after half the time of the 400 °C result.	Conditions: 1 mol % H_2S at 400 °C, pressure: 2-20 atm. At higher pressures, the sulphur loading values were considerably higher, reaching estimated values as high as 97 % of the maximum loading capacity at 20 atm. At 2 atm, sorbent utilization was only 52 % of the maximum capacity. Possibly, the diffusion of H_2S to the interior of the pellet is enhanced at higher pressure.

Note that TGA refers to thermogravimetric apparatus

Table 3.9 Effect of pellet size, space velocity, H_2S inlet concentration on Zn- based sorbents (Botha, 2010)

Researcher	Sorbent	Reactor Type	Pellet Size	Space Velocity	H_2S inlet concentration
Woods *et al.* (1990)	Zinc titanate	TGA	The smaller pellets (3.2 mm) reacted appreciably faster than larger pellets (4.8 mm). Similar results were obtained at other temperatures.	-	Concentration was varied from 0.25-2.5 mol % at 1 atm and 705 °C. As expected the global rate increased with increasing H_2S concentration.
Lew *et al.* (1992 b)	ZnO	TGA	[Inlet concentration only] Concentration was varied from 1-3 mol % at 1 atm and 500 °C. The reaction rate increased with increasing H_2S concentration.		
Li *et al.* (1997)	ZnO-MnO	TGA	[Pellet size only] The initial and final reaction rates were significantly increased with a decrease in the pellet size from 4mm to 3.3mm.		
Turton *et al.* (2004)	ZnO	TGA	[Pellet size only] No difference in reaction rate between size fractions from 37-137 μm.		
Sánchez *et al.* (2005)	Z-Sorb III	Fixed bed	[Space velocity only] Conditions: 10 atm, 400 °C, gas space velocities of 3500 h-1 to 10 000 h-1. At higher velocity, sulphur uptake by the sorbent is lower. In addition to diffusion resistance, a possible explanation would be that, at the higher velocity, the bed length might be shorter than the sorption front. Breakthrough of the higher velocity occurred at about one third of the lower velocity result		

Note that TGA refers to thermogravimetric reactor

As was mentioned, the reaction between H_2S and ZnO is a gas solid reaction. Chapter 4 will explain in detail the occurrence and limitations of gas-solid reactions and the models that explain their occurrence.

Chapter 4

GAS-SOLID REACTION MODELLING

4.1 Introduction

Gas-solid reactions have a wide range of application in the chemical and metallurgical industries. Examples of these include coal gasification, reduction of metal oxides (iron ore to iron), roasting of sulphides, incineration of solid waste, calcination of limestone among many others. Understanding of these reactions is essential in the designing of experiments and interpretation of the experimental results. In addition the performance of industrial equipment in which these reactions occur can be improved.

The general form of the gas-solid reaction is shown in equation 4.1:

$$aA_{(g)} + bB_{(s)} \leftrightarrow cC_{(g)} + dD_{(s)} \qquad (4.1)$$

Where *a, b, c* and *d* are stoichiometric coefficients. Szekely et al. (1976) explained the mechanism of gas-solid reaction system of a single particle with a stream of moving gas. Study of single particle systems is much easy and the results can be extrapolated to the more complex multi-particle systems which is relevant in this study. The overall reaction mechanism may involve the following steps (Szekely et al., 1976) also illustrated in Figure 4.1:

1. Mass transfer of the gaseous reactant from the bulk of the gas stream to the external surface of the solid particle
2. Diffusion of the gaseous reactant through the pores of the solid matrix
3. Adsorption of the gaseous reactant on the surface of the solid matrix
4. Chemical reaction at the surface of the solid matrix
5. Desorption of the gaseous product from the surface of the solid matrix
6. Diffusion of gaseous reaction product through the pores of the solid matrix
7. Mass transfer of the gaseous product from the external surface of the solid to the bulk of the gas stream

From the steps mentioned above it can be summarised that gas-solid reactions are characterised by external mass transfer, pore diffusion, adsorption/desorption and chemical reaction phenomenon. Whichever of these factors exhibit the highest resistance to the reaction it is termed as the rate controlling process and the overall rate of reaction is dependent on its rate. Apart from these main factors, the reaction can also be affected by heat transfer both within the reacting solid (conductive) and between the solid and the surrounding gas (convective and possibly radiative). Heat transfer and the

reaction process may lead to changes in the solid structure (sintering or pore structure changes) also affecting the progress of the reaction. The flow of gases and solids in the reactor could also be another factor to consider (Szekely et al., 1976).

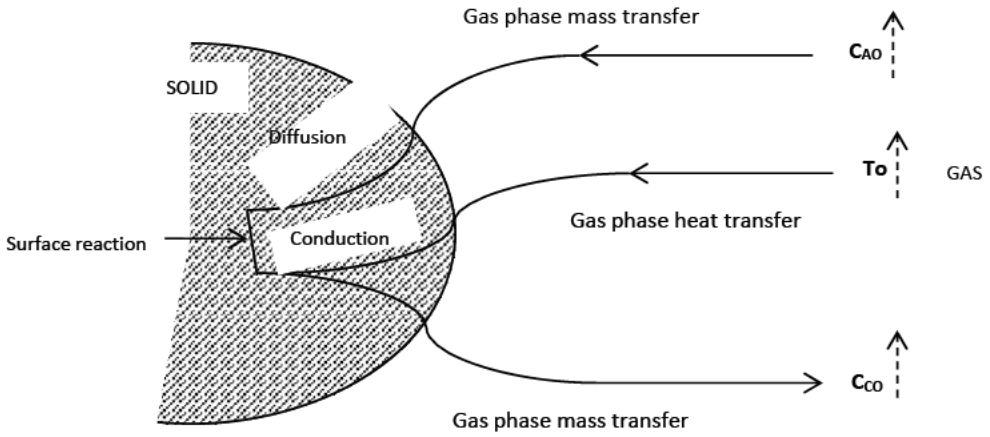

Figure 4.1 Reaction of a single solid pellet with a gas (Szekely et al., 1976)

4.1.1 Mass transfer effects

The rate of mass transfer can be described and measured by the use of mass transfer coefficient which is determined by the flow and physical characteristics of the species in the system. The mass transfer coefficient is available from a variety of correlations. For any particle-fluid system, the correlations can be described by equation 4.2 (Szekely et al., 1976):

$$N_{Sh} = A + BN^m N^n \qquad (4.2)$$

For example, the Ranz and Marshall Equation for of 0-200 is shown in equation 4.3 (Szekely et al., 1976):

$$N_{Sh} = 2.0 + 0.6N^{1/2}N^{1/3} \qquad (4.3)$$

$$N_{Sh} = \frac{Lh_D}{} \qquad (4.4)$$

$$= \frac{}{\mu} \qquad (4.5)$$

$$= \frac{\mu}{} \qquad (4.6)$$

Where:

N_{Sh}	Sherwood Number	(-)
	Schmidt Number	(-)
	Reynolds Number	(-)

h_D	External mass transfer coefficient	(m/s)
	Characteristic length (diameter for a sphere)	(m)
	Binary diffusion coefficient	(m^2/s)
	Superficial velocity	(m/s)
	Fluid density	(kg/m^3)
μ	Fluid viscosity	(Pa.s)

The results obtained from the correlation of Ranz and Marshall for the range of Reynolds and Schmidt numbers usually encountered in gas-solid reactions were identical with other researchers (Skezely et al., 1976).

4.1.2 Pore diffusion effects

Diffusion through the pores of a porous solid provides access for the reacting gas to the solid surface and the removal of the gaseous products. For the case of a non-porous solid, pore diffusion may occur if the product layer formed is porous. This type of diffusion is more complex compared to molecular diffusion where the gaseous molecules are in constant contact with each other. This process is thus affected by (Szekely et al., 1976 and Klobes et al., 2006):

- The size of the pores; if the pores are small the laws of molecular diffusion cease to exist and Knudsen diffusion (the collision between the gas molecules and the solid surface is higher than the collision between the gas molecules themselves) becomes significant.
- The types of pores present in the solid particle determines the path in which the fluid will take and whether the pores are accessible by the gaseous reactant as shown in Figure 4.2. In Figure **4.2** the pore labelled (a) is a closed pore in which no external fluid can access. If path (cec) or (ced) is followed that's an open through pore whereas pore (f) and (b) are open blind pores. It can be seen that the path is very tortuous and not straight.

- Occurrence of pressure gradients within the solid may occur and thus movement due to pressure gradient must be considered.
- The area occupied by the solid that is the shaded part in figure 4.2 is not available for diffusion.

Figure 4.2 Cross-section of a porous solid particle (Klobes et al., 2006)

Therefore to be able to determine the rate of diffusion the molecular diffusion laws are considered with an additional effective diffusivity term which caters for the above mentioned factors. There are several equations that show how to calculate the effective diffusivity and one of them is as shown in equation 4.7-4.10 (Seader and Henley, 2006):

$$= \quad (\text{—}) \tag{4.7}$$

$$= \left(\frac{1}{\text{—}} + \frac{1}{\text{—}}\right)^{-1} \tag{4.8}$$

$$= \frac{\bar{u} d_p}{3} \tag{4.9}$$

$$\bar{u} = \left(\frac{8}{\text{——}}\right)^{0.5} \tag{4.10}$$

Where:

	Effective diffusion coefficient	(m^2/s)
	Combined diffusion coefficient	(m^2/s)
	Diffusion coefficient of solute A in solvent B	(m^2/s)
	Knudsen diffusion coefficient	(m^2/s)
ū	Mean molecular velocity	(m/s)
	Molecular mass	(g/mol)
	Absolute temperature	(K)
	Gas constant	(J/mol.K)
	Particle porosity	(-)
	Particle tortuosity	(-)

4.1.3 Chemical reaction effects

The chemical reaction process involves three steps; the adsorption of the reactant gas on the surface of the solid to form a surface complex, the chemical reaction and desorption of the gaseous products. For gas-solid reactions this type of process is referred to as chemisorption as opposed to just adsorption. This is because adsorption is of two types; physical adsorption and chemisorption. Physical adsorption involves the interaction of the gas to the solid surface by van der Waals forces which are very weak and can occur to any surface under similar conditions. Chemisorption on the other hand involves the formation of chemical bonds between the gas and the solid and a significant heat of reaction may result in the process. Chemisorption like any other chemical reaction is specific to different reactants at different reaction conditions. The expression of the rate of chemical reaction can be very complicated if all the steps involved during the reaction are to be considered because of many parameters. As a result most studies have come up with simplified rate expressions like the empirical power law giving the value of the activation energy and equilibrium expressions like the Langmuir–Hinshelwood-Hougan-Watson type showing rate of surface adsorption and desorption.

Experiments to study the controlling step can be done in a thermo gravimetric apparatus where reaction temperature, sorbent particle size and space velocity are easily varied using a single pellet. The chemical reaction step is normally more sensitive to temperature. Therefore by increasing reaction temperature the probability of chemical reaction step controlling is high but only if the increase in temperature does

not alter the structure of the solid particle (sintering) otherwise the diffusion steps resistances will take control. Particle size variation can also determine which step exhibits the highest resistance. Levenspiel (1979) gave some relationships between time and particle size (radius) to determine the rate controlling mechanism:

- If $t \alpha R^{1.5-2.0}$ then film diffusion is in control
- If $t \alpha R^{2.0}$ then ash layer diffusion is in control
- If $t \alpha R$ then chemical reaction is in control

4.2 Mathematical Models for Gas-Solid reactions

Mathematical models were developed to predict how the gas-solid reactions will proceed under varying conditions (sorbent size, temperature, space velocity) and in that way enable researchers design their experiments accordingly. In general a good model should be a close depiction of reality and can be used without too many mathematical complications (Levenspiel, 1999). A discussion of mathematical models for gas-solid reactions which are applicable to the HGD process using zinc oxide will follow. These models are based on single pellet but a model in a packed bed reactor will be outlined. Many models for gas-solid reactions have been detailed in literature but this study will restrict discussion to only two; shrinking core model and grain model. This is because these two types of models have been used extensively to describe the desulphurisation process using zinc oxide sorbent.

4.2.1 Shrinking core model

The shrinking core model developed by Kunii and Yagi (1955) assumes that the reaction occurs from the outer surface of the solid particle and proceeds with a sharp interface to the interior of the particle. As the interface moves towards the core of the particle a product layer (ash layer) is left behind and the unreacted core reduces in size. If the product formed scales off then the original size of the particle reduces otherwise it remains unchanged (Figure 4.3). Shrinking core model is based on the below assumptions (Doraiswamy and Sharma, 1984):

- The solid particle is non-porous
- The particle size remains unchanged as the reaction proceeds
- The reaction is 1st order and irreversible
- The process is isothermal
- There is equi-molar counter diffusion of gases through the outer gas film and product layer
- The reaction interface is assumed stationary at any time while the diffusion flux is calculated to find the concentration profile (Pseudo-steady state approximation)

Based on these assumptions, the steps involved in the modelling of the overall reaction and the corresponding kinetic expressions are derived below. These equations are based on the general gas-solid reaction equation 4.1.

4.2.1.1 Film diffusion controlling

When diffusion through the bulk gas surrounding the particle is rate controlling the rate of moles of disappearing per unit time for a single particle is correlated to the mass transfer coefficient by:

$$\frac{-dN_A}{} = 4\pi R^2 k \quad (\quad - C \quad) \qquad (4.11)$$

Assuming irreversible reaction, the equilibrium concentration $= 0$

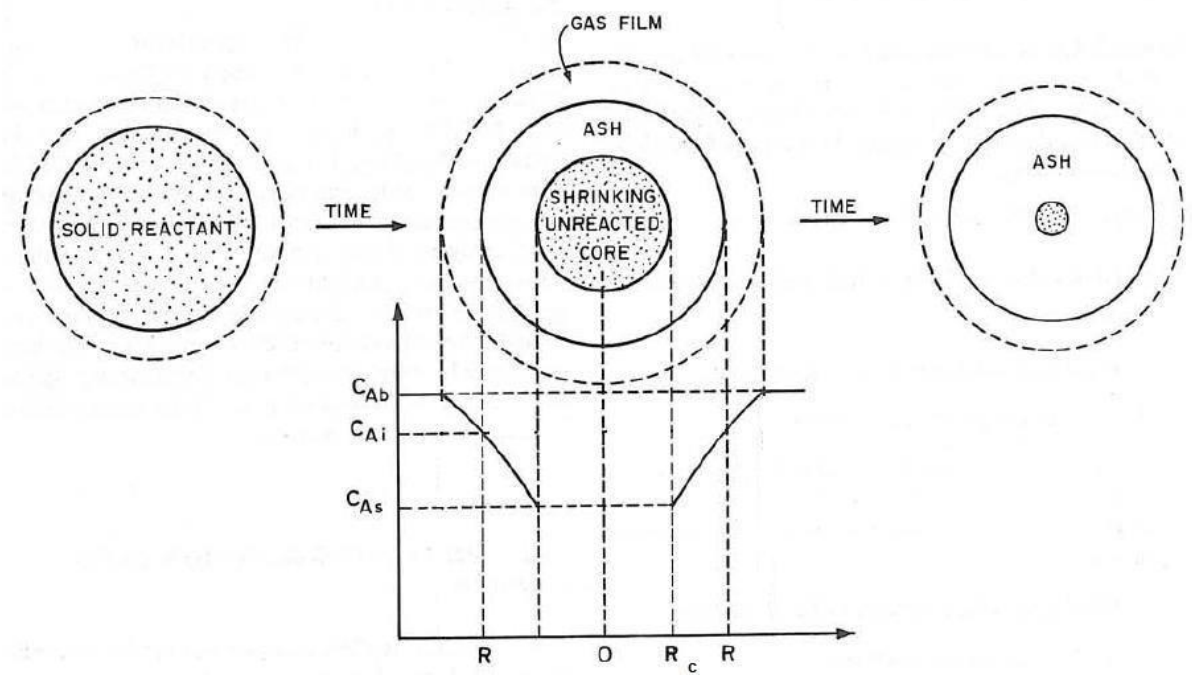

Figure 4.3 Shrinking Core Model for unchanging particle size (Doraiswamy and Sharma, 1984)

Number of moles of solid reactant present in the particle is:

$$= \qquad (4.12)$$

Where is the solid molar density of the particle and is the volume of the particle.

Disappearance of is related to the decrease in radius of the unreacted core as:

$$-dN_B = -\rho_B V_p = -\rho_B d\left(\frac{4}{3}\pi r_c^3\right) = -4\pi\rho_B r_c^2 dr_c \qquad (4.13)$$

From the stoichiometry of equation 4.1

$$-dN_B = -bdN_A \qquad (4.14)$$

Combining equations 4.11, 4.13 and 4.14 give the rate of reaction in terms of the unreacted core radius

$$\frac{-\rho\ r^2\ dr}{2} = \qquad (4.15)$$

Rearranging and integrating gives

$$= \frac{}{3}[1 - (\frac{}{R})^3] \qquad (4.16)$$

For a spherical particle the fractional conversion is given by

$$X = 1 - (\_)^3 \qquad (4.17)$$

Substituting equation 4.17 into 4.16 gives the relationship between reaction time and the fractional conversion for gas film diffusion control reaction

$$= \frac{}{3} \qquad (4.18)$$

Equation 4.18 shows a linear relationship between reaction time and fractional conversion . By plotting against we get a straight line therefore we can use this criterion to determine whether the reaction is controlled by gas film diffusion or not. The mass transfer coefficient can as well be obtained from the slope of the straight line if the other parameters are known.

4.2.1.2 Product layer diffusion controlling

When diffusion through the product layer is controlling, assuming pseudo-steady state approximation the rate of reaction of at any instant is related to the flux of , to the product layer by

$$-\frac{dN_A}{} = 4\pi R^2 J \qquad (4.19)$$

The flux through the product layer is defined by Fick's Law as

$$= \qquad (4.20)$$

Substituting equation 4.20 into 4.19, separating variables and integrating between where = and where = gives

$$-\frac{}{dt} = 4\pi D_e(C_{Ab} - C_{Ae})\left(\frac{1}{r} - \frac{1}{R}\right)^{-1} \qquad (4.21)$$

Assuming irreversible reaction and substituting equations 4.12 and 4.13 into equation 4.21 then by separating variables and integrating yields

$$= \frac{^2}{6}\left[1 - 3\left(\frac{}{R}\right)^2 + 2\left(\frac{}{}\right)^3\right] \qquad (4.22)$$

The fractional conversion depends on therefore substituting the relationship between and as shown in equation 4.17 into equation 4.22 gives the relationship between time and the fractional conversion for a reaction that is controlled by the diffusion through the product layer below

$$= \frac{^2}{6}[1 - 3(1 - X)^{2/3} + 2(1 - X)] \qquad (4.23)$$

Plotting $[1 - 3(1 - X)^{2/3} + 2(1 - X)]$ against time t would result in a straight line and thus a criterion to determine whether the diffusion through the product layer is controlling. The slope of the straight line can also be used to calculate the effective diffusivity D_e if the values of the other parameters are known. Jothimurugesan and Harrison (1990) have shown that diffusion through the product layer is the dominant resistance in HGD processes using metal oxides.

4.2.1.3 Chemical reaction controlling

When chemical reaction is rate controlling, the rate of reaction is dependent on the available surface area for reaction of the unreacted core. Assuming a first order irreversible reaction the rate of reaction of is given by

$$-\frac{dN_A}{} = 4\pi r^2 kC \qquad (4.24)$$

Where is the coefficient of chemical reaction. Substituting equations 4.12 and 4.13 into 4.24 gives

$$-\rho \frac{}{} = bkC \qquad (4.25)$$

Integrating equation 4.25 from = 0, = = = gives

$$t = \frac{}{} (R - r) \qquad (4.26)$$

Equation 4.26 can be written inform of fractional conversion to give

$$t = \frac{\rho_B}{} (1 - (1 - X)^{1/3}) \qquad (4.27)$$

This gives a relationship between time and fractional conversion for a reaction that is controlled by the chemical reaction step.

Essentially more than one resistance affects the reaction and therefore combining all the three individual resistances expressions and eliminating the intermediate concentrations gives the rate of reaction at any instant as the particle is being converted. By using the time and fractional conversion equations 4.18, 4.23 and 4.27 an expression giving the time required to reach any conversion is

$$t_{all\ resistances} = t_{film\ alone} + t_{product\ layer\ alone} + t_{chemical\ reaction\ alone} \qquad (4.28)$$

Substituting equations 4.18, 4.23 and 4.27 into 4.28 gives the time and conversion expression as

$$= \frac{}{3} + \frac{^2}{6}[1 - 3(1 - X)^{\frac{2}{3}} + 2(1 - X)] + \frac{}{}(1 - (1 - X)^{\frac{1}{3}}) \qquad (4.29)$$

And the overall rate of reaction is given by

$$-r_A = \frac{}{\frac{1}{} + \frac{(R - r_c)r_c}{} + \frac{^2}{^2}} \qquad (4.30)$$

One of the limitations of the shrinking core model is the assumption of the solid being non-porous. Therefore the structural properties of the solid are neglected. Thus when using the shrinking core model to fit experimental data for a porous solid material, the results are likely to deviate. Shen and Smith (1965) introduced a parameter to the shrinking core model for the case where the solid product layer formed does not have an equal volume to the solid reactant which will result in change of particle size. was defined as:

$$= \frac{}{} \qquad (4.31)$$

For the case of sulphidation to , can be defined as:

$$= \frac{/}{/} \qquad (4.32)$$

Where and are the densities of and respectively and and are the molar masses of and respectively.

Another limitation of the shrinking core model is the assumption that the effective diffusivity is constant within the product layer. Krishan and Sortichos (1993) showed that this is not the case in their study of limestone sulphidation with SO_2 in a TGA. They further modified the model by introducing an effective diffusivity to the product layer that is assumed to vary with distance from the external surface of the particle.

Despite these limitations some studies using the shrinking core model have been successful with good agreement between experimental data and the model predictions.

Yanxu et al., (1997) performed studies on the ZnO-H_2S reaction using the shrinking core model. The experiments were performed in a TGA at temperatures 200-400 ^{0}C. Their results indicated that at high temperatures and low conversion the chemical reaction resistance controlled the rate whereas at low temperature and high conversion the diffusion through the product layer took over. There was good agreement between experimental data and the model results.

Hepworth et al. (1997) performed hot coal gas desulphurization using Mn- based sorbents in both TGA and a packed bed reactor. They used a single pellet shrinking core model then later extrapolated it into a packed bed model. The results for both TGA and packed bed were in good agreement with the predicted values.

4.2.2 Grain Model

In the grain model the particle is assumed to be composed of many non-porous grains of equal size and shape (i.e. spherical, cylindrical and plate like). Each grain then reacts according to the shrinking core model as shown in Figure 4.4. The process involves mass transfer of the reactant gas from the bulk of the gas stream to the surface of the particle. The gas then diffuses between the grains followed by diffusion through the product layer of each grain to the surface of the unreacted core for the chemical reaction. Four steps exhibit resistance to the overall rate:

- Bulk gas diffusion resistance
- Pore diffusion resistance
- Ash layer diffusion resistance
- Chemical reaction resistance

This model is based on the following assumptions

- Pseudo steady state approximation

- Isothermal process
- Equi-molar counter diffusion
- A first order reaction with respect to the gaseous reactant concentration
- Irreversible reaction

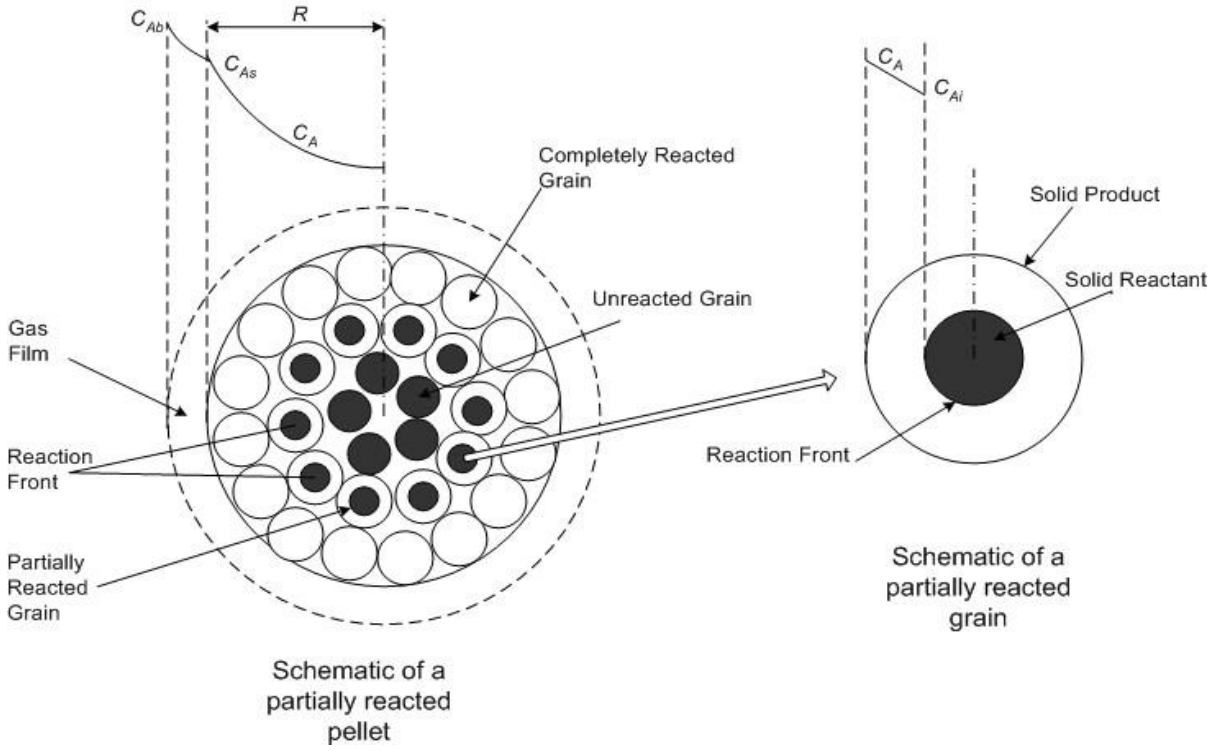

Figure 4.4 Schematic presentation of Grain Model (Zhang, 2004)

Szekely et al. (1976) came up with mathematical expressions in terms of dimensionless parameters based on the combination of conservation of the gaseous reactant and product with the solid reactant mass balance. The governing equations represented by the dimensionless parameters showed that a parameter σ similar to Thiele modulus for heterogeneous catalysis combined both the kinetic and structural properties and it measured the relative magnitude of chemical reaction and diffusion rates. It was defined as:

$$= \quad_{,0}\left[\frac{3(1-\varepsilon)k}{\quad_{,0}}\right]^{1/2} \qquad (4.33)$$

Where

,0	Original size of the pellet	(m)
,0	Original size of the grain	(m)
	Grains effective diffusivity	(m^2/s)
	Reaction coefficient	(m/s)
	Pellet porosity	(-)

By evaluating this value it was possible to determine which mechanism rate is controlling. To further simplify the solution, they came up with two asymptotic behaviour of the system:

1. When σ → 0, pore diffusion is negligible and the concentration within the pellet is uniform therefore :

$$t^{+} = 1 - (1 - X)^{\frac{1}{Fg}} \qquad (4.34)$$

Where $^{+}$ is a dimensionless time defined as:

$$^{+} = \frac{}{_{,0}} \qquad (4.35)$$

is the grain shape factor. For spheres, cylinders and flat plates are 3, 2, and 1 respectively. is similar to which is the particle shape factor.

2. When σ → ∞, the concentration driving force for the reactions drops to zero and diffusion through the product layer controls the reaction and therefore:

$$^{+} = \frac{2}{18}[1 - 3(1 - X)^{\frac{2}{3}} + 2(1 - X)] \qquad (4.36)$$

3. When both resistances are in control Szekely et al. (1976) proposed an approximate solution for time and conversion as:

$$t^{+} = 1 - (1 - X)^{\frac{1}{3}} + \frac{2}{18}[1 - 3(1 - X)^{\frac{2}{3}} + 2(1 - X) + \frac{2}{}] \qquad (4.37)$$

Where is the Sherwood number

4.3 Packed bed reactor modelling

One of the objectives of this study was to come up with a gas-solid reaction model that will predict the effect of operating conditions on the desulphurisation performance of the sorbent in a fixed bed reactor. The general shrinking core model was used because of its numerical simplicity. Fitting parameters like effective diffusivity and reaction coefficient were obtained from previous published experimental data (Jothimrugesan and Harrison, 1990). The assumptions made for the derivation of the mathematical expressions are:

- Isothermal system
- Equi-molar counter diffusion
- Plug flow system

Assuming plug flow of gas the mass balance of component is

$$\frac{}{} + \frac{}{} + = 0 \qquad (4.38)$$

For low pressure systems the second term on the left hand side can be neglected and equation 4.38 becomes

$$\frac{}{} + = 0 \qquad (4.39)$$

At

$$= 0, \quad = \ _0 \qquad (4.40)$$

Mass balance on solid reactant

$$(1 - \varepsilon)\frac{\partial C_B}{} = -br \qquad (4.41)$$

At

$$= 0, \quad = \ _0 \qquad (4.42)$$

Rate of consumption of , is defined as

$$= \frac{1}{} \qquad (4.43)$$

Relating the rate of reaction of to the rate of reaction of a single spherical particle with original size gives

$$r = \frac{3(1-\varepsilon)\, dN_A}{4^{3}} \qquad (4.44)$$

Substituting the global rate of reaction for a shrinking core model equation 4.30 in terms of conversion yields

$$= \frac{3(1-\varepsilon)C_{Ab}}{}\left[\frac{1}{} + \frac{R}{}\left((1-X)^{-1/3} - 1\right) + \frac{1}{k(1-X)^{2/3}}\right]^{-1} \qquad (4.45)$$

Substituting in equations 4.39 and 4.41 and introducing dimensionless variables gives

$$\frac{\partial C^{\star}}{\partial z^{\star}} = \frac{-r_A L}{0} \qquad (4.46)$$

$$\frac{}{\partial t^{\star}} = \frac{}{C_{A0}u} \qquad (4.47)$$

By implementing a numerical method based on Euler's forward difference for space and forward difference for time method equations 4.46 and 4.47 can be solved with the boundary conditions

$$C^{\star} = 1 \; at \; z^{\star} = 0 \; at \; all \; t^{\star} \qquad (4.48)$$

$$X = 0 \; at \;\; t^{\star} = 0 \; at \; all \;\; z^{\star} \qquad (4.49)$$

Chapter 5

EXPERIMENTAL METHODS

5.1 Experimental Design

This study involved two sets of experimental work both having specific objectives. In the production of syngas using the mixed liquid hydrocarbons fuel, the main objectives were:

- Production of syngas which contains H_2S
- Identification of the syngas composition at fixed operating conditions

The second part of the experiment which involved the HGD of the produced syngas the objectives of the experiments were:

- To study the effect of temperature variation on the desulphurization capability of ZnO
- To study the effect of sorbent size variation on the desulphurization capability of ZnO
- To study the effect of sorbent surface area variation on the desulphurization capability of ZnO
- To study the effect of gas flow rate variation on the desulphurization capability of ZnO

To establish the above HGD objectives, a plot of the concentration of H_2S with time referred to as breakthrough curve was drawn. The breakthrough time at which the H_2S concentration exiting the reactor exceeds 100ppm was noted and used to calculate the sulphur sorption capacity (Appendix B). Sulphur sorption capacity evaluates the utilization of the sorbent in the bed during sulphidation.

Thus the experimental work had to be planned accordingly to achieve the above mentioned objectives in the most economical way possible. Montgomery (2012) details the advantages of having an experimental design as:

- It improves the process yields
- Less time is used in the development of the process
- It reduces overall cost since there are less trial and error procedures
- It reduces results variations and brings closer conformance to the targeted requirements

The main aim of any experiment is to perform a series of test by performing purposeful variations of the input variables to a system and observe how they affect the output response. These input variables can be called factors that affect or can affect the output response of a system. Experimental factors can be divided into two (Montgomery 2012):

- Design factors- These are factors that are selected for study and they are easy to change during experimental work
- Held constant factors- These are factors that exert an effect on the process but are difficult to vary in an experiment

For the gasification process, the operating conditions were held constant at the chosen conditions. These fixed conditions were obtained from literature survey and used in a simulation program to identify the expected syngas composition.

For the desulphurization experiments, a 2*2 factorial design was adopted in studying the effect of temperature and sorbent size variation on the desulphurisation process at their high (550 ^{0}C and 2.03mm) and low levels (350 ^{0}C and 1.63mm). These variations of temperature and sorbent size were performed separately at high (>20m^2/g) and low surface area (5.3m^2/g) and high (3430h^{-1}) and low (610h^{-1}) average space velocity. Factorial experiment designs are very useful as opposed to one factor at a time approach which is time consuming and does not show interaction between varied factors. A factorial design involves selecting a factor and varying it at different levels and observing the response at each level. For the experiment to be complete a series of four experiments have to be performed to ensure that all combinations of the factors have been tested. For a good experiment, it is always good to randomly perform the runs to avoid systematic errors and also replicate each run many times possible depending on the cost and time available for each experiment. A 2*2 factorial design can be represented by a square and each corner of the square indicates the treatment combinations ((1), a, b and ab) obtained by varying the factors at the different levels; high (+) and low (-). Combination (a) denotes the effect of sorbent size at 2.03mm diameter and temperature at 350 ^{0}C, (b) denotes the effect of temperature at 550 ^{0}C and 1.63mm sorbent size, ab denotes effect of both sorbent size and temperature at their high levels (2.03mm and 550 ^{0}C) whereas (1) denotes the effect of both factors at their low levels (1.63mm and 350 ^{0}C) resulting in a complete design. Figure 5.1 shows a 2*2 design for the desulphurisation experiment with temperature and sorbent size varied at two levels to study their effect on the sorbent sulphur sorption capacity. The set of experiment was planned to be replicated twice and is summarised in Table 5.1.

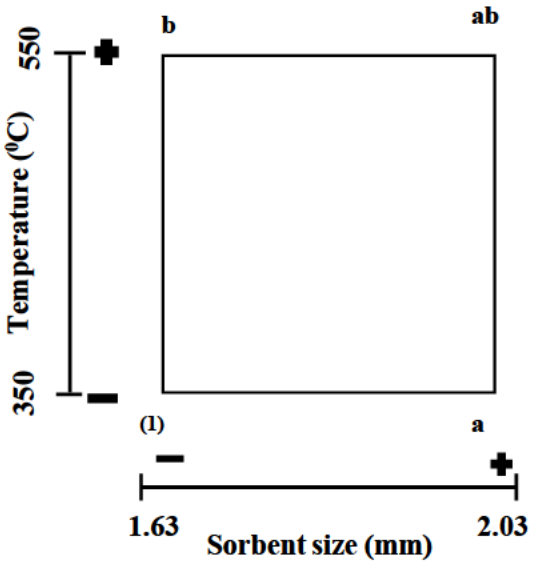

Figure 5.1 A Sketch of a 2*2 Factorial Design

Table 5.1 Summary of all the experiments in HGD

Run		**High surface area low space velocity**		**Low surface area high space velocity**		**Low surface area Low space velocity**	
	Label	**Temperature**	**Sorbent size**	**Temperature**	**Sorbent size**	**Temperature**	**Sorbent size**
1&5	(1)	-	-	-	-	-	-
2&6	a	-	+	-	+	-	+
3&7	b	+	-	+	-	+	-
4&8	ab	+	+	+	+	+	+

In a factorial design it is possible to know the overall effect or the main effect of each factor. The main effect of a factor is the change in response caused by the change in the level of that factor averaged over the levels of the other factors (Montgomery, 2012). This gives details of the magnitude and direction of each individual factor and hence knowledge of which factor is more significant and at what level consequently optimising the system. The main effect of each factor and their interaction magnitude are

calculated by equations 5.1, 5.2 and 5.3 where is the number of replicates performed (Montgomery, 2012). In this study 2 replicates were performed and the sum of the response at each combination was used to calculate the main effect. A variance analysis was performed to verify the results of the main effect calculations.

$$= \frac{1}{2}[a + ab - (1) - b] \qquad (5.1)$$

$$= \frac{1}{2}[b + ab - a - (1)] \qquad (5.2)$$

$$= \frac{1}{2}[ab + (1) - a - b] \qquad (5.3)$$

The results of the main effect and their interactions can be used to draw a surface response curve which will show the direction for optimum conditions to obtain the sorbents maximum sulphur sorption capacity. To be able to draw the surface response curve a first order regression model was developed. The model is described by equation 5.4.

$$y = \beta_o + \beta_1 x_1 + \beta_2 x_2 + \beta_{12} x_1 x_2 + \in \qquad (5.4)$$

Where

Sorbent sulphur sorption capacity %

Average of all response at all levels

1 A half of the main effect of temperature

2 A half of the main effect of sorbent size

12 A half of the interaction effect

1 Variable representing temperature

2 Variable representing sorbent size

1 2 Variable representing the interaction between the two factors

$\in$ Random error value

Denoting for temperature at any level and and for temperature at the set high and low level respectively, for sorbent size at any level and and for sorbent size at the set large and small level respectively with minimal interaction (therefore ignoring the interaction variable term $_1 _2$) $_1$ and $_2$ can be calculated from (Montgomery,2012):

$$_1 = \frac{T - (T_L + T_H)/2}{(T_H - T_L)/2} \tag{5.5}$$

$$_2 = \frac{S - (S_L + S_H)/2}{(S_H - S_L)/2} \tag{5.6}$$

5.2 Equilibrium Model Procedure

For this study Advanced System for Process Engineering (ASPEN) software package was used to model the gasification process. ASPEN does not have a gasification in-built model; therefore one of the unit operation models, the Gibbs reactor was used. The criterion as explained in Section 2.2 uses the minimisation of Gibbs free energy and makes use of equations 2.1-2.4 in the same section to predict the equilibrium composition of Syngas. This model is normally used when the reactions occurring are not known and are high in number due to many reactants reacting. The model requires complete information of (Figure 5.2):

- All the reactants and their flow rates
- All expected products
- The reactors operating temperature and pressure

The expected products were obtained from literature survey for products obtained during gasification. The operating temperature and pressure were also obtained from literature. A sensitivity analysis on the program was performed varying temperature from 0 ^{0}C to 1500 ^{0}C to obtain the optimum operating temperature for the process. Initial flow rates were obtained from Botha (2010) and were slightly changed as the composition of syngas was observed from the simulation program.

The assumptions made for using these criteria were:

- The rate of the gasification reactions are first enough and the residence time long enough to reach the equilibrium state.
- There is perfect mixing between the reactants.

- The process operates at isothermal conditions.
- The process is adiabatic.
- The gas behaves in an ideal manner (which is possible at high temperatures and low pressures).

From this model the equilibrium composition of syngas produced and the optimum reaction temperature were deduced.

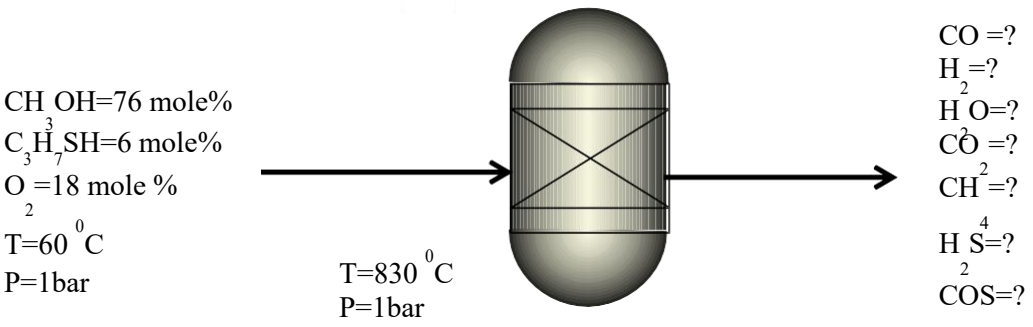

Figure 5.2 Flow diagram of the simulation process

Botha (2010) used the minimization of Gibbs free energy and Lagrange undetermined multipliers with constraint of mass balance using similar fuel mixture as the one used in this study. The results obtained in this study were compared to Botha (2010).

5.3 Equipment Description

The process of production of syngas and desulphurization were performed in two distinct set of equipment which were arranged in a manner similar to the industrial set-up. This section will describe the equipment in detail as well as the equipment used for improving the surface area of the sorbent. Figure 5.3 shows the description and flow of material for the whole experimental set-up and Figure 5.4 shows a picture of the whole equipment in the laboratory.

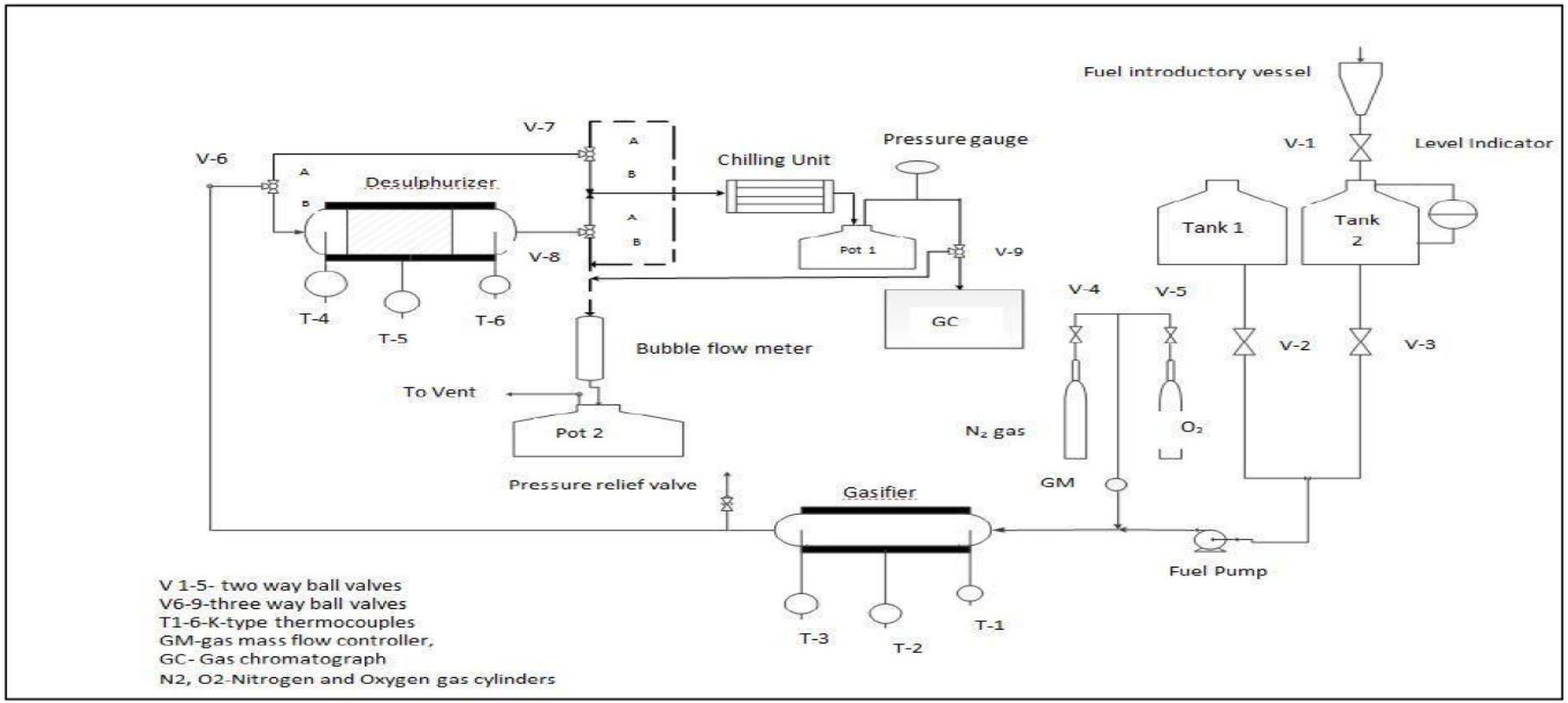

Figure 5.3 Process Flow Diagram

Figure 5.4 Equipment Lab set-up

5.3.1 Gasification process equipment description

The gasification reactor was fabricated by GM Heating (Pty) Ltd and was accompanied by its own tubular furnace. The reactor was made up of a 316 stainless steel material capable to resist H_2S corrosion. Mechanical strength was not that important since the system pressure was to be at atmospheric. The tubular reactor had an I.D. of 37mm and was 600mm long. It was slid at the centre of the ceramic furnace and was threaded on both sides to allow pipe fittings on the inlet and the outlet. Temperature inside the reactor was monitored by K-type thermocouples fitted at the inlet, centre and outlet of the reactor. The centre thermocouple was 300mm long extending up to the middle of the reactor where it was assumed that all the syngas components are formed. It was 6mm thick to withstand the high temperatures in the reactor to avoid warping. The outlet thermocouple on the other hand was 200mm long and 6mm thick as well. The centre thermocouple was connected to temperature control panel whereas the other two were connected to a temperature measuring device whose output signal was transmitted digitally to a personal computer (PC) temperature monitoring program. From literature survey and the sensitivity analysis performed during simulation of the gasification process it was agreed that a temperature of 830 ^{0}C should be set as the gasification reaction temperature. At 830 ^{0}C all of the syngas components are formed and do not vary with increase in temperature. Thus the control panel was set to measure a temperature of 830 ^{0}C and from the steady state studies of the unit it was established that the system attains steady state though after a long time. The furnace housing the gasification reactor and the inlet and outlet pipes (1/2 inch stainless steel) were thoroughly lagged using glass wool as shown in Figure **5.4** to prevent heat loss to the surrounding through convection.

The feed to the gasification reactor included liquid methanol and a liquid mixture of methanol and 2-propanethiol (fuel) with O_2 gas as oxidant. The fuel was pumped by a Watson Marlow 101U/R peristaltic pump and the flow of the gas was controlled by an Alicat Scientific gas mass flow controller (GM). The peristaltic pump had a range of 0-0.594cm^3/s and was calibrated using the fuel. The calibration curve is given in Appendix A. The GM had a maximum range of 1.024 standard litres per minute (SLPM) with a maximum oxygen flow control of 1.340g/min. An equation to calculate the amount of oxygen in SLPM was then derived using the maximum ranges of the equipment (equation 5.7). A pump was not required for oxygen since the cylinder was already under pressure controlled by a pressure regulator fixed on the gas cylinder. The cylinder was located outside the experiment set-up laboratory for safety purposes.

$$_2(\quad) = \frac{_2(\ /\ )}{1.30859} \qquad (5.7)$$

The pipes from these two pieces of equipment to the reactor were 1/4 inch 316 stainless steel pipes and before they reached the reactor entrance they were coiled around the furnace. The purpose of coiling the pipe was to use the heat transferred from the furnace to the piping's to vaporize the fuel so that there is proper mixing of the fuel and the oxidant for efficient reaction. Methanol and 2-Propanethiol have low boiling points of 64 ^{0}C and 67 ^{0}C respectively. From the equilibrium simulation it was set to work with 86 % and 14 % by mass of methanol and 2-propanethiol. These values were determined using trial and error by observing the composition of syngas during simulation the results of which will be given in chapter 6. Oxygen concentration for partial oxidation from literature was supposed to be within 5-20 mole % at constant fuel flow (Matsumoto et al., 2008). Preliminary experiments worked with oxygen concentration of 18 mole% and a fuel flow rate of 0.108cm^3/s which resulted in very high space velocity of syngas at an average of 3430 h$^{-1.}$ This brought about a low sorbent sulphur sorption capacity for this particular set up though other researchers have worked with even higher flow rates than this. It was decided to lower the fuel flow rate to 0.042cm^3/s and maintain oxygen concentration at 18 mole% which resulted in a space velocity at an average of 610h^{-1}. The difference in fuel flow rates had an effect in the composition of syngas produced because of short residence time in the gasifier. Table 5.2 shows the flows of each component in the feed at O_2 and fuel flow rates of 4.85cm^3/s and 0.042cm^3/s respectively. Prior to gasification the whole system was purged by N_2 gas in a gas cylinder and the flow was controlled by the same GM set at 0.5 SLPM until no H_2S could be detected from the gas chromatograph (GC) analysis.

Table 5.2 Feed flows at Oxygen flow of 4.85cm^3/s and fuel flow of 0.042cm^3/s

Feed	**cm^3.s^{-1}**	**g.s^{-1}**	**Moles.s^{-1} (10^{-3})**
Methanol	0.03700	0.029267	0.913395
2-propanethiol	0.00602	0.005062	0.066460
Oxygen	4.85000	0.006936	0.216730
Total	4.895	0.041265	1.242179

The feed to the gasification reactor were contained in 3 litre tanks made of PVC material. The methanol tank (Tank 1) had a removable lid whereas the fuel tank (Tank 2) was sealed completely but had an inlet hole fitted with an O-ring that connected the tank to a separatory glass funnel which was completely covered and directed towards the extractor fan to prevent the smell of 2-propanethiol from spreading to the entire building. When refilling the fuel, the glass funnel was detached from the O-ring and taken to a fume cupboard where the measuring took place. The fuel tank had a silicone pipe which acted as a side glass to show the level of the fuel. Silicone pipe was used because it is resistant to H_2S corrosion. The inlet to the peristaltic pump from the fuel tank also had a silicone pipe. The top part of the side glass pipe connected to the tank had to be opened when refilling to release the vacuum created through pumping. The purpose of having the methanol tank was for using methanol to start-up the partial oxidation process until the system attained steady state. Running the fuel could have been very costly since the price of 2-propanethiol was 25 times higher than methanol. Once the system was steady the methanol tank was closed (V-2) and the fuel tank valve opened (V-3) to start production of a H_2S containing syngas.

Syngas produced initially by-passed the desulphurisation reactor until a consistent concentration of H_2S was registered from the GC. The by-passing was made possible by the use of the three-way ball valves (V6-8) by changing position to either A or B shown in Figure 5.3. Table 5.3 shows the action taken by each valve and which path the gas was flowing.

Table 5.3 Valve positions for different actions

ACTION	V-6	V-7	V-8
Bypass desulphurisation reactor to bubble flow meter and vent	A	A	Closed
Syngas direct to GC for analysis prior desulphurisation	A	B	Closed
Syngas to desulphurisation then bubble flow meter and vent	B	Closed	B
Syngas to desulphurisation then GC analysis	B	Closed	A

The flow of syngas exiting the gasification reactor was measured by a laboratory bubble flow meter in a 50 cm^3 column before being vented. The vented gas had to first pass through a conical flask (pot 2) half-way filled with water. The purpose of the pot was to cool the gas and condense steam to prevent water from flowing back as well as significant amounts of condensate in the outlet pipes. In addition it gave a clear visual indication of gas flowing through bubbling of water in the flask.

5.3.2 Desulphurization reactor description

A Carbolite (UK) manufactured tubular furnace was used to provide heat to the reactor. The furnace had an I.D. of 38 mm and was 400 mm long. It had its own control panel where temperature could be easily varied. It had a maximum operating temperature of 1000 ^0C with a constant heating zone of 100 mm long which was sufficient to supply constant heat to the reaction bed. The furnace was cylindrical and had a hollow opening on both sides where the reactor could slide through it without getting stuck. The desulphurization reactor used was fabricated in the UKZN workshop. The reactor was made up of a 316 stainless steel pipe which could withstand the corrosive nature of H_2S. It had an I.D. of 27 mm and was 400 mm long to fit well in the furnace. The pressure through the system was atmospheric and therefore mechanical strength of the reactor was not very important. The tubular reactor was threaded on the inlet side where a socket could be fit to provide the gas seal and connection to the inlet pipe. Similar work was done on the outlet side to provide connection fittings to the exit pipe. The inlet socket had three connections on it. The gas inlet fitting, the gas sampling fitting, the inlet K-type thermocouple and a 200 mm long and 6 mm thick K- type thermocouple which ran co-axially inside the reactor tube to measure the temperature of the reaction bed. Figure 5.5 shows a cross section of the inlet socket with its fittings.

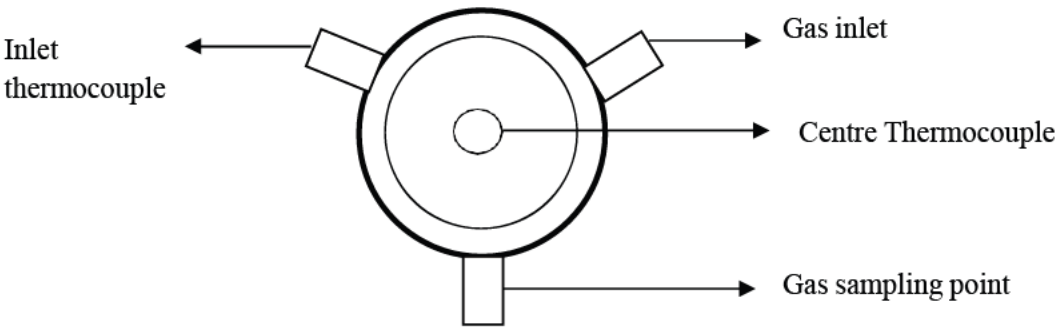

Figure 5.5 Cross-section of the inlet socket

The sorbent bed inside the reactor had to be fixed to prevent channeling of the gas flow and have a defined reaction front. The bed was created by fitting an adjustable mesh grid on to the center thermocouple extending inside the reactor bed. The mesh grid had the following properties:

- The mesh was big enough to prevent pressure build up inside the reactor and smaller than the largest particle to prevent sorbent slip
- Fit well inside the reactor to prevent sorbent slip
- Resistant to H_2S corrosion and non-reactive with the other components of syngas and the sorbent
- Maintain its shape under the high temperature environment

Since the reactor was horizontal a spacer was fitted on the lower side of the bed and another filter with similar properties like the mesh grid was placed on it to hold the sorbent. Previous studies on HGD had a short spacer and from the preliminary results it was evident that the bed was not fixed due to inconsistent results during desulphurization. Another spacer was fabricated and added to rise up the bed and provide a completely packed fixed bed. Another fixed bed was created on the thermocouple by having another adjustable mesh fitted on it. This bed supported the 20 mm diameter glass beads that were used as a filter trap for any particulate matter coming from the gasifier. Figure 5.6 shows a pictorial of the reactor tube, the inlet socket with its fittings, the center thermocouple with the two adjustable mesh grids, the two spacers and the filter of the lower side of the bed.

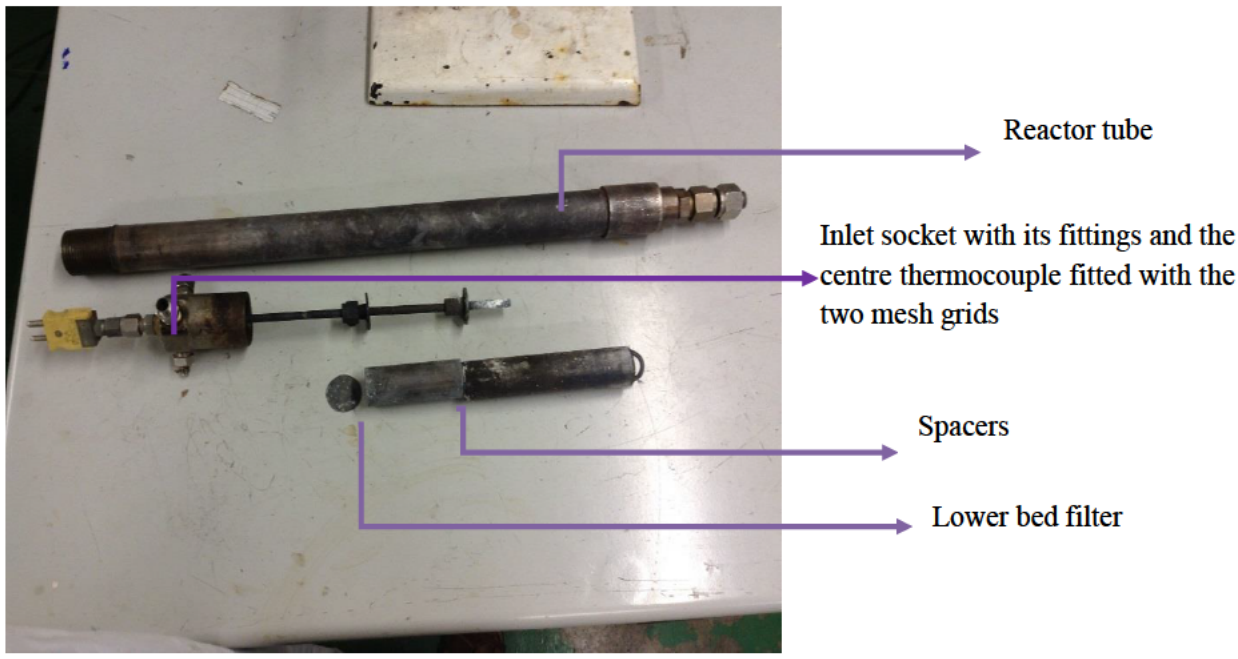

Figure 5.6 Desulphurisation Reactor and its fittings

Pressure drop across the packed reactor was calculated using Ergun equation adopted from Szekely et al. (1976) using both the large and small particle sizes and was very negligible. The pressure obtained was 0.028Pa and 0.264 Pa for large and small sizes respectively. Further details on the calculation and parameters used are in Appendix B. To ensure there were no side wall effects the ratio of the reactor diameter to the particle diameter had to be > 10. Therefore the choice of particle sizes had to be chosen wisely to comply with this requirement. Details of obtaining the particle diameter are given in section 5.4.2. The average sizes obtained were 2.06 mm and 1.63 mm for large and small particles respectively. If D is the reactor diameter (27 mm) and d_p the particles diameter the ratio D/d_p obtained was 13.1 and 16.5 for large and small particles respectively which were all > 10. Similar to gasification process the gas flow was measured by the bubble flow meter before being vented out through pot 1.

5.3.3 Gas Sampling and Analysis Equipment Description

To determine the concentration of H_2S produced and removed as well as the composition of syngas, Shimadzu GC 2014 and Shimadzu GC 2010 were used respectively. Shimadzu GC 2014 was equipped with a Flame photometric detector (FPD), Inertcap 5MS/NP capillary column of length 30m, I.D. of 0.25mm with a wall thickness of 0.25µm. Helium gas was used as the carrier gas and Hydrogen and Air Zero were reference gases. These gases had to be pure because any impurity like hydrocarbons can react with the columns stationery phase and cause poor separation. For optimum separation and good response, the GC pressure gauges for Hydrogen and Air zero were set at 100 kPa and 40 kPa respectively. Helium was also used as a make-up gas and was set at a pressure of

18 kPa to increase the flow of gas across the detector. Therefore the pressure of gas flowing from the cylinders had to be regulated by fitting high quality gas cylinder regulators. The split mode was used to avoid the production of broad and tailing peaks due to high concentration of H_2S in syngas. It entails the mixing of the hot sample with the carrier gas which are then divided into two streams depending on the split ratio. One stream enters the column (carrier gas flow) and the other is vented out (split flow). Normal split ratios range from 1:20 and 1:200 (Colin, 2003).The advantages of split mode include (Colin, 2003):

- It is independent on the solvent used for sample
- It is independent on the column temperature
- Does not cause problems like band broadening due to slow sample transfer from the injector to the column

FPD detector was chosen because of its selective and sensitive properties towards sulphur and phosphorous compounds. It can detect sulphur and phosphorous containing compounds at very low concentrations of up to 200ppb and 10ppb respectively with a maximum detection for sulphur compounds of up to 10000ppm. It can also detect some metals like tin, boron and arsenic. The operating conditions of the GC are shown in Table 5.4.

Table 5.4 GC fitted with FPD detector operating conditions

Injection Temperature	^{0} C	200.00	
Carrier gas	Helium		
Carrier gas Pressure	kPa	132.00	
Total Flow	ml/min	179.50	
Split Ratio	-	1:90	
Detector Temperature	^{0} C	250.00	
OvenTemperature Program	**Isothermal**		
	Rate(^{0}C/min)	Temperature (^{0}C)	Hold Time (min)
	-	40.00	2.00

This particular GC was connected to the experimental set-up and sampling was done on-line through the sampling valve (V-9). V-9, a rotary valve with 6 ports and an external sample loop of 1ml was operated manually by switching the position of the valve to either position A or B as

shown in Figure 5.7. In position A the sample from the experiment accumulates in the 1ml ±0.05 loop and the excess vented out through V-8. This takes about 5 sec and the valve is switched to position B where the carrier gas sweeps away the entire sample in the loop and send it to the GC for analysis. The pressure of the sample in the loop was given by the pressure gauge located prior to the valve; whereas the temperature of the gas was given by the temperature recorded on the chiller temperature control panel. The gas had to be passed through the chiller to condense any steam and cool the gas before accumulating in the sample loop. Cooling the gas was essential since a high temperature sample can evaporate the stationery phase of the column whereas the presence of water in the sample would lower the sensitivity of the detector as well as decrease column life. The condensed steam was collected in a knock out pot (pot 1).The sample valve and the GC were connected by a thin stainless steel capillary tubing which was chemically inert.

Figure 5.7 V-9 Sampling positions (Valco Instruments Co. Inc, 2009)

It was not possible to detect and quantify the other components of syngas using the GC connected to the set-up because FPD was a selective detector for only sulfur and phosphorous compounds. Therefore to analyze the composition of syngas a Shimadzu 2010 GC fitted with a thermal conductivity detector (TCD) and a packed CARBOXEN 1000 column of 4.6m in length, an I.D. of 2mm with a film thickness of 0.5µm was used. TCD is a universal detector that responds to the difference between the conductivity of the pure carrier gas and the carrier gas containing sample (Colin, 2003). The operating conditions of the GC are shown in Table 5.5. The commonly used carrier gases are Hydrogen and Helium because of their low molecular weight and high thermal conductivity thus increasing the detector response (Colin, 2003). For this particular GC analysis was done by drawing samples from the experiment sampling points using a gas tight syringe with a valve mechanism to close the passage way. The capacity of the syringe was 1ml ± 0.05 similar to the sample loop of the GC fitted with FPD for consistency. The sample was then injected into the

injector port of the GC through a silicone rubber septum into a glass liner and carried away by the carrier gas to the column for separation.

Table 5.5 Operating conditions of GC fitted with a TCD detector

Injection Temperature	^{0} C	250.00	
Carrier gas	Helium		
Carrier gas flow	ml/min	30.00	
Detector temperature	^{0} C	300.00	
OvenTemperature Program	**Programmed**		
	Rate(^{0}C/min)	Temperature (^{0}C)	Hold Time (min)
	0	35.00	5.00
	20	225.00	5.00
Total run time			19.50

5.3.4 Surface area improvement equipment description

Among the factors that were being studied in desulphurisation process was the effect of varying sorbent surface area to the sorbent sulphur sorption capacity. A process adapted from Robison (1987) was used but customized according to the available equipment. It involved chemical treatment of the low surface area (bulk) by increasing its moisture content then reacting it with CO_2 in a packed bed reactor to form basic Zinc Carbonate ($Zn_5(CO_3)_2(OH)_2$). This was followed by an oxidation process to decompose the basic zinc carbonate back to using compressed air. Figure 5.8 and 5.9 show the process flow diagrams for both carbonation and oxidation processes respectively.

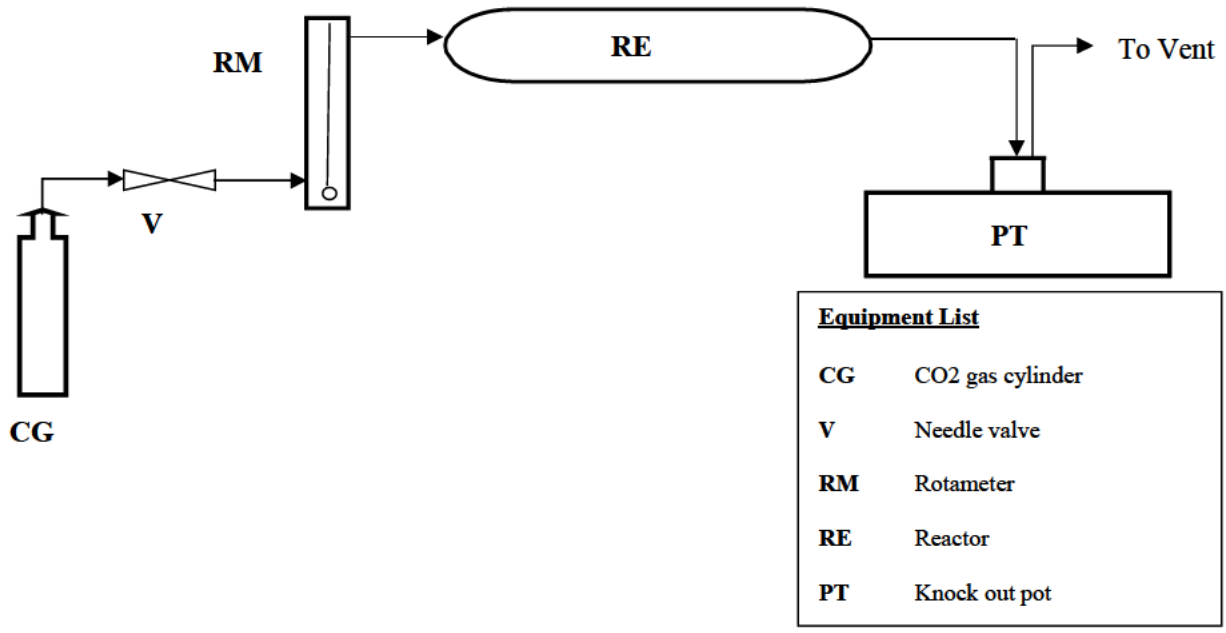

Figure 5.8 Flow diagram of Carbonation process

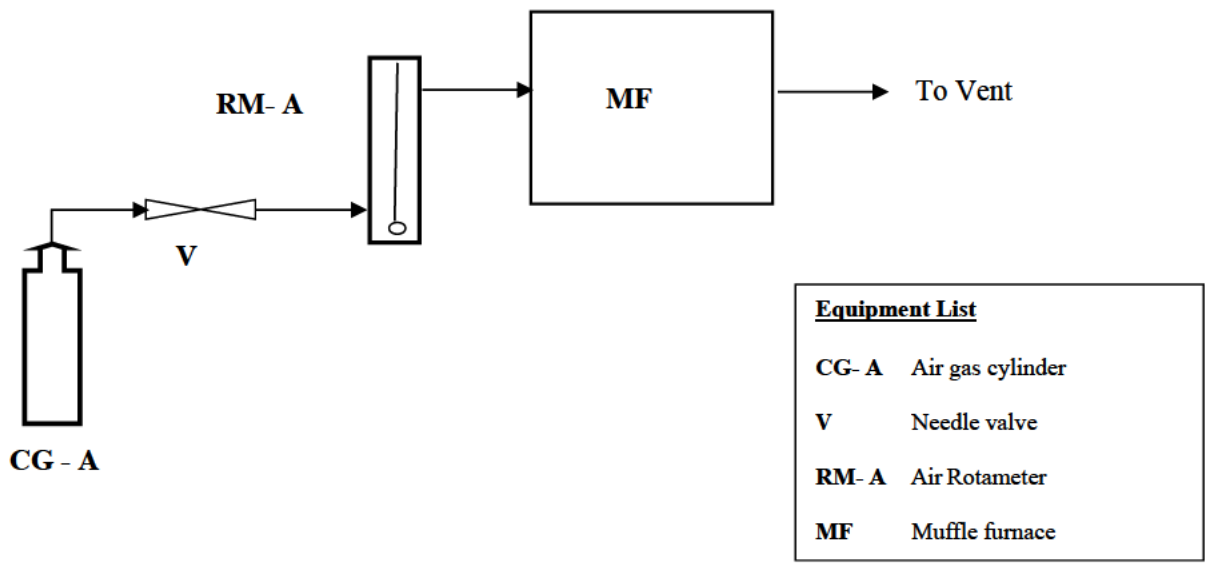

Figure 5.9 Flow Diagram of Oxidation Process

During carbonation the reactor that was used is the same as the one used for the desulphurisation process only that in this case no glass bead bed was created. The advantage of using this reactor was that the length of the sorbent bed could be increased by adjusting the top mesh grid attached to the centre thermocouple therefore more sorbent could be treated. In addition the reactor had its own furnace to provide the heat required for the process and was set to operate at 65 ^{0}C ± 5 ^{0}C. The temperature of the bed was monitored from the PC temperature program and the sensing devices were the K-type thermocouple located at the inlet, centre and outlet of the reactor. The flow of CO_2

gas entering the reactor was measured by a rotameter (RM) by adjusting the needle valve (V) to ensure that the bobbing ball position is at 4liters/min. The rotameter was calibrated using CO_2 gas prior the experiment and the calibration curve is given in Appendix A. CO_2 gas came from a gas cylinder whose pressure was regulated by a gas regulator and the gauge pressure was set at 5 kPa.

In decomposition process, the sorbent which had been carbonated was placed in a ceramic tray and placed inside a muffle furnace. A muffle furnace is a kind of furnace where the heating element is insulated by a material which muffles the heat and thus does not come into direct contact with the materials to be heated. The transfer of heat inside the chamber to the material to be heated is through radiation. The volatiles released from the heating process are vented out through a hole inside the furnace or by slightly opening the doors of the furnace to a level which will not interfere with the furnace set temperature. It also has an inlet hole where the compressed air flowing at 2liters/min measured by the rotameter (RM-A) was admitted. The furnace had its own digital temperature control panel where the temperature could be set. The process was operating at a temperature of 330 ^{0}C ± 5 ^{0}C.

5.4 Experimental Procedures

5.4.1 Gas Analysis

The produced syngas composition and the level of desulphurisation of H_2S in the syngas with time had to be established. The most appropriate way of performing this analysis was through gas chromatography. As was described in section 5.3.3 Shimadzu GC 2014 and 2010 were used for this purpose. In gas chromatography it is possible to identify and quantify a component by performing qualitative and quantitative analysis. In qualitative analysis, pure samples of the component expected to be in the gas mixture of unknown composition are injected into the GC and the time they exit from the column is noted. This time is called the retention time. Retention time is what is used to identify a particular component of a gas in a gas mixture. Each component in the mixture has its own retention time depending on the interaction between the stationery phase of the column and the component itself. The components that are more soluble with the stationery phase take more time to be eluted and thus have long retention times and vice versa. Therefore it is critical to select a column that has good interaction between the sample and the stationery phase for good separation. Separation is also dependent on the GC operating conditions thus all the parameters like temperature, flows and pressures must be set accordingly.

The syngas produced was expected to contain CH_4, H_2, CO_2, CO, H_2O and H_2S. To identify these gases a qualitative analysis had to be performed. Pure gas cylinders of all these gases were procured from AFROX. The purity of each gas is given in Table 5.7. The gas cylinders were fit with gas

sampling fittings and gas was then drawn by injecting the syringe on a septum. The gas samples in the syringe were then injected to the GC manually and the retention times were noted.

Table 5.6 Purity of the gases used for qualitative analysis.

Gas	**Purity (%)**
Methane (CH_4)	99.50
Hydrogen (H_2)	99.50
Carbon Dioxide (CO_2)	99.00
Carbon Monoxide (CO)	99.30
Hydrogen Sulphide (H_2S)	5.00 (95 % N_2)

The identification of H_2S was done on both GCs but the other components analysis was done on the GC fitted with TCD. Water detection on the GC fitted with FPD was not possible because all the water expected to be produced was condensed by the chiller prior GC analysis. For the TCD analysis water was expected to be present but identification using GC was not performed. The composition of water was done gravimetrically by weighing Pot 1 prior start of experiment then weighing it again at the end of the experiment to note the mass of water collected. This was then converted to moles assuming ideal gas law. The retention times for all the gases analysed qualitatively are given in chapter 6.

The next procedure was to quantify the gases by performing a quantitative analysis. A GC responds by yielding a peak area that is proportional to the amount of sample injected as shown in equation 5.8 (Raal and Mühlbaeur, 1998):

$$= \qquad (5.8)$$

Where

Response factor

No of moles of component *i*

Peak Area of component *i*

Therefore to be able to come up with a complete method of quantification calibration procedures had to be established. This was done by obtaining a relationship (calibration curve) between the peak areas of a known quantity of a substance which is then used to estimate the amount of that

substance in a sample of unknown concentration. This method of calibration is known as the absolute method. To perform the calibration, a concentration range of calibration standards is prepared based on the expected range of the substance in the sample of unknown concentration. The standards are then injected into the GC and the corresponding peak areas noted. A plot of the peak area against the standard concentration gives the calibration curve. It is always advisable not to try to extrapolate quantities beyond the calibration range especially if the calibration curve is non-linear (since it is not always linear). When injecting same volumes of a standard into the GC, it is not possible to obtain the exact same peak areas, for this reason it is good to work with area ratios to correct for the differences (Raal and Mühlbaeur, 1998):

$$\frac{x_i}{x_j} = \frac{x_i}{x_j} = \frac{x_i}{x_j} \quad (5.9)$$

Where:

Mole fraction

, Any pair of components in a mixture

An alternative to the absolute method of GC calibration described above is the internal standard method. In this method a constant amount of a substance is added to the sample before analysis. For example in equation 5.9 component *j* could be the standard with constant amount and the area ratios between the standard and the substance of unknown concentration are used to construct the calibration curve. This process is more advantageous since it caters for any variability in the injection volume and it is mostly used in gas-liquid chromatography. Generally, for accurate calibrations the flow rates, temperature, injection method, split ratios and all other parameters that affect the response of the GC must be consistent and stable throughout the calibration process.

For this study the absolute method was adapted and samples were injected manually using a gas tight syringe. Since there would be some errors associated with the injected volume, the same sample was injected three times in a random manner and the response observed. The random injection was beneficial because the responses obtained had very minimal deviations.

The range of calibration for each gas to be quantified was based on the expected percentage mole fractions obtained from the equilibrium simulation. To obtain the volume of standards to be injected the following assumptions were made:

- The gas behaves in an ideal manner.
- The sample during calibration and experimentation is at room temperature.
- The pressure of the sample during calibration and experimentation is at 1 atmosphere.

During experimentation the amount of sample to be analysed was set to be 1ml which was the capacity of the sample loop. Therefore the number of moles in 1ml was calculated for each gas. For CH_4, H_2, CO and CO_2 the compressibility factor *Z* was included into the ideal gas equation and were obtained from tables at 25 ^{0}C and 1atm pressure (Perry and Green, 1999). To obtain the exact number of moles in the 1ml volume for the specific gases, the value of the number of moles in 1 ml was multiplied by the purity of each gas. Once this was calculated the specific volume for each standard within the range could be calculated. These volumes were then injected to the GC and the peak areas obtained were plotted against the corresponding mole fractions to obtain the calibration curves. The calibration curves for all the gases are given in Appendix A. Table 5.8 shows the parameters used for each individual gas to come up with the calibration standards. Table 5.9 shows an example of H_2 calibration standard volumes used. For the rest of the gases their calibration standards are given in Appendix A. When performing H_2S calibrations, limitations of the minimum volume were experienced because of the capacity of the syringes available. Fortunately the response at low concentrations was linear and thus extrapolation could be performed.

Table 5.7 Parameters used during GC calibration

Component	***Z*(25^{0}C,1atm)**	**Expected Mole fraction (%)**	**Calibration range Mole fraction (%)**	**Volume in 1 mole (litre)**	**Exact Moles In 1ml (µmoles)**
H_2	1.0005	61.57	0 – 100	24.478	40.6487
CO	0.9997	32.78	0 – 50	24.458	40.5994
CO_2	0.9949	0.68	0 – 1.0	24.341	40.6712
CH_4	0.9982	1.81	0 – 2.5	24.422	40.7453
H_2S	1.0000	2.03	0 – 2.2	24.470	2.04330

Table 5.8 H_2 calibration standards

Sample	% Mole Fraction	Exact Moles (µmoles)	*Volume injected (ml)
1	0	0.0000	0.0
2	20	8.1297	0.2
3	40	16.2595	0.4
4	60	24.3892	0.6
5	80	32.5190	0.8
6	100	40. 6487	1.0

* Value rounded off to accommodate syringe calibrations

5.4.2 Sorbent Preparation

Spherical pellets of zinc oxide (99.5 mass % purity) were procured from M.R. Zinc Oxide (Pty) Ltd in a 25 kg bag of varying sizes. To have sorbents of different sizes, screens were used to perform the separation. It was decided to work with size ranges of 1180 – 1700 µm and 1700 – 2000 µm. Once separated the bulk density and average geometric particle diameters from each class was measured. The bulk density was measured by using a vial of 21.6 mm in diameter and 76mm in height. The weight of the empty vial was measured and recorded. The sorbents were then densely packed into the vial by shaking down the container with the particles until full and the weight of the vial with the particles was measured and recorded. By calculating the volume of the vial and dividing the mass of the sorbent the bulk density was obtained. This process was done three times for each class and a mean of the bulk densities recorded. To measure the average particle diameters of sorbent in each class, 30 particles from each class were randomly picked and using Vernier calliper under magnifying glass the diameter was measured. This process was repeated three times randomly for each class and a mean was taken.

5.4.3 Preparation of the high surface area sorbent

The criteria behind this method was that it is possible to prepare an active or a highly dispersed sorbent without a binder by partially converting the parent material to its basic carbonate and thermally decomposing it back by evolution of a volatile material (Robinson, 1978). The high surface area sorbent was thus prepared from some of the separated above. For effective conversion to basic zinc carbonate the moisture content of the bulk prior carbonation had to be above 15 %. Other factors that affect the conversion to basic zinc carbonate include the initial bulk density (the conversion is inversely proportional to the bulk density) and its

porosity. For this study there was no much control over the latter two factors since the used was procured and not synthesized in the lab. The sorbents moisture content was measured using a moisture analyser in the laboratory prior manually spraying it with water to increase the moisture content. The process of increasing the moisture content was to be in such a manner that the physical nature of the sorbent is not impaired. After increasing the moisture the sorbent was weighed and the mass recorded. This was essential for calculating the conversion to basic zinc carbonate once carbonation was done. Calculating the conversion based on mass was possible since was the limiting reactant in the reaction (equation 5.10). To achieve a surface area of above 20 m^2/g, the conversion was to be above 20 %. The sorbent was then packed into the reactor and the temperature on the furnace set to 65 ^{0}C. The reaction temperature was monitored from the PC temperature software. Once it reached the set point, CO_2 gas was allowed to flow for 3 hours. After 3 hours, the CO_2 flow was stopped, the furnace switched off and the reactor opened to remove the sorbent which was then weighed and the conversion calculated according to equation 5.11.

$$5ZnO + 2CO_2 + 3H_2O \rightarrow Zn_5(CO_3)_2(OH)_6 \qquad (5.10)$$

$$= \frac{W_t - W_0}{0.349W_0} \qquad (5.11)$$

Where:

	Conversion at time t	(-)
	Weight of sorbent at time t	(g)
0	Initial Weight of sorbent	(g)

As carbonation continued the muffle furnace was turned on to hasten the process. The temperature was set to 330 ^{0}C and left to reach the set point. This temperature was neither to exceed 350 ^{0}C otherwise it will affect the surface area and the physical nature of the sorbent nor be below 300 ^{0}C due to incomplete decomposition. After carbonation and once the muffle furnace was ready, the carbonated sorbents were weighed again and then poured on a ceramic tray and placed inside the muffle furnace for decomposition. Compressed air was allowed to flow at a rate of 2 litres/min and the process allowed to run for 2 hours. At the end of 2 hours the air flow was stopped and the tray removed from the furnace safely by wearing heat resistant gloves. The tray was left in open air for some time to cool and then finally weighed and its bulk density measured. The weighing of before and after oxidation was done to observe any weight loss which was expected to occur since

has an approximately 7 times lower molecular weight than the basic zinc carbonate. The bulk density of the now active ZnO was expected to increase by 5 – 15 % more than the parent ZnO.

5.4.4 Sorbent Characterisation

5.4.4.1 Brunnauer – Emmet – Teller (BET) Surface area and Pore volume measurements

Micrometric TriStar II 3020 Surface area and porosity equipment in the School of Physics and Chemistry Westville campus UKZN was used to determine the BET surface area, pore size distribution, adsorption isotherm and pore volume of the fresh sorbents. Nitrogen gas at 77 K was used as the adsorptive. The sorbents were initially degassed using N_2 for 1 hour at 90 ^{0}C then the temperature was ramped up to 200 ^{0}C and was held there for 12 hours.

5.4.4.2 Field Emission Scanning Electron Microscopy / Energy Dispersive X-ray spectroscopy (FESEM/EDX)

A Zeiss ULTRA PLUS FESEM/EDX Oxford system using AZTEC software from the Microscopy Unit in Westville campus UKZN was used to characterise the surface morphology and spatial elemental composition of the fresh and spent sorbents. The sorbents were crushed to powder and poured on to a specimen nut coated with a double tape which enabled the sample to stick on it. The nut was then placed in POLARON SC500 for gold coating for 8- 10 minutes and the sample was analysed.

5.4.4.3 Transmission Electron Microscopy (TEM)

A JEOL 1010 TEM from the Microscopy Unit in Westville campus UKZN was used to analyse the particles morphology and their size for both fresh and spent sorbents. The samples were crushed into very fine powder and about 1 g was put in a plastic vial and was filled with ethanol. The vial was then covered tightly and placed in an ultrasonic bath for 10 – 15 minutes to disperse all the particles. A drop of the solution was then placed on a copper grid coated with carbon and left to dry before analysis.

5.4.5 Fuel Preparation

To maintain the 86 mass % and 14 mass% of methanol and 2- propanethiol respectively, these two liquid hydrocarbons had to be weighed. The separatory glass funnel attached to the fuel tank was removed and taken to the analytical lab where measurement was done under a fume hood. Using a weighing balance 615 g of methanol and 100 g of 2-propanethiol were weighed and mixed together to make up a 715 g mixture of fuel. Another clean beaker was used to weigh 100 g of methanol which was poured into the methanol tank. This methanol was used during start-up of the process.

5.4.6 Procedure for Production of Syngas and Desulphurisation

Loading the desulphurisation reactor

Depending on the design combination (small or large particles of either low or high surface area) to be experimented:

- Using a mass balance 30g of the sorbent was weighed into a beaker carefully to prevent sorbent disintegration.
- The desulphurisation reactor tube and the spacers were cleaned to remove any carbon deposits.
- The two spacers were then returned back into the reactor tube and the mesh at the bottom of the bed put back to its position.
- The weighed sorbent was poured into the reactor tube, and a torch was used to check the condition of the sorbents inside the tube.
- An anti-seize grease was applied on the inlet threads of the reactor tube before screwing the socket holding the centre thermocouple for ease of opening the reactor during off-loading of the sorbents.
- Before completely screwing the socket to the tube, the socket was fitted half-way into the reactor tube that is the bottom mesh grid attached to the thermocouple was completely inside the tube and the top mesh grid outside the tube. This was to enable the glass beads to be filled between the two mesh grids.
- Once the beads completely filled the space between the two mesh grids the socket was lowered down the tube carefully and tightly screwed.
- The loaded reactor tube was then brought into horizontal position and slid into the furnace.
- Anti-seize grease was applied on the reactor outlet tube threads and screwed onto the outlet of the system.
- The inlet of the desulphurisation reactor was finally reconnected to the outlet of the gasification reactor.

Production and desulphurisation process

- The gasifier was switched on and temperature was set to 830 ^{0}C. This process took about 3 hours for the set temperature to be attained.
- Once the gasifier reached the set temperature, the GM was switched on and the flow was set to control N_2 gas at 0.5SLPM.
- The N_2 gas cylinder was opened and the gas was allowed to pass through the gasifier bypassing the desulphurisation reactor and vented out.

- The purging process was left to run for 1 - 2 hours and at this time the desulphurisation reactor was loaded.
- Once the reactor was loaded, its furnace was switched on to either 350 or 550 ^{0}C depending on which design combination was being experimented.
- The GC was turned on ready for analysis.
- The chiller was also turned on to cool any gas sent to the GC.
- After 2 hours of gasifier purge with the bypass still on, a sample was sent to the GC, to test if there are any H_2S peaks. If there were peaks, purging was left to continue until there were no more peaks detected.
- Once the gasifier was clean (no sulphurous compounds detected) the N_2 gas was directed to purge the desulphurisation reactor by switching the bypass. No peak was expected to be detected when doing analysis of the gas exiting the desulphurisation reactor
- The N_2 gas cylinder was closed and the N_2 valve turned off.
- The O_2 valve was then opened and the GM set to control the flow at 4.85cm^3/s (0.291SLPM).
- The peristaltic pump was switched on and set at 0.042cm^3/s (7 rpm).
- The methanol tank outlet valve was opened and allowed to flow to the gasifier to react with the opened O_2 gas.
- This was allowed to go on until the system attained steady state (indicated on the PC temperature log and the temperature control panel for the gasifier). The process took about 15-30minutes.
- Once steady state was attained the methanol valve was closed, and the bypass to the desulphurisation reactor turned on to ensure the gas produced does not go to the reactor. The methanol valve must be closed first before the fuel pump opened to avoid mixing of the pure methanol and the fuel through backflow.
- Fuel valve was opened and fuel allowed to flow to the gasifier to react with O_2 and produce H_2S containing syngas.
- Gasification proceeded and after 30 minutes the first sample was sent to the GC for analysis.
- The 2nd sample was taken after 10minutes and their concentration compared for consistency. If the concentration of H_2S was not consistent sampling of the syngas continued until consistency was reached.
- Once consistency was established the bypass was turned off and syngas allowed to flow to the desulphurisation reactor and the time onset of this process was noted down.
- Sampling of the gas exiting the desulphurisation reactor was done after every 5 minutes until when the exit H_2S concentration exceeded 100ppm which was set as the breakthrough

concentration and the time was also noted. 100 ppm was chosen since it is the limit required for sulphurous compounds in syngas to be used in IGCC.

- Samples of the syngas produced were drawn at the sampling point located on the desulphurisation reactor socket using a 1 ml gas tight syringe and injected into the GC fitted with the TCD after every 30 minutes from the onset of desulphurisation to analyse the composition. This continued until the end of desulphurisation process.
- From the onset of gasification process gas flow was measured by the bubble flow meter after every 30 minutes until the end of the process.
- Pressure measurements were also recorded from the pressure gauge after every 30 minutes together with the chiller temperature.
- Once the breakthrough concentration was exceeded, the flow was switched back to bypass and the desulphurisation furnace turned off.
- 3 more samples from the gasifier were sent to the GC for analysis after 10 minutes interval to compare their consistency with the initial concentration.
- Thereafter the fuel valve was closed and the methanol valve opened for about 1 hour to flash out the remaining fuel which contained 2-propanethiol.
- The peak areas from the GC were exported to an excel sheet for concentration calculations using the calibration curve and a breakthrough curve for the experiment was plotted.
- The GC was then shut down accordingly.
- After 1 hour, the methanol valve was switched off, the O_2 gas cylinder closed, the chiller, pump, gasifier and GM turned off.
- Once the desulphurisation reactor had cooled down, it was unthreaded from the pipe fittings and the reactor was pulled out.
- The socket was unscrewed slowly pulling out the centre thermocouple and the glass beads collected in a beaker.
- The reactor was then lowered gently to pour out the sorbent into a beaker.
- A torch was used to inspect inside of the tube to see whether there were any sorbent trapped inside.
- The sorbent was then finally weighed.
- The reactor was cleaned using soapy water and a cleaning brush to remove any carbon deposit layer on the reactor tube walls.

5.5 Equipment and Process Safety

These study involved the use of raw materials, process conditions and products which were sources of hazard and therefore for the safety of the research proper measures had to be put in place. Table 5.10 and 5.11 give details of the hazardous raw material, products and process conditions and the

measures taken to prevent the hazard. Some of the information was taken from manufacturer material safety data sheet (MSDS) and Perry and Green (1999).

Table 5.9 Process condition related hazards and precaution

Condition	**Hazard**	**Precaution**
High temperature	Cause a burn when in direct contact Cause fire when in contact with flammable material Backflow of hot gas	All surfaces which were hot were insulated using glass wool material. Loose material when working in the lab was prohibited. Non- return valves were installed on the fuel and gas feed lines.
Pressure	Cause explosion	A pressure relief valve was installed after the gasifier that released pressure beyond 3 bar
Pipe fittings and Connections	Create pressure build up and ultimately cause an explosion Source of leakages	There were no many bend corners on piping's and the connections were NPT type to prevent leakages

Table 5.10 Raw material related hazards and prevention measures

Material	Nature of Hazard	Hazard	Precaution
Methanol	Toxic & Flammable Liquid	Cause fire when in contact with heat source. Damages skin when in contact with liquid.	The methanol piping was leak free. Safety gloves were worn when handling it
2- Propanethiol	Toxic & Flammable Liquid	Cause fire when in contact with heat source. Cause eye irritation and bad odour	The piping was leak free and no heat source around Safety gloves, gas mask and goggles were worn
Oxygen gas	Flammable & Explosive	Explosion since it's under high pressure. Can cause and enhance fire.	Proper pressure regulators were fitted. Kept outside the lab.
Hydrogen gas	Flammable & Explosive	Cause fire and explosion	Proper pressure regulators were fitted. Lab was well ventilated
Hydrogen sulphide	Flammable, Explosive & Toxic	Cause fire and explode since its under pressure Cause unconsciousness if inhaled. Limits include not more than 50ppm for 10 minutes	Proper pressure regulators were fitted Safety gloves, respirator and goggles were worn System was leak free. H_2S produced was diluted before venting out Lab was well ventilated
Carbon monoxide	Toxic & Explosive	Cause anoxia when inhaled for long times at 50 ppm concentration Can explode	Safety gloves, respirator and goggles were worn System was leak free CO produced was diluted before venting out Lab was well ventilated Proper pressure regulators were fitted
Carbon dioxide	Toxic & Explosive	Can explode Can cause asphyxiation when exposed for long time	Safety gloves, respirator and goggles were worn System was leak free CO_2 produced was diluted before venting out Lab was well ventilated Proper pressure regulators were fitted
Methane	Toxic, Flammable & Explosive	Can Explode Cause fire when in contact with heat source Can cause asphyxiation when exposed for long time	Safety gloves, gas mask and goggles were worn System was leak free CH_4 produced was diluted before venting out Lab was well ventilated Proper pressure regulators were fitted

Chapter 6

RESULTS AND DISCUSSION

6.1 Gasification process and Equilibrium Model results

Production of syngas containing H_2S by partially oxidising a mixture of methanol and 2-propanethiol was achieved. Prior to gasification and desulphurisation process analysis the components expected to be in the syngas were identified and quantified through calibration of the GC. The GC fitted with FPD was calibrated for H_2S only, and the GC fitted with the TCD detector was calibrated for the other components of syngas including H_2S. TCD being a universal detector has a limitation of 1000ppm for sulphurous compounds and therefore could not be used as a detector during desulphurisation where concentrations of below 10ppm were expected. Table 6.1 shows the retention times of the gases using both the TCD and the FPD detectors.

Table 6.1 Retention time of syngas components using GC fitted with TCD and FPD

Component	Retention Time TCD (minute)	Retention Time FPD (minute)
H_2	0.49	-
CO	2.12	-
CO_2	9.97	-
CH_4	6.73	-
H_2S	11.09	1.41
N_2	1.65	-

During gasification only sulphurous compounds could be analysed online as the process continued since the GC connected to the experimental set-up was fitted with the FPD detector. Figure 6.1 shows the peaks of the sulphur compounds present in the syngas. It was assumed that all of the sulphur from the 2-propanethiol was to be converted to H_2S but this was not the case. Two other sulphur compounds peak 2 and 3 eluted during analysis although they were not identified during calibration. From desulphurisation process analysis (further details are given in section 6.2.5) peak 3 was identified to be COS. During gasification apart from H_2S, COS is the second sulphur

compound mainly produced through oxidation of the sulphur element in the fuel by carbon monoxide present in the syngas through equation 6.1.

$$CO + S \rightarrow COS \qquad \Delta H_R = +63kJ/mol \qquad (6.1)$$

During gasification process analysis the peak area percentages of peak 2 and 3 compared to peak 1 (99%) were very negligible.

For desulphurisation process to commence it was imperative that the concentration of H_2S produced during gasification be consistent or within an acceptable range. This was established after approximately 30 – 45 minutes of switching off the flow of methanol and allowing the fuel to flow and react with the oxygen. Figure 6.2 and 6.3 show plots of the concentration of H_2S produced during all gasification runs at fuel flow rates of 0.108cm^3/s and 0.042cm^3/s respectively. At fuel flow rate of 0.108cm^3/s the concentration of syngas produced was low because of the short reaction time during gasification. The H_2S concentration was between 0.5 – 1mole % (5000 – 10000ppm). At 0.042cm^3/s fuel flow rate the concentration of H_2S produced was between 1-1.5 mole % (10000 – 15000ppm). Although the concentration of H_2S obtained after lowering the fuel flow was not exactly as expected (2.04 mole %) further reduction of the fuel flow was impossible because of long experimental hours.

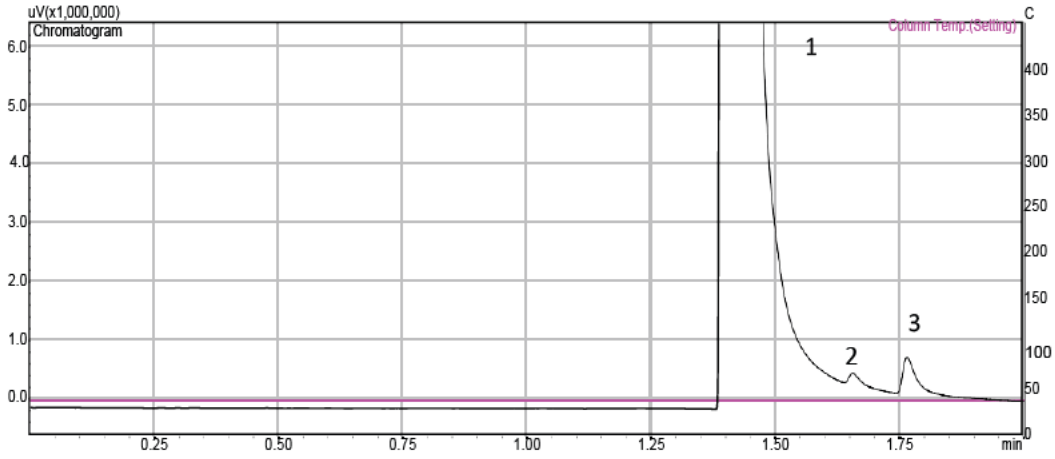

Figure 6.1 Chromatograph showing peaks of sulphur compounds detected in the syngas using FPD (Peak 1-H_2S, Peak 3-COS)

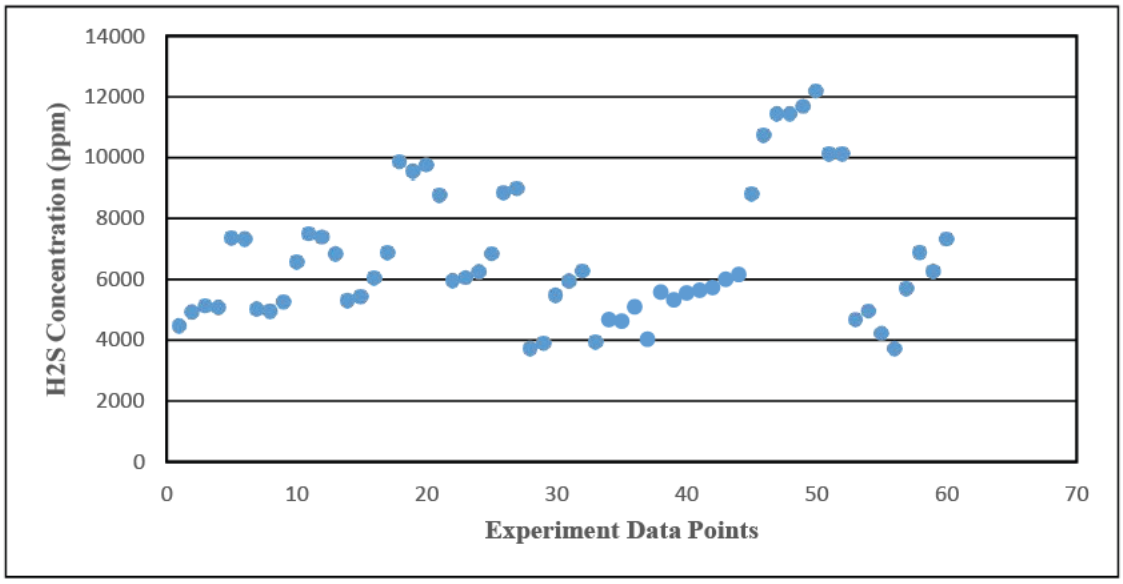

Figure 6.2 Concentration of H_2S produced during all gasification runs at 0.108cm^3/s fuel flow rate

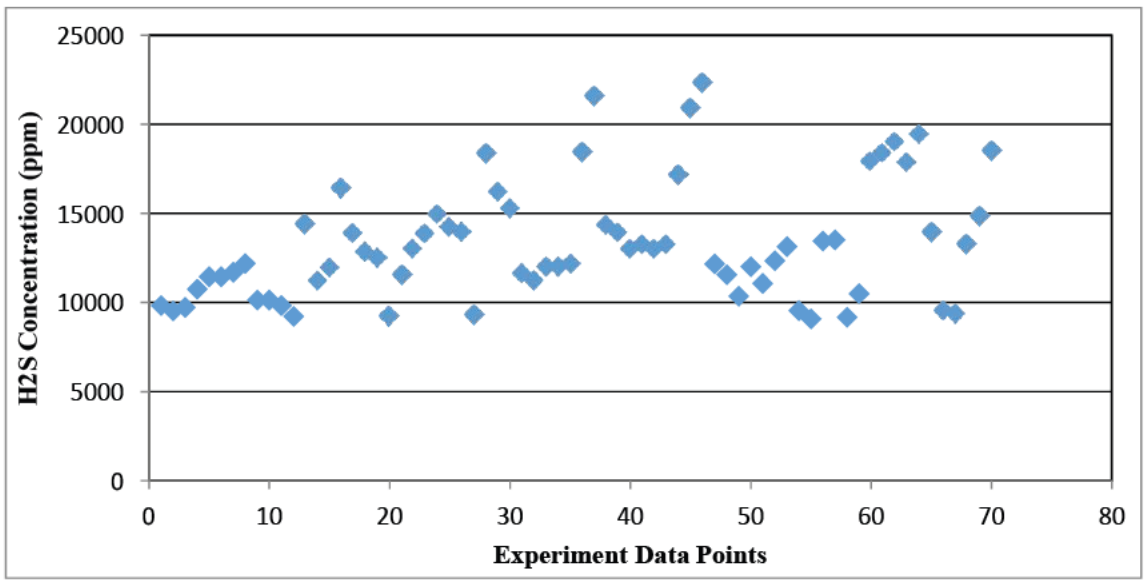

Figure 6.3 Concentration of H_2S produced during all gasification runs at 0.042cm^3/s fuel flow rate

The production of syngas containing H_2S from partial oxidation of the fuel mixture used in this study can be compared to research done by Thompson et al., (1982) and Edouard et al., (2013). Thompson et al., (1982) studied the thermal decomposition of 2-Methyl 2- propanethiol at 300-500^{0}C. The major product from the 0-97% decomposition was H_2S with minimal amounts of elemental sulphur and residual sulphur. The reaction time was between 10 to 120 seconds. They proposed a free radical chain type of decomposition mechanism. Edouard et al., (2013) studied the efficient way of converting methyl mercaptan into hydrocarbons and H_2S using protonic zeolite

catalyst at high temperatures. They first thermally decomposed it without the presence of a catalyst and the conversion to dimethyl sulphur and H_2S obtained was low (3%). By using a catalyst high conversions at temperatures below 427^{0}C converted methyl mercaptan at equilibrium to dimethyl sulphur and H_2S, but above 427 ^{0}C H_2S and hydrocarbons (light alkanes and aromatics) were produced as shown in Figure 6.4.This shows that it is possible to produce H_2S by partially combusting the mixture of fuel as used in this study.

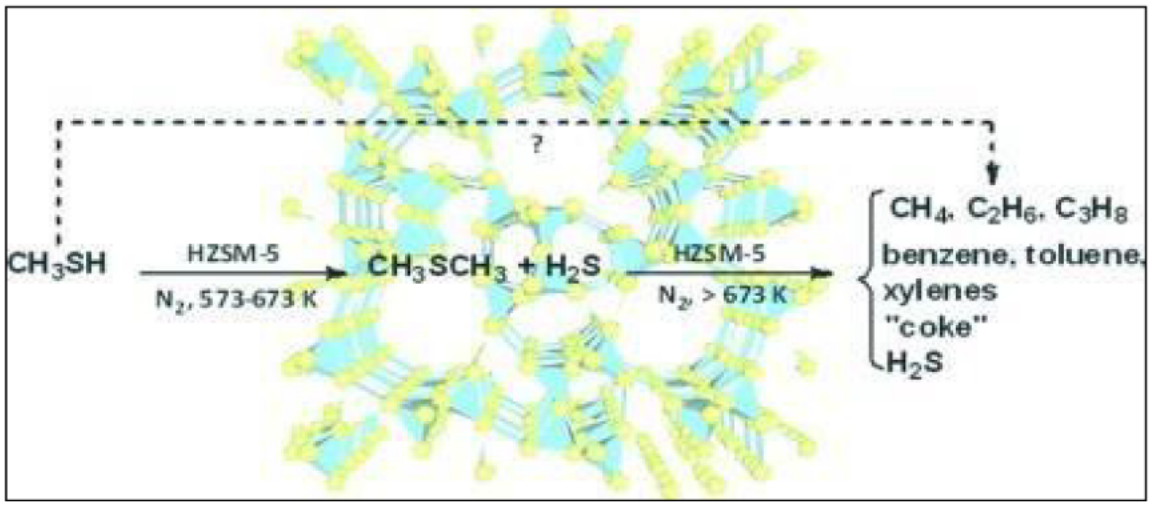

Figure 6.4 Mechanism of catalytic transformation of methly mercaptan to H_2S and Hydrocarbons at temperatures above 427 ^{0}C (Edouard et al., 2013)

The other components of syngas were analysed with the GC fitted with TCD. The analysis was done after the commencement of the desulphurisation process. This was because the sampling point was located on the socket covering the desulphurisation reactor. Therefore gas could only be sampled when it was flowing into the reactor for desulphurisation. A gas tight syringe of 1 ml capacity was used to draw the sample. The sample was then injected into the GC and analysis done. Figure 6.5 shows the peaks of the gases produced during gasification. The H_2 peak in Figure 6.5 is negative because the GC was using Helium as the carrier gas. Helium has a lower thermal conductivity compared to that of Hydrogen. At low concentrations of Hydrogen the Helium/Hydrogen mixture thermal conductivity has little effect on the detector and positive peaks results having an overall linear response. As the concentration of Hydrogen increases, the Helium/Hydrogen mixture thermal conductivity brings about a change in the detector response resulting into a negative peak with an overall non-linear response. In our study very high Hydrogen concentrations (100 mole %) were used which resulted in a quadratic calibration curve (Appendix A). Similar results were obtained by Snavely and Subramaniam, (1998). The best carrier gas to use when analysing Hydrogen is Argon but it lowers the sensitivity of the detector towards the other components of syngas. Conclusion that peak 7 and 8 are sulphurous compounds was made

because they also eluted during analysis of the syngas produced using FPD as shown in Figure 6.1 that is peaks 2 and 3 respectively.

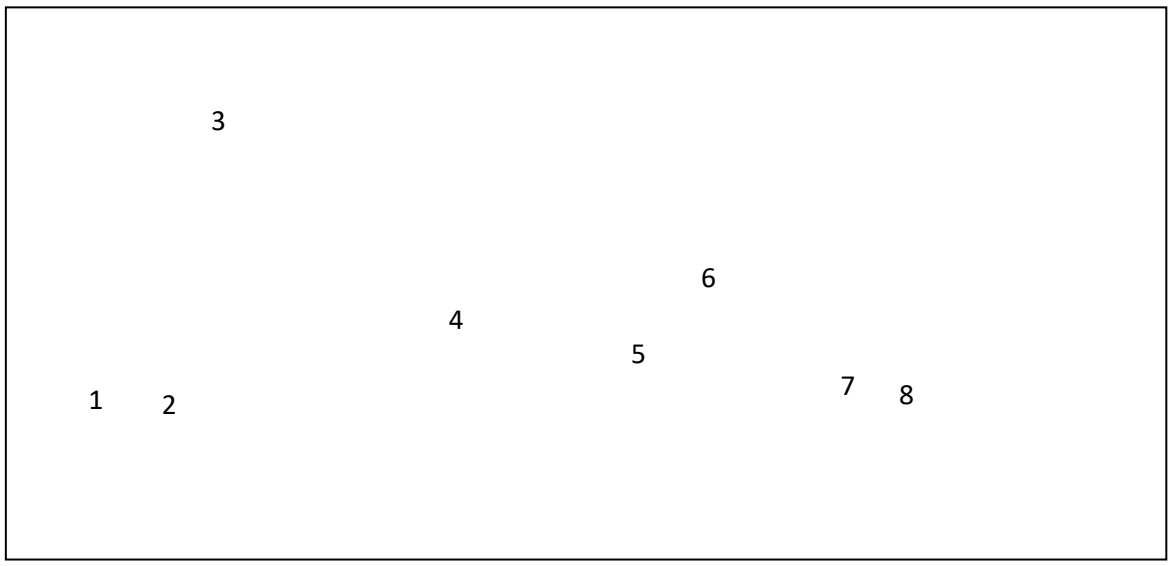

Figure 6.5 Chromatograph showing peaks of the different syngas components detected using GC with TCD (1. H_2, 2. N_2, 3. CO, 4. CH_4, 5. CO_2, 6. H_2S, 7. Sulphur compound, 8. COS)

A model of the gasification process was created using the ASPEN plus simulation programme prior the experimental work by direct minimization of Gibbs energy. Using this criterion it was possible to predict the syngas composition at equilibrium and the optimum reaction temperature to achieve a H_2: CO ratio of 2:1. The pressure was maintained at 1 atmosphere throughout. Apart from high pressure having a positive effect in the production of CH_4 and CO_2, the advantage of operating at high pressures depends on the downstream processes. In IGCC for example the gas turbine requires a pressure of 20bar therefore operating gasification process at high pressures than 20bar saves in compression energy and results in compact systems. Unfortunately high pressure operations are limited to the type of feed, solid feed stocks being at a disadvantage. In this study working at atmospheric pressure was an advantage since it simplified the equipment and the process at large. Figure 6.6 obtained from sensitivity analysis done on the simulation shows the effect of temperature on the equilibrium composition of syngas. It also gives the optimum reaction temperature. It is clear that at temperatures above 800 ^{0}C the H_2/CO ratio of 2:1 can be achieved by using the set flows of fuel and oxidant (0.042cm^3/s and 4.867cm^3/s). H_2O, CH_4 and CO_2 concentrations are seen to decrease with increase in temperature and H_2S and COS are not affected by the change in reaction temperature. On the other hand H_2 and CO concentration increases with increase in temperature up to an optimum level where they all become steady. From Figure 6.6 the optimum reaction temperature was thus chosen to be 830 ^{0}C.

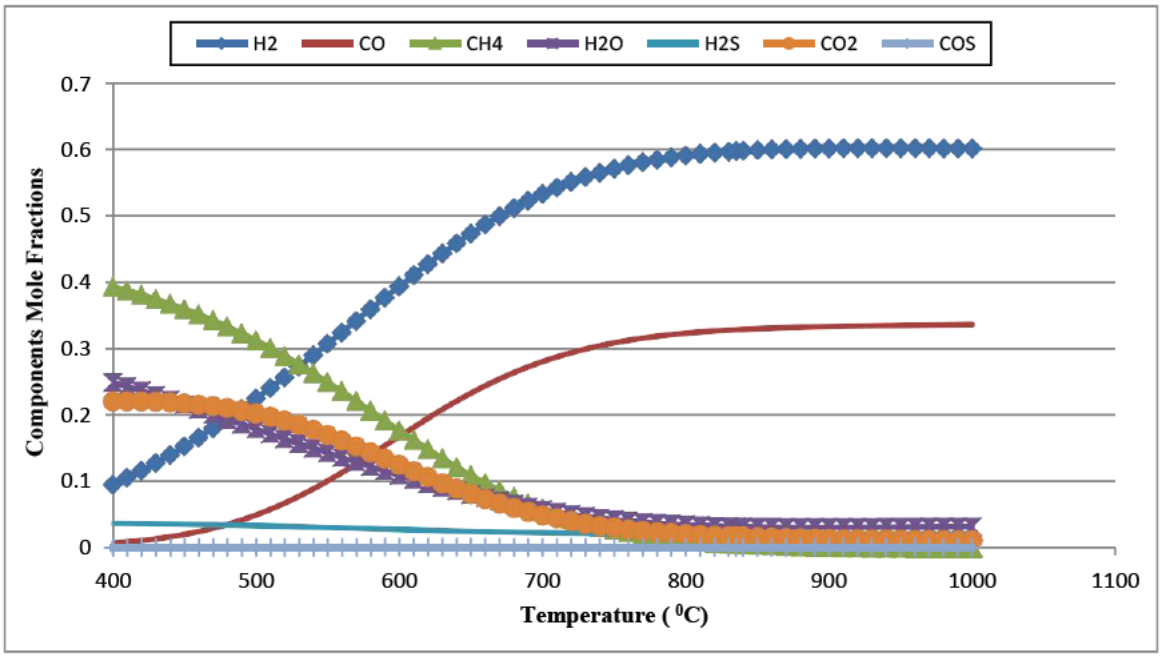

Figure 6.6 Effect of Equilibrium composition of syngas with varying reaction temperature

The results of the equilibrium model used in this study were compared to the work of Botha, (2010). Botha, (2010) used the minimization of Gibbs free energy and Lagrange undetermined multipliers with constraint of mass balance using an O_2/Fuel ratio of 0.0989. This study used an O_2/Fuel ratio of 0.219. Table 6.2 compares the equilibrium composition of syngas obtained by varying the O_2/Fuel ratio. From the comparison there is a distinct difference in the concentration of CO_2, CH_4 and H_2O. High O_2 /fuel ratio levels favour the production of CO_2 and H_2O and consequently low levels of CH_4. This is because of the high levels of oxidant present during gasification favouring combustion products. It can be seen that the amount of H_2S and COS are very similar. The concentration of H_2S is independent on reaction temperature and the O_2/Fuel ratio. It only depends on the amount of sulphur present in the fuel whereas COS production is dependent on process pressure and the amount of CO produced in the syngas as indicated in equation 6.1.

Table 6.2 Comparison of syngas equilibrium composition by varying the O_2/Fuel ratio

Gas Components	**Botha (2010) % mole fractions at O_2/Fuel ratio of 0.0989**	**Model % mole fractions at O_2/Fuel ratio of 0.219**
H_2	60.91	60.01
CO	33.48	33.1
CO_2	0.61	1.47
CH_4	1.76	0.29
H_2S	2.04	2.03
H_2O	1.15	3.09
COS	0.05	0.05
TOTAL	100	100

Figure 6.7 and 6.8 compares syngas equilibrium composition of the model and average compositions of all gasification runs performed at fuel flow of 0.042cm^3/s, O_2 flow of 4.867cm^3/s, reaction temperature of 830 ^0C and 1 atmosphere. The model as well as the experimental analysis were carried out on a wet basis.

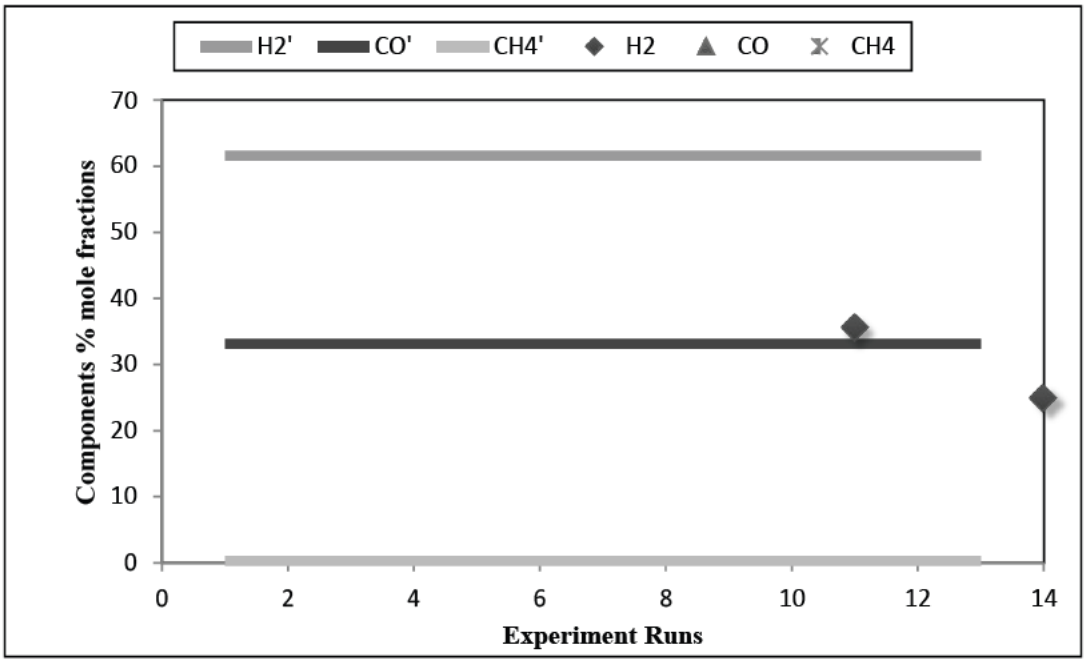

Figure 6.7 Comparison of model and averaged experimental equilibrium composition of H_2, CO and CH_4 at 0.042cm^3/s fuel, 4.867cm^3/s O_2 at 830 ^{0}C and 1 atm (H_2', CO' and CH_4' are the predicted values)

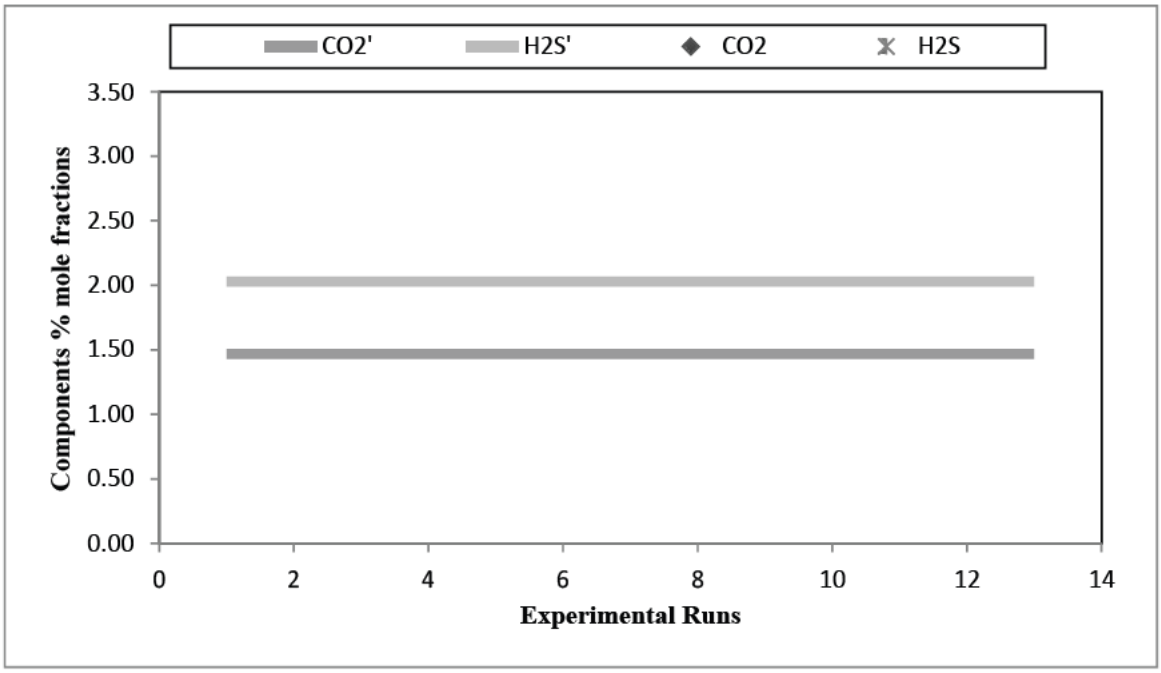

Figure 6.8 Comparison of model and averaged experimental equilibrium composition of H_2S and CO_2 at 0.042cm^3/s fuel, 4.867cm^3/s O_2 at 830 ^{0}C and 1 atm (H_2S', and CO_2' are the predicted values)

At thermodynamic equilibrium the high temperature and low pressure in the reactor favour production of H_2 and CO and limits formation of CO_2, CH_4 and H_2O. This contributes to the composition of syngas obtained from the experiment. Good agreement was seen between the model

and experimental data for CO but there was a slight deviation with CH_4 and H_2 as shown in Figure 6.7. The other components; CO_2 and H_2S were not in good agreement with the predicted values as shown in Figure 6.8. From the experiment, the amount of water collected after condensation was so little that it was difficult to quantify. This explains why more H_2 and CH_4 were produced than was predicted. CO_2 was expected to be high but since there was very small quantity of water the condition was unfavourable for water gas shift reaction (equation 2.19) and methane reforming reaction (equation 2.1). In addition the high temperature in the reactor was favourable for the Boudouard reaction (equation 2.17) further reducing the CO_2 concentration. From Figures 6.1 and 6.4 it is shown that two other sulphur compounds were present. This explains the low H_2S concentration obtained from the experiment in opposition to what was predicted. A H_2: CO ratio of 1.97:1 was obtained.

$$CO + H_2O \leftrightarrow CO_2 + H_2 \qquad (\Delta H_R = -41\,MJ/kmol) \qquad (2.19)$$

$$CH_4 + H_2O \leftrightarrow CO_2 + 3H_2 \qquad (\Delta H_R = +206\,MJ/kmol) \qquad (2.1)$$

$$C + CO_2 \leftrightarrow 2CO \qquad (\Delta H_R = +172\,MJ/kmol) \qquad (2.17)$$

6.2 Desulphurisation Results

During desulphurisation the effects of sorbent size, reaction temperature, sorbent surface area and space velocity on the sorbent sulphur sorption capacity was evaluated. Results and discussions of each of these effects in relation to the sorbent sulphur sorption capacity given in percentage weight (mass of sulphur absorbed per 100 g of ZnO) will be detailed.

6.2.1 Effect of sorbent surface area on desulphurisation

The BET surface area analysis of a particle gives information about the sorbent reactivity and the adsorption capacity of a particle in terms of pore volume, pore size distribution and particles surface area per unit mass. As the surface area is increased the particle size reduces and the pore volume increases. Table 6.3, 6.4 and 6.5 show the results of the properties of the sorbent before and after increasing the surface area of the commercial zinc oxide (bulk zinc oxide). The results show that the process was a success and the surface area did increase. The bulk densities obtained from the new sorbents were high indicating an increase in pore volume as the size reduced. Evidence of the size reduction was in the length of the sorbent bed in the reactor. The bed length for the large particles and small particles for bulk zinc oxide were 5.83 cm and 5.12 cm respectively and for the increased surface area sorbent were 4.39 cm and 4.25 cm for large and small particles respectively. These bed lengths were for 30g of sorbent loaded in all cases. Figures 6.9 and 6.10 show the adsorption isotherm of the fresh bulk zinc oxide for the large and small particles respectively. Bulk zinc oxide sorbents of all sizes show type II kind of isotherms as classified by the International

Union of Pure and Applied Chemistry (IUPAC) (Sing et al., 1985). This type of isotherms depict unrestricted monolayer-multilayer adsorption a characteristic of nonporous or macro porous sorbents. Conclusion that the bulk zinc oxide is a macro porous material is supported by the pore size distribution graphs Figures 6.11 and 6.12 which gave an average value of 130nm and 97nm for large and small particles respectively. Macro pores are classified to have a width (size) of > 50nm. This conclusion is also supported by particle size analysis done on TEM micrographs for fresh bulk ZnO sorbents using a computer software for size analysis which gave an average value of 175-211nm. Macro porous materials are also characterised by small specific surface areas as depicted by the bulk zinc oxide ($5.3 m^2/g$ in Table 6.3). In sorption the main role of macro porous sorbents is to provide route or channels for the reagent to access the small pores in the material (Everrent, 1972)

Table 6.3 Bulk Zinc Oxide properties

Sorbent	Size class (mm)	Average size (mm)	Bulk Density(g/cm^3)	Particle density (g/cm3)	Surface Area (m^2/g)	Pore volume (cm^3/g)
Small	1.18 -1.70	1.63	1.0235	1.1828	5.2758	0.0230
Large	1.70 – 2.00	2.06	0.8994	0.9906	5.3581	0.0262

Table 6.4 Small particles properties after treatment to increase surface area

Run	Moisture Content (%)	Initial ZnO Mass (g)	% Conversion	Final ZnO Mass (g)	Final ZnO Bulk Density (g/cm^3)	% Bulk density increase	Surface Area (m^2/g)	Pore volume (cm^3/g)
1	22.31	80.00	18.92	70.88	1.2342	13.83	15.89	0.1190
2	23.47	86.01	20.34	72.94	1.2354	20.7	22.99	0.1515
3	19.78	83.10	22.01	72.44	1.2391	21.1	35.33	0.2149
4	20.25	60.00	20.06	51.55	1.2256	16.49	23.39	0.1843

Table 6.5 Large particles properties after treatment to increase surface area

Run	Moisture Content (%)	Initial ZnO Mass (g)	% Conversion	Final ZnO Mass (g)	Final ZnO Bulk Density (g/cm^3)	% Bulk density increase	Surface Area (m^2/g)	Pore volume (cm^3/g)
1	21.56	83.00	24.10	71.69	1.2098	34.5	24.54	0.2006
2	20.18	80.20	35.05	73.01	1.1757	30.7	38.50	0.2189
3	21.8	85.00	17.53	72.20	1.1936	20.65	16.08	0.1366
4	19.71	76.00	22.62	65.01	1.1099	17.09	22.68	0.1695

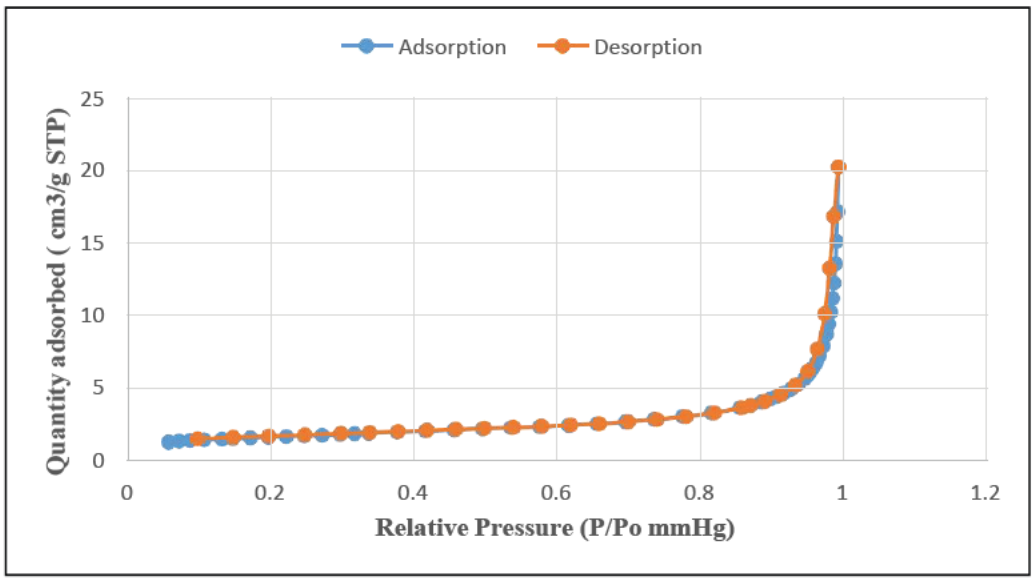

Figure 6.9 Fresh bulk ZnO large particles Adsorption Isotherm

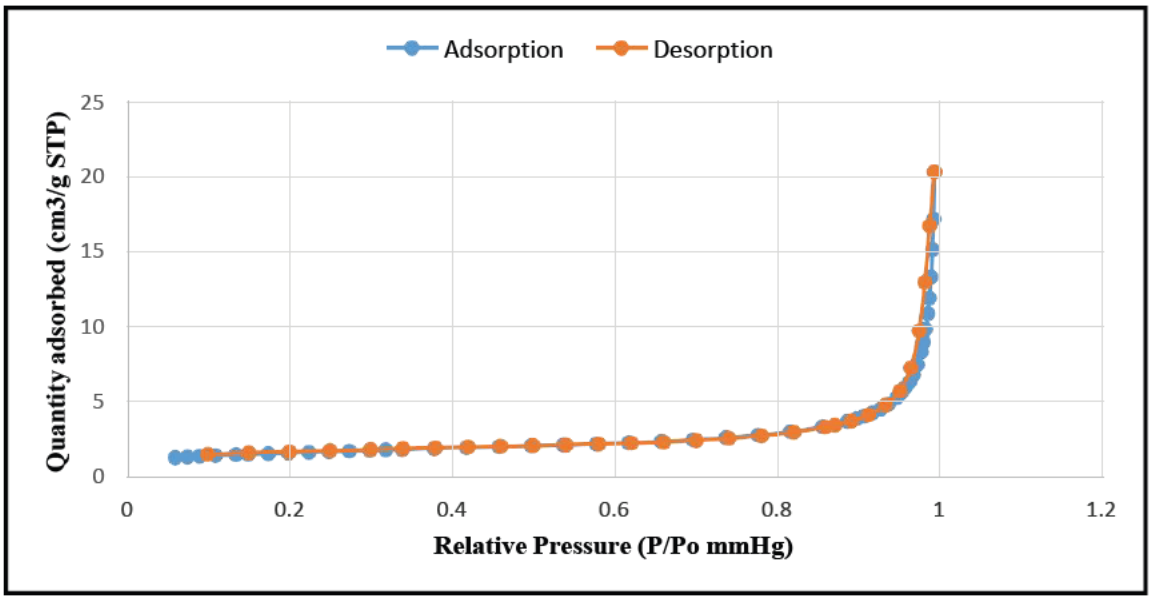

Figure 6.10 Fresh bulk ZnO small particles Adsorption Isotherm

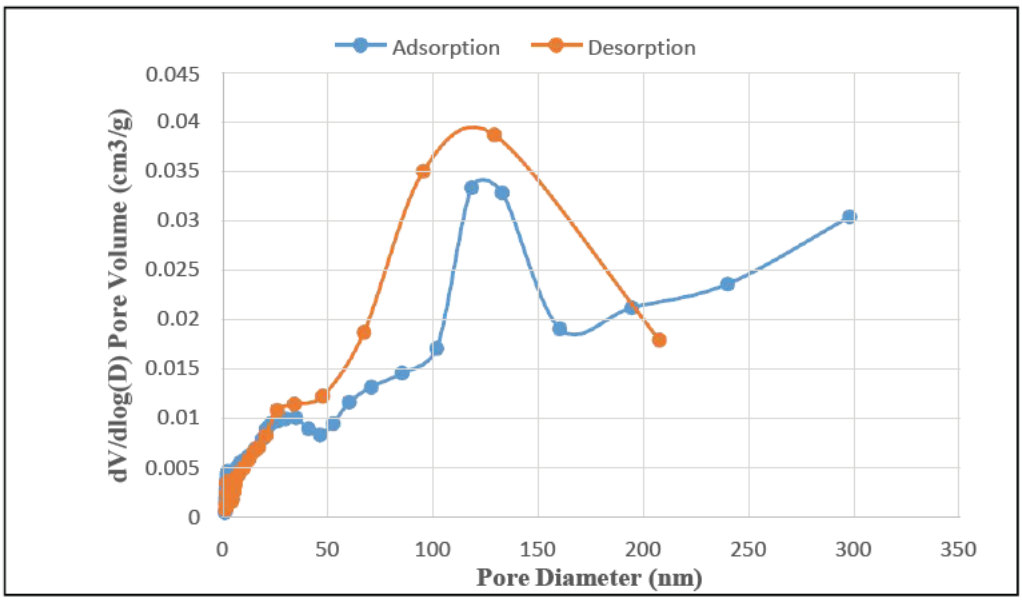

Figure 6.11 Fresh bulk ZnO large particles size distribution

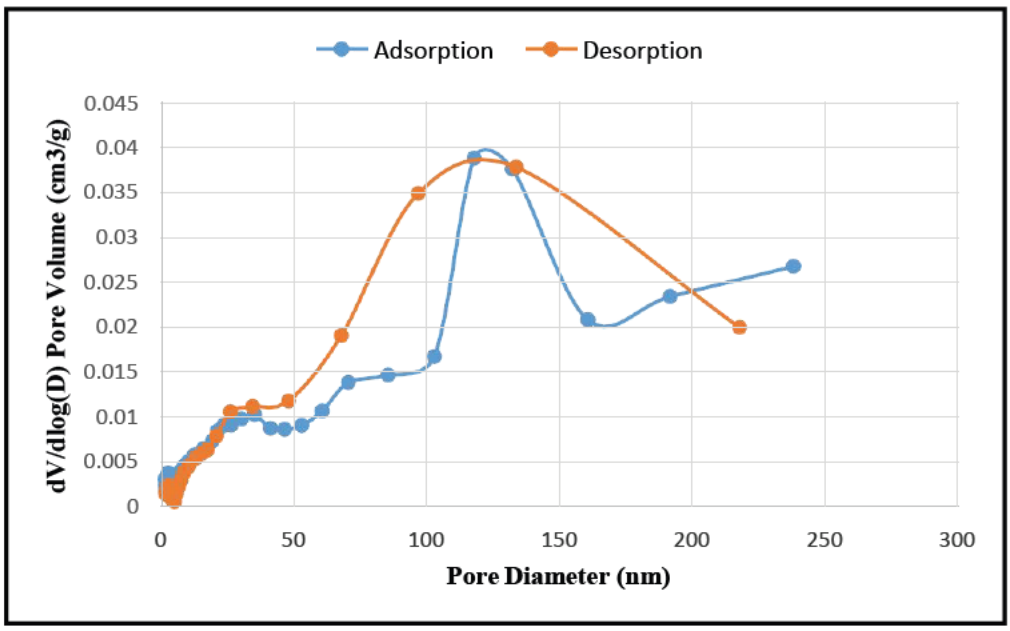

Figure 6.12 Fresh bulk ZnO small particles size distribution

On the other hand the increased surface area sorbents show a type IV kind of isotherm shown in Figure 6.13 and 6.14. This is evident by the formation of the hysteresis loop which is related to capillary condensation that occurs in mesoporous sorbents. Capillary condensation occurs when a gas condenses into a liquid like phase at a pressure less than the saturation pressure of the bulk liquid resulting in complete pore filling (Trunschke, 2013). The pore size distribution graphs Figure 6.15 and 6.16 together with particle size analysis done on the TEM micrographs support the

mesoporous characteristics of these sorbent. The highest peak on the size distribution graphs gave an average size of 17nm and 25 nm for large particles and small particles respectively. TEM analysis gave an average of 30-48nm. Mesopores are classified to have size ranges of between 2 – 50 nm. In sorption process mesoporous sorbents are more effective than macro porous sorbents because the latter have a larger surface area to volume ratio enabling more sorption of the reagent.

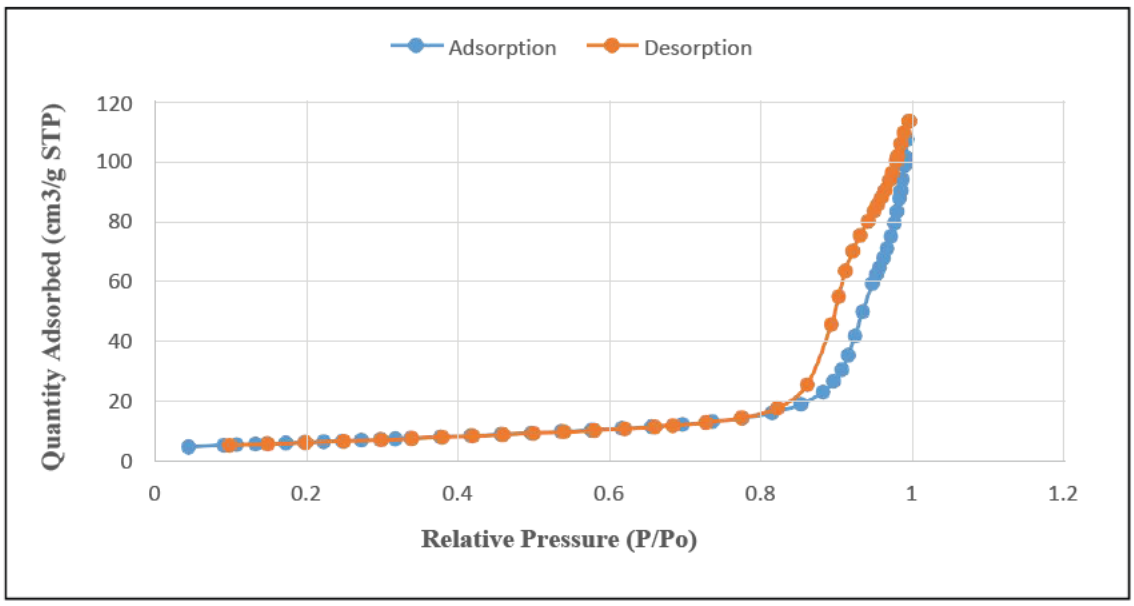

Figure 6.13 Fresh increased surface area ZnO large particles Adsorption Isotherm (Run 4 in Table 6.8)

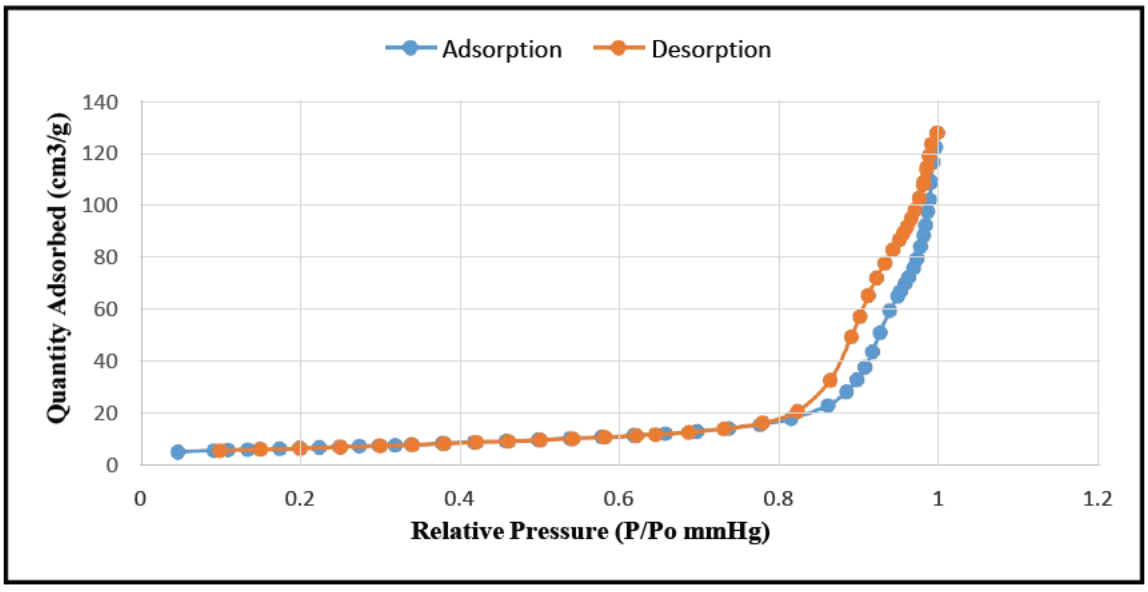

Figure 6.14 Fresh increased surface area ZnO small particles Adsorption Isotherm (Run 4 in Table 6.7)

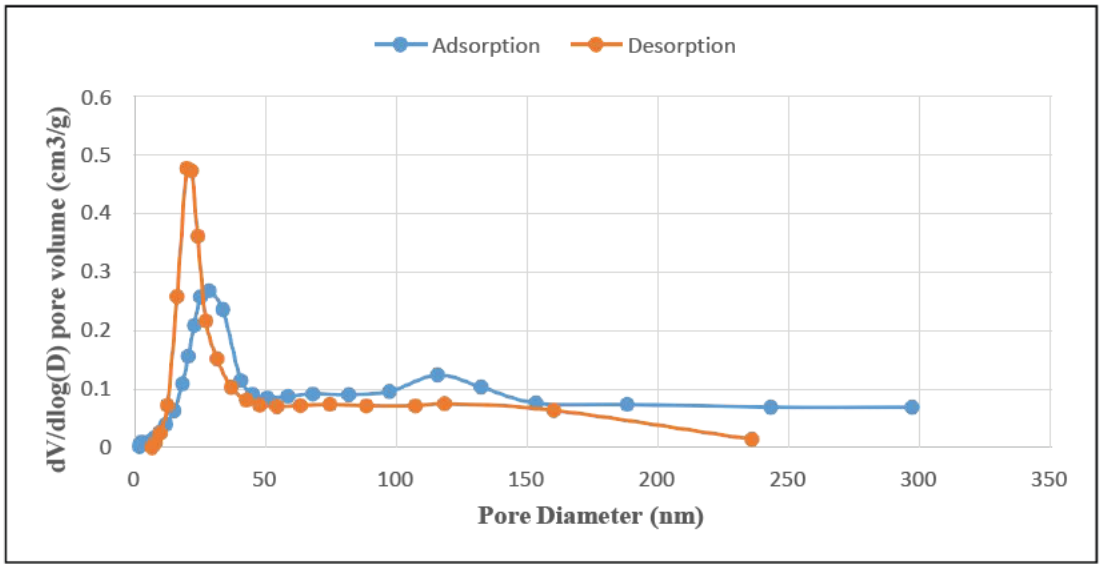

Figure 6.15 Fresh increased surface area ZnO large particles size distribution (Run 4 Table 6.8)

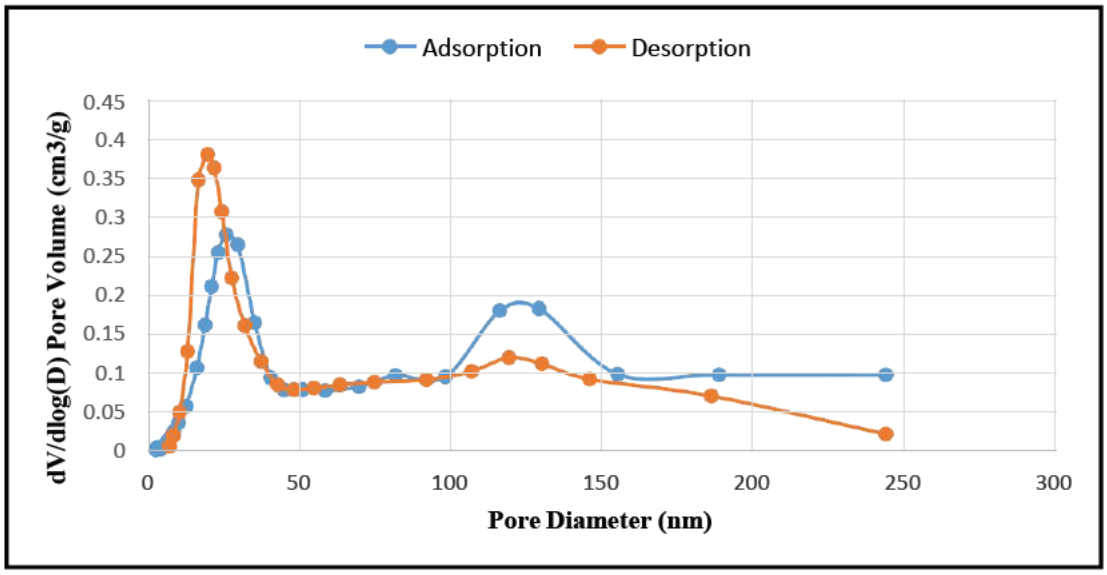

Figure 6.16 Fresh increased surface area ZnO small particles size distribution (Run 4 Table 6.7)

From the above characterisation of the sorbents used, it was thus expected that the increased surface area sorbent should exhibit high sulphur sorption capacities. To evaluate the effect of varied surface area, experiments at both low surface area (5.28m^2/g and 5.36m^2/g for small and large particles respectively) and increased surface area (Average of 24.4m^2/g and 25.45m^2/g for small and large particles respectively) at an average space velocity of 610h^{-1} were used in the 2*2 experiment design. Table 6.6 give details of the labels used which are similar to the factorial design combinations.

Table 6.6 Abbreviations used for various Particle size and Temperature combinations

Combination	Meaning
SPLT	Small particle (1.63 mm) at low temperature (350 ^{0}C)
BPLT	Large particles (2.03 mm) at low temperature (350 ^{0}C)
SPHT	Small particles (1.63 mm) at high temperature (550 ^{0}C)
BPHT	Large particles (2.03 mm) at high temperature (550 ^{0}C)

The results given in Table 6.7 and the breakthrough curve Figure 6.17 compared to the results given in Table 6.8 and the breakthrough curve Figure 6.18 for the low surface area at the same space velocity indicate a poor performance for the increased surface area sorbent. The increased surface area sorbents had extremely low sulphur sorption capacity in all combination through the short breakthrough time at the breakthrough point. On the other hand the low surface area had long breakthrough times and consequently higher sulphur sorption capacities. This could have resulted because of sorbent damage either during the process of increasing the surface area and the range of temperature used during desulphurisation.

Table 6.7 Results of experiments at high surface area and average space velocity of 610h^{-1}

Run	Combination	Initial H_2S concentration (ppm)	Space Velocity (h^{-1})	Breakthrough time (minute)	Sulphur sorption Capacity (Wt. %)
1	SPLT	14464	780.56	20	0.2299
2	BPLT	15428	526.96	5	0.0471
3	SPHT	12826	636.79	170	1.071
4	BPHT	15821	456.43	60	0.3678
5	SPLT	15780	676.55	25	0.2719
6	BPLT	13443	565.43	15	0.1322
7	SPHT	14557	593.88	100	0.6668
8	BPHT	11345	625.44	40	0.2489

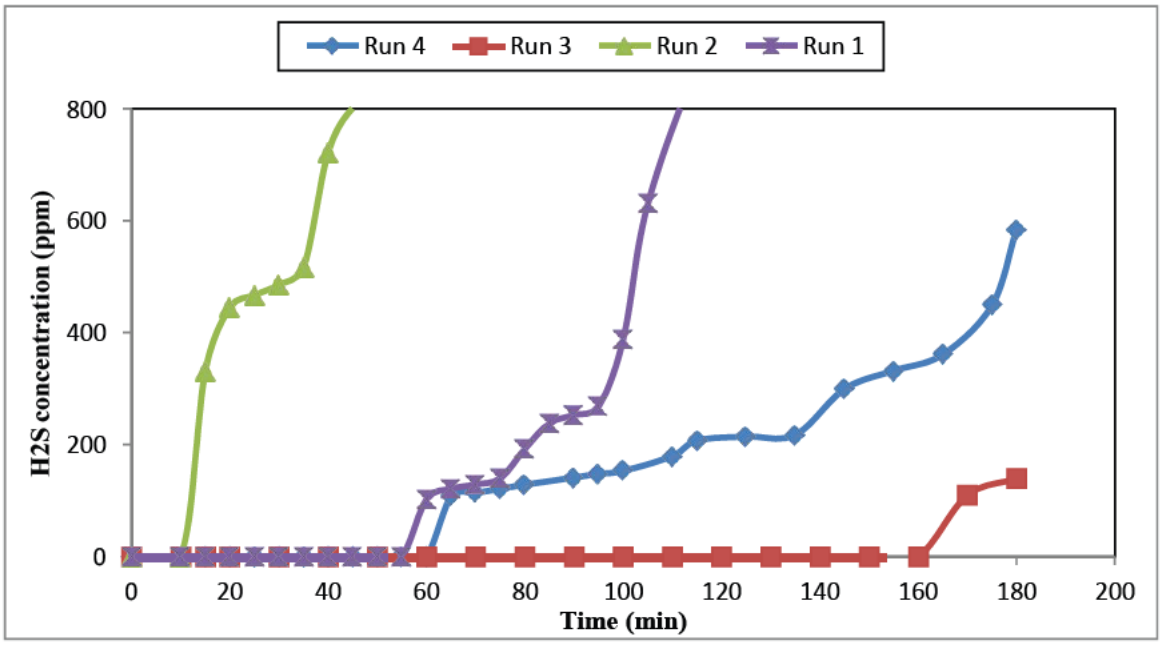

Figure 6.17 Breakthrough curve of experiment at high sorbent surface area and an average space velocity of 610h^{-1} (Run 1-4 as indicated in Table 6.7)

Table 6.8 Results of experiment at low surface area and an average space velocity of 610h^{-1}

Run	Combination	Initial H_2S concentration (ppm)	Space Velocity (h^{-1})	Breakthrough time (minute)	Sulphur sorption capacity (Wt. %)
1	SPLT	15790.00	680.00	340	3.7197
2	BPLT	9712.00	560.14	300	1.8926
3	SPHT	13443.00	574.28	285	1.6970
4	BPHT	13916.23	633.89	80	0.6195
5	SPLT	12158.00	654.44	345	2.7950
6	BPLT	9743.00	580.10	290	1.9010
7	SPHT	11703.00	625.01	295	1.6643
8	BPHT	9551.74	546.94	95	0.4358

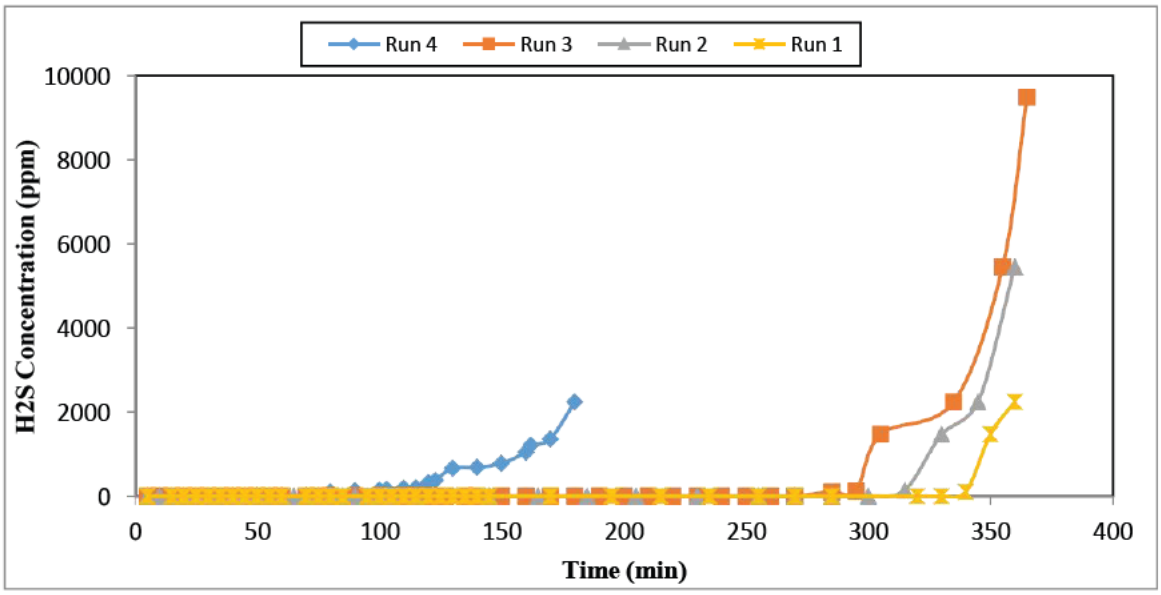

Figure 6.18 Breakthrough curve of experiment at low surface area and an average space velocity of 610h^{-1} (Run 1-4 as indicated in Table 6.8)

During the process of increasing the surface area the bulk zinc oxide was first converted to basic zinc carbonate then decomposed back to zinc oxide. In the decomposition of carbonates relatively high local partial pressures of CO_2 exists, this coupled with the effect of operating conditions like temperature result in sintering of the resulting product for this case zinc oxide (Bolis et al., 1989 and Maciejewski and Oswald, 1985). This is evident from the TEM micrograph of the increased surface area sorbent Figure 6.19 which shows partial large arrays of single crystals with no sharp edges detaining the crystallites. This is in contrast with the TEM micrograph of the bulk zinc oxide Figure 6.20 which shows well defined single crystals of hexagonal shapes. SEM micrographs Figure 6.21 and 6.22 also show a change in morphology as compared to bulk zinc oxide Figure 6.23. The sintering effect on the sorbent was worsened during the sulphidation process by the range of temperature used in this study. A study done by Corrie and Kenneth, (2002) to show the unique chemical reactivity of Nano-crystalline metal oxides towards H_2S gave an optimum sulphidation temperature of 250°C for zinc oxide Nano-crystalline structures. Beyond this temperature the Nano particles showed a decrease in reactivity and consequently low sulphur sorption capacity caused by the sintering effect. The sintering effect results in reduction of the particle's pore volume. Thus the little sulphur that was captured using the increased surface area sorbents is from the part of the sorbent that was not converted to basic zinc carbonate during the carbonation process. SEM and TEM micrographs Figure 6.21, 6.22 and 6.24 of the fresh increased surface area sorbents show that not all the zinc oxide was converted by depicting a mixture of the hexagonal crystals with agglomerated microcrystals. The process condition for the production of zinc oxide plays a major role in the form of zinc oxide produced and consequently its application. Most bulk zinc oxide are prepared by the common methods referred to as French and American processes (Moezzi et al.,

2012). In these processes, zinc metal is heated to very high temperatures > 1400 ^{0}C to form zinc vapour which is oxidised at high temperatures as well. The oxide formation process kinetics is so fast resulting in well-defined crystals of low surface area (3-5m^2/g). On the other hand the kinetics of the decomposition of the salts is slow at low temperatures resulting in densely packed aggregates of compact small particles and high surface area (Bolis et al., 1989). Bolis et al., (1989) studied the effect of form on the surface activity of differently prepared zinc oxide. Their conclusion was that a high surface reactivity of zinc oxide is not necessarily related to high surface area but to the abundance of specific active sites of which is highly dependent on the method of preparation of the zinc oxide. In their study bulk zinc oxide had the highest adsorption capacity towards CO and H_2 compared to two zinc oxides decomposed from a carbonate and an oxalate salt. This was because of the highly crystallite morphology of the bulk zinc oxide with well-defined crystal edges. This also explains why the low surface area had higher sulphur sorption capacities than the increased surface area zinc oxide.

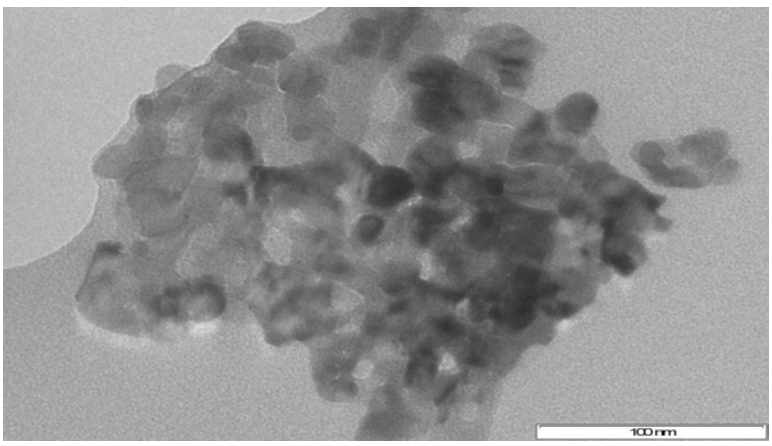

Figure 6.19 Low resolution TEM micrograph of Fresh increased surface area small ZnO particles

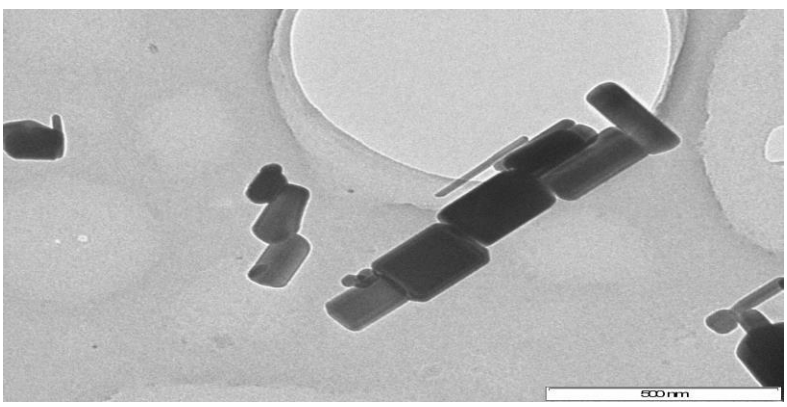

Figure 6.20 Low resolution TEM micrograph of fresh low surface area ZnO particles

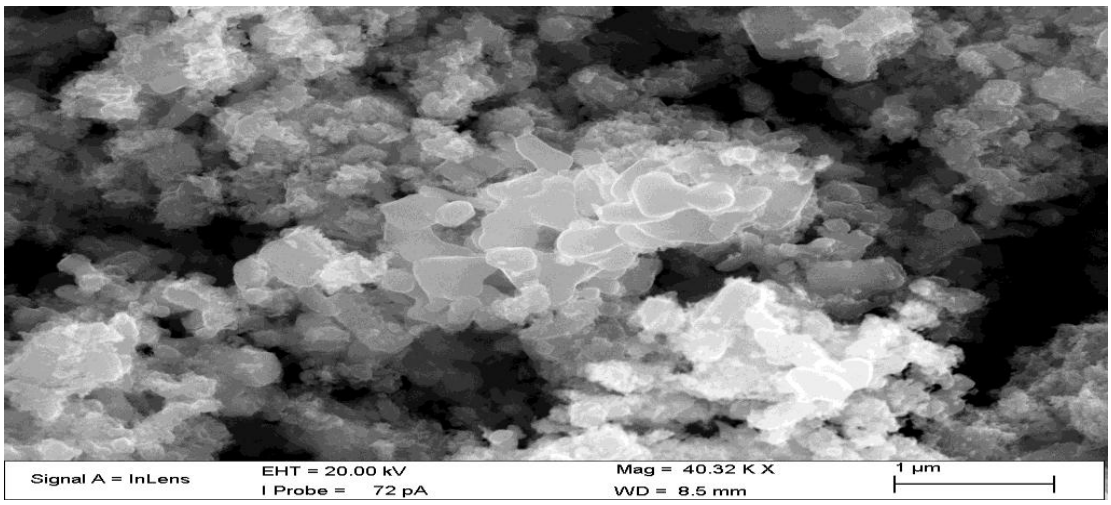

Figure 6.21 SEM micrograph of fresh increased surface area ZnO large particles

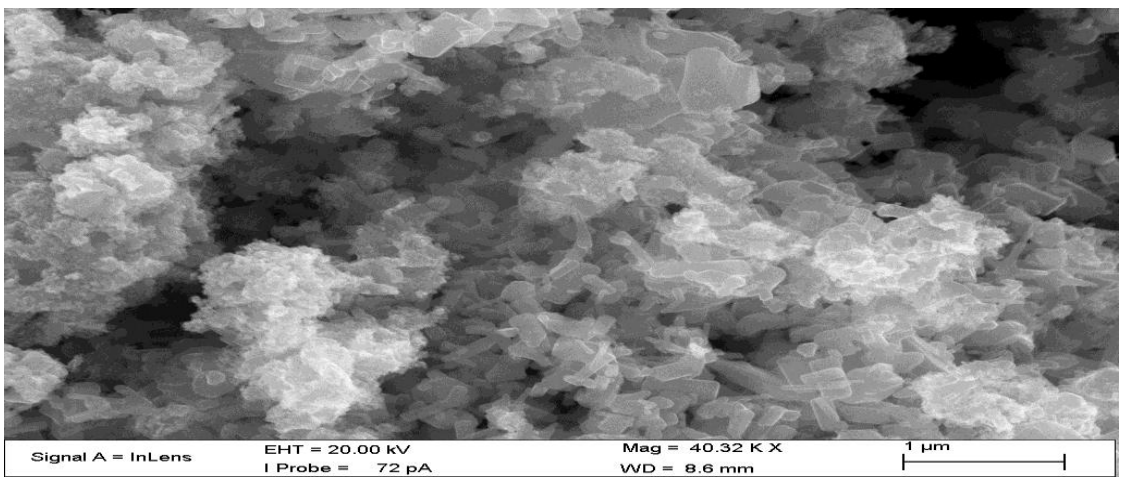

Figure 6.22 SEM micrograph of fresh increased surface area small ZnO particles

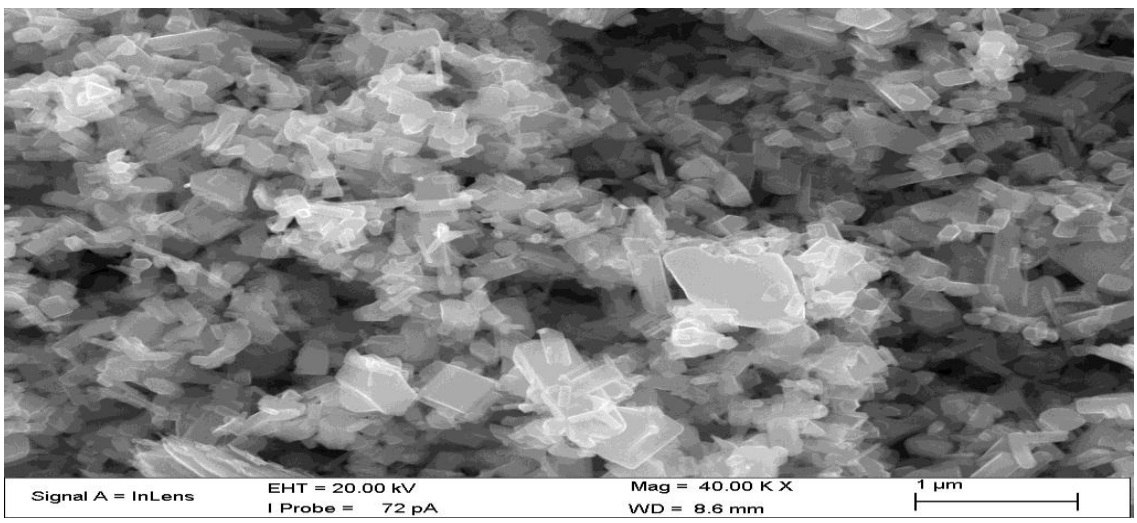

Figure 6.23 SEM micrograph of fresh low surface area ZnO particles

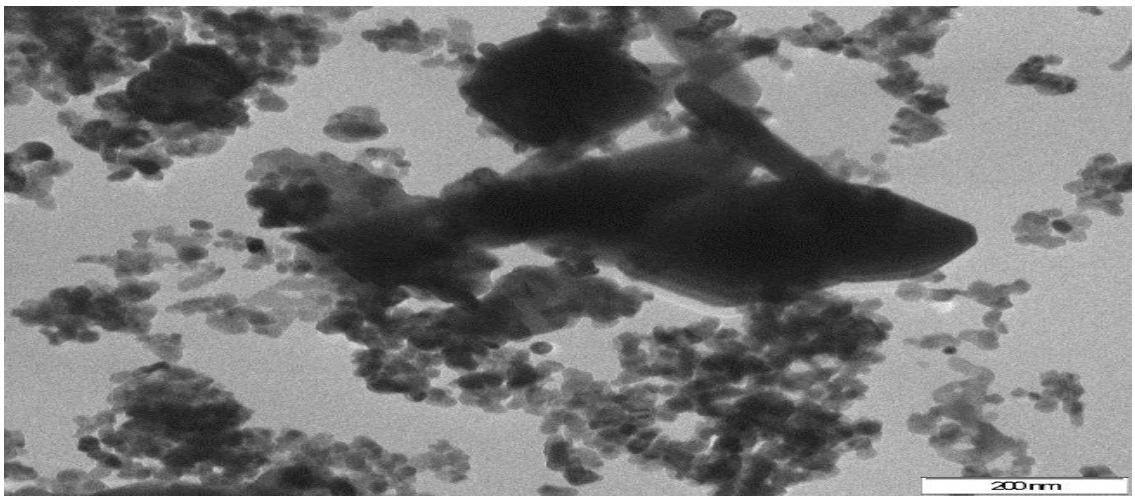

Figure 6.24 Low resolution TEM micrograph of fresh increased surface area large ZnO particles showing a mixture of hexagonal crystals and agglomerated microcrystals

6.2.2 Effect of sorbent particle size on desulphurisation process

The breakthrough curves Figure 6.17, 6.18 and 6.25 as well as the results shown in Tables 6.7, 6.8 and 6.9 clearly show that small particles desulphurization ability is higher than the large particles by the long desulphurisation time before reaching breakthrough point and the high sulphur sorption capacities. This is because the smaller the particle size the more effectively the volume available for reaction is utilized. This is as a result of reduced diffusion distances and consequently increased high rates of reaction. Another factor that shows the superiority of the small particles is its bulk density. The bulk density of smaller particles for both bulk and increased surface area sorbents is higher than the large particles as shown in Table 6.3 and 6.4. The bulk density is directly proportional to the weight of sorbent that can be charged into the reactor. That means for the same reactor volume more of the small particles are loaded than the large particles. This reason makes small sorbent sizes suitable. Despite this there is a limit to the size of the particles to be charged into the reactor which depends on the pressure drop across the bed.

6.2.3 Effect of temperature on desulphurisation process

In this study temperature was varied from 350 – 550 ^{0}C. The temperature profiles for run 1-4 of all the experiments performed are given in Appendix C. For the runs in which the temperature started from 0 ^{0}C to the set point shows that at the beginning of desulphurisation, the temperature increased rapidly then dropped down and stabilized. This is because the sulphidation reaction is exothermic with a heat of reaction of -78kJ/mol. Thereafter it stabilized showing that the process was isothermal. In the other desulphurisation experiments the temperature had to be lowered to the set point. This is because in a day two experiments at different levels could be performed therefore

once the temperature drops to ± 5 ^{0}C of the set point the desulphurisation process was started and with the flow of gas inside the reactor temperature drops down steadily and then stabilizes. From the results of all combination it can be seen from sulphur sorption capacity obtained in Tables 6.7, 6.8 and 6.9 that there was no much influence of temperature observed. It was expected that since the process is dependent on the activation energy it will be highly dependent on temperature according to the Arrhenius equation but this was not the case. This might be because at the temperature range of this study, the extent of reaction is essentially the same. The small differences may be attributed to diffusional resistance, which is known to be the rate limiting step in spherical pellets. Similar results of minimal influence of temperature have been reported in literature (Everett and Monaco, 1994, Siriwardane and Cicero, 2000 and Sánchez-Hervás, 2005).

6.2.4 Effect of space velocity on desulphurisation process

Preliminary experiments into this study operated with a space velocity on average of 3430h^{-1}. This was at a fuel flow of 0.108cm^3/s. The sorbent used for these experiments was the bulk zinc oxide with low surface area. It was observed that at this space velocity the breakthrough point was reached so fast with the longest time being 40 min using small particles at low temperature (Figure 6.25 and Table 6.9). The rest of the experiments were even worse. At 40 minutes a sulphur loading capacity of 1.036 Wt. % was obtained which was low compared to all the runs performed at the low space velocity of 610h^{-1} using the low surface area sorbent where the minimum was 95 minutes. At high space velocity the residence time across the sorbent bed is reduced and consequently lower the contact time between the sorbent and the gas which result in low utilization of the sorbent. Short bed lengths with respect to the absorption front could also be a reason for the poor performance at high space velocities. In addition gas-solid reactions are more diffusion resistant therefore at high space velocities little gas gets to diffuse into the bulk of the solid resulting in low sulphur sorption capacities.

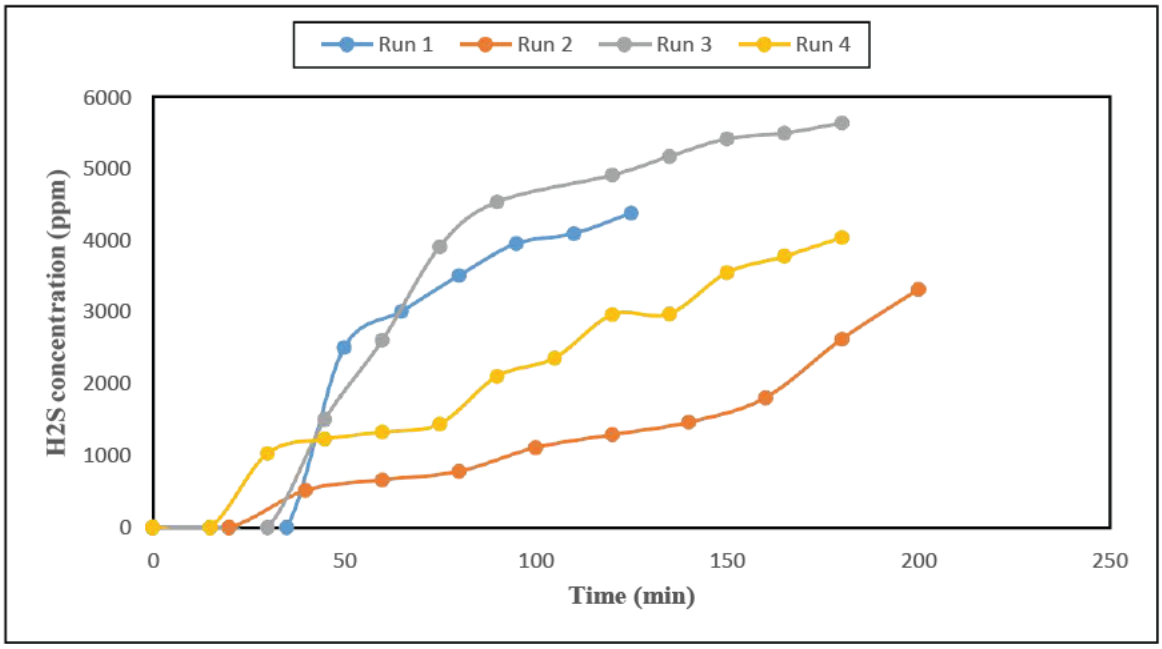

Figure 6.25 Breakthrough curve of experiments at low surface area sorbent and an average space velocity of 3430h^{-1}

Table 6.9 Results of experiment at low surface area and an average space velocity of 3430h^{-1}

Run	Combination	Initial H_2S concentration (ppm)	Space velocity (h^{-1})	Breakthrough time (minute)	Sulphur sorption capacity (Wt. %)
1	SPLT	4940.89	3313.82	35	0.5839
2	BPLT	5896.08	2625.85	20	0.3591
3	SPHT	8913.62	4011.71	30	0.8274
4	BPHT	7319.93	3299.32	15	0.3180
5	SPLT	6525.23	3896.01	40	1.0361
6	BPLT	5575.43	3260.46	20	0.4215
7	SPHT	9462.20	3655.27	25	0.6669
8	BPHT	7076.15	3389.17	10	0.2104

6.2.5 Other factors that affected the desulphurisation process

From all the experiments performed it was evident that reactions at low surface area and low space velocity yielded better results than the rest. But looking at the overall effectiveness of the sorbent at all levels considering the expected results, it is clear that the sorbent was underutilized even at this set of conditions. For this study sulphur sorption capacity was expected to be 19.5 Wt. % when the sorbent is fully sulphated that is 100 % conversion of zinc oxide to zinc sulphide. This amounts to 5.85g of sulphur captured with a theoretical time at full sulphidation of 30 and 40.58 hours at low and high temperatures respectively. Equations for calculating the sulphur sorption capacity, maximum mass of sulphur captured and theoretical time for complete sulphidation are given in section B.2 of Appendix B. The best results were obtained at low surface area with a space velocity of $680h^{-1}$ at 350 ^{0}C using sorbent with average diameter of 1.63mm as shown in Table 6.8. The time at which the exit concentration of H_2S exceeded 100ppm was 340 minutes yielding a sulphur sorption capacity of 3.72 Wt. %. This gives a conversion of 20%. Despite this the sorbent showed very high efficiencies of 99% calculated from the initial concentration of H_2S with respect to the concentration at any time during desulphurisation before breakthrough point. The sorbent was capable to lower the H_2S concentration to below 10ppm.

Apart from the factors discussed above other factors could have resulted in the underutilization of the sorbent as was observed during the experimental work and analysis of the sulphated sorbent. During online GC analysis of the gas exiting the desulphurisation reactor peak 3 as shown in Figure 6.1 was increasing with time even beyond the H_2S peak (Figure 6.26). Its quantity increased drastically as the concentration of H_2S approached breakthrough point. This behaviour occurred at low temperature reactions. At high temperatures this peak did not behave like this and maintained its gasification concentration. This phenomenon has also been reported by other researchers who identified this gas as COS (Li and King, 2006, Novochinskii et al., 2004 and Shanguan et al., 2011).

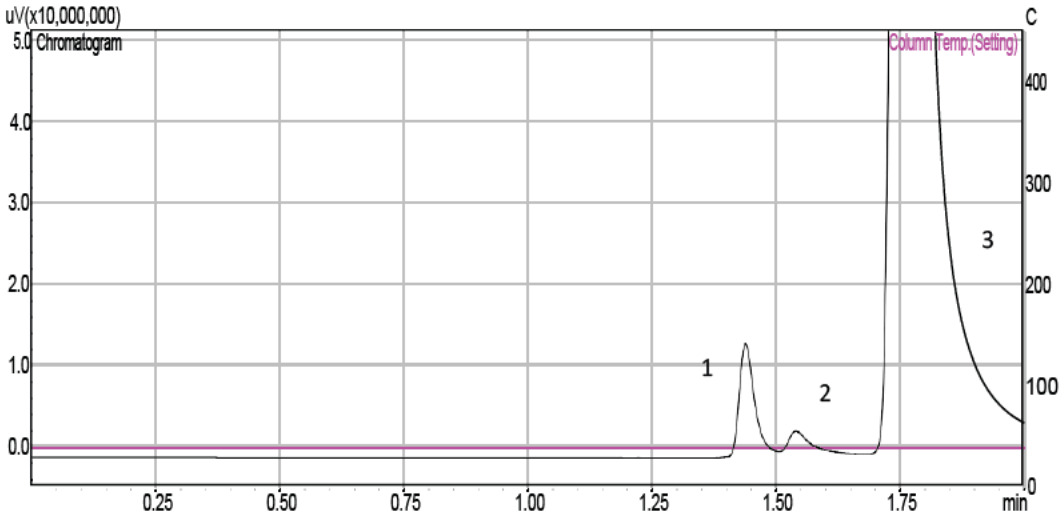

Figure 6.26 Chromatograph showing increasing size of peak 3 (COS) as peak 1 (H_2S) reduces at 350 ^{0}C during desulphurisation process

COS is formed in the reducing environment of the desulphurisation reactor by the reduction of H_2S by CO and CO_2 in the syngas by reactions shown in equations 3.7 and 3.8. For this study the reaction shown by equation 3.8 is unfavourable because of its endothermic nature and it requires CO_2 concentration of above 20 % of which in this study CO_2 concentration was about 1.6 %. Thus the COS that was being produced was from the reaction indicated by equation 3.7. The reduction of H_2S by CO is favoured by low temperatures and high concentrations of H_2 in the gas stream of which was satisfied for this study. Novochinskii et al., (2004) reported that the influence of CO on COS/H_2S ratio reduces with increasing temperature of which for their study was above 400 ^{0}C. This could be the reason why at high temperature reactions this phenomenon was not observed. This conversion of H_2S to COS during desulphurisation lowers the sorption capacity of the sorbent since zinc oxide is not capable of absorbing COS.

$$H_2S + CO \leftrightarrow COS + H_2 \qquad \Delta H^0 = -10.9kJ/mol \qquad (3.7)$$

$$H_2S + CO_2 \leftrightarrow COS + H_2O \qquad \Delta H^0 = 30.3kJ/mol \qquad (3.8)$$

The other reason that could have attributed to the low sulphur sorption capacity by the sorbent is the deposition of solid carbon onto the surface of the sorbent. Initial assumptions were that no carbon would be produced but that seemed not to be the case. Silica glass beads were placed inside the reactor in a bed to be able to adsorb any carbon present of which was evident from the beads removed after the reaction. Carbon was adsorbed on the surface of the glass beads as shown in

Figure 6.27. Despite this precaution some of the carbon was also adsorbed onto the surface of the sorbent. This was evident from the greyish colour of the sorbents removed after desulphurisation. The sorbent had a mix of pale yellow indicating H_2S sorption and grey showing presence of carbon deposition (Figure 6.28). EDX analysis on the spent sorbent also showed some presence of carbon on to the sample (Figure 6.29, 6.30). A mapping procedure was done on the EDX image to show the distribution of sulphur and carbon elements onto the surface of the sorbent grains this is shown in Figure 6.31. Carbon formation during gasification can be attributed to the below reactions at thermodynamic equilibrium without the presence of catalyst (Nikoo and Amin, 2010):

$$CH_4 \leftrightarrow C + 2H_2 \qquad \Delta H_{298} = 74.9kJ/mol \qquad (6.2)$$

$$2CO \leftrightarrow C + CO_2 \qquad \Delta H_{298} = -172.4kJ/mol \qquad (6.3)$$

$$CO_2 + 2H_2 \leftrightarrow C + 2H_2O \qquad \Delta H_{298} = -90.0kJ/mol \qquad (6.4)$$

$$H_2 + CO \leftrightarrow H_2O + C \qquad \Delta H_{298} = -131.3kJ/mol \qquad (6.5)$$

At the operating conditions of this study equation 6.2 is more favourable than the others. This is because high temperature does not improve exothermic reactions but promotes endothermic reactions. In addition more of H_2 was formed as was expected and thus could have resulted from the decomposition of CH_4 as shown in equation 6.2. Hydrogenation of CO_2 and CO shown in equations 6.4 and 6.5 could not have occurred since little water was collected during experimentation. Therefore the carbon deposit in this case could have resulted from the decomposition of CH_4. This carbon was then transported to the desulphurisation reactor by the flowing syngas and adsorbed on the surface of zinc oxide blocking the pores for H_2S sorption.

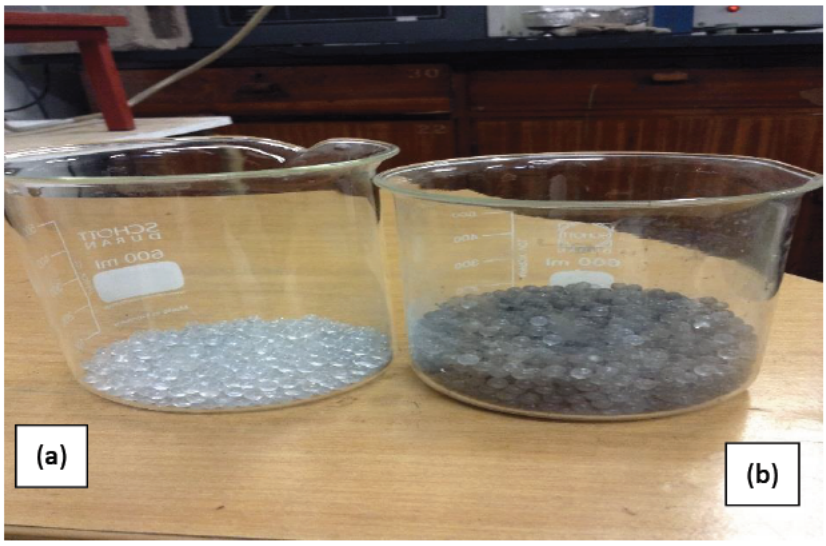

Figure 6.27 Glass beads used to adsorb any carbon present in the syngas (a) before (b) after desulphurisation

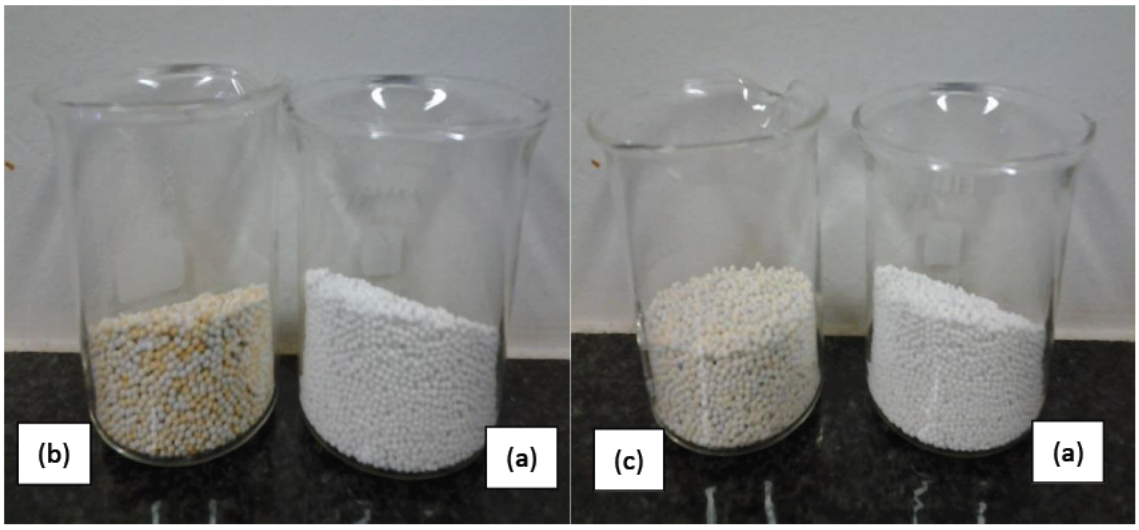

Figure 6.28 Sorbent (a) before (b) increased surface area after (c) low surface area sorbent after desulphurisation

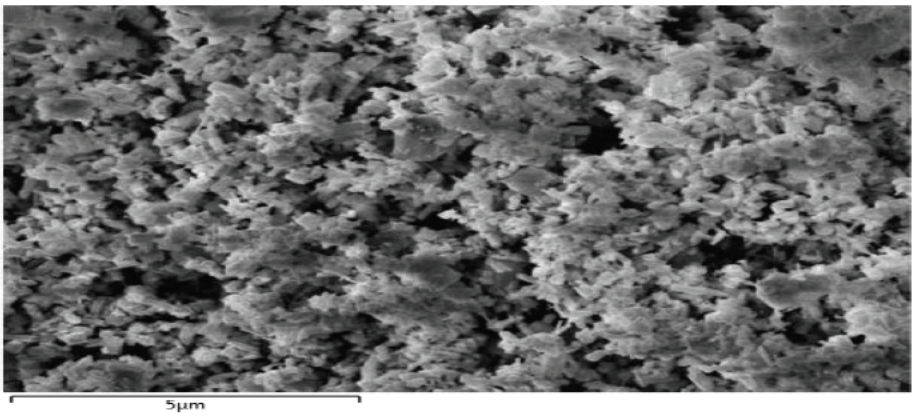

Figure 6.29 EDX micrograph of low surface area small particles at low temperatures after desulphurisation

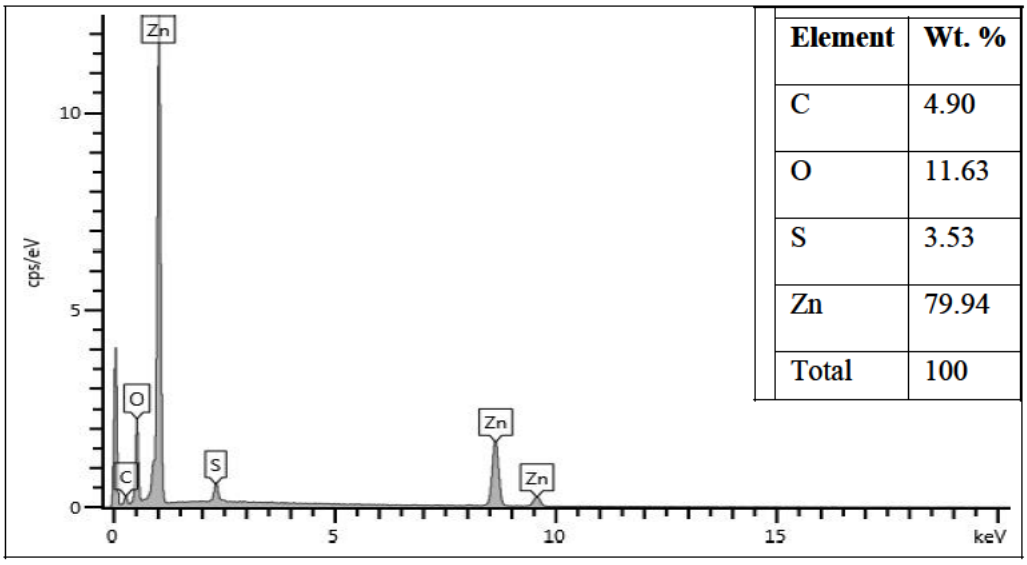

Element	Wt. %
C	4.90
O	11.63
S	3.53
Zn	79.94
Total	100

Figure 6.30 EDX elemental analysis of low surface area small ZnO particles at low temperature after desulphurisation

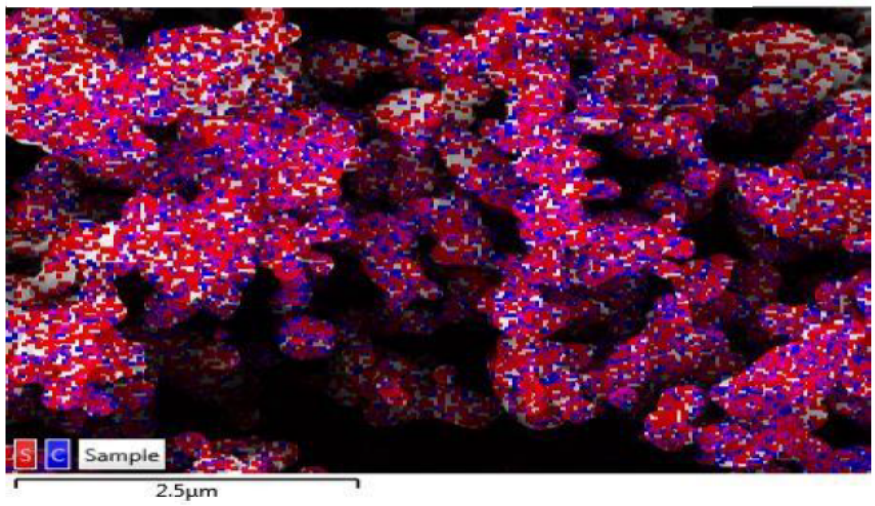

Figure 6.31 EDX micrograph showing distribution of sulphur element (red spots) and carbon element (blue spots) on the surface of the sorbent particles

6.3 Statistical Analysis of the Desulphurisation process

The 2*2 factorial experiment design was adopted as was mentioned earlier on to observe the effect of sorbent size and temperature at their low and high levels, at varied sorbent surface area and space velocity on the ability of the sorbent to absorb H_2S. Random experiments were performed according to the design in duplicates and the sorbent sulphur sorption capacity was calculated for each run. The total of the response at each combination was noted and was used to calculate the main effect of each factor and the interaction value between the two factors. The mean response was also

calculated and was used to plot the interaction graph. The main effect value of each factor indicates which factor has more control on the response and at what level. Whereas the interaction value indicate if the two factors being studied are dependent or independent on each other towards the response. For this statistical analysis results obtained using sorbent with low surface area at average space velocity of $610h^{-1}$ were used. Table 6.10 gives the response obtained at all experiment combination with the total and mean responses. Table 6.11 gives the results of the variance analysis performed after calculation of the main effects and interaction to check their significance. The main effects were calculated by the equation defined in section 5.1 in Chapter 5.

Table 6.10 Response, total response and mean response obtained at all combinations

Run	Label		Sulphur sorption capacity (Wt. %)		Total Response (%)	Mean Response (%)
			Run 1	Run 2		
1 &5	SPLT	(1)	3.72	2.80	6.52	3.26
2 & 6	BPLT	a	1.89	1.90	3.79	1.90
3 & 7	SPHT	b	1.70	1.66	3.36	1.68
4 & 8	BPHT	ab	0.62	0.44	1.06	0.53

Table 6.11 Variance analysis of the experiment design

Variations	Main Effect	Sum of Squares	Degree of Freedom	Mean square	F- Value
Temperature	-1.4725	4.3365	1	4.3365	185.3953
Sorbent size	-1.2575	3.1626	1	3.1626	135.2086
Interaction	0.43	0.3698	1	0.3698	15.8098
Error	-	0.09367	4	0.0234	
Total	-	7.9624	7	-	

From Table 6.11 the values of the main effect for both temperature and sorbent size are negative. This indicates that to obtain maximum sulphur sorption capacity the temperature and the sorbent size should be at their low levels (<350 ^{0}C and < 1.63mm). The magnitude of the main effects shows that temperature has a greater effect on the response than sorbent size only at their low levels. This is true as indicated by the mean response on Table 6.10. It can be seen that the sulphur sorption capacity of the large particles at low temperature is higher (1.9 Wt. %) than the small particles at high temperature (1.68 Wt. %). If at all the effect of sorbent was higher than temperature the reverse could have been seen. The value of the interaction is very small compared to the main effects of

each factor. To verify the results obtained by calculating the main effect and interaction a variance analysis was performed on the response obtained from both runs. From Table 6.11 the F- values support that temperature has more effect on the response than sorbent size from the large value obtained (185), whereas it's clear that there was no interaction between the two factors from the very small value of interaction obtained (15). This is also verified by the interaction curve shown in Figure 6.32. In Figure 6.32 two parallel lines of the large (L) and small (S) particles at different temperature level was obtained. This clearly shows there was no interaction between the two factors. In addition the gradient of each line is negative verifying that the two factors are effective at their low levels.

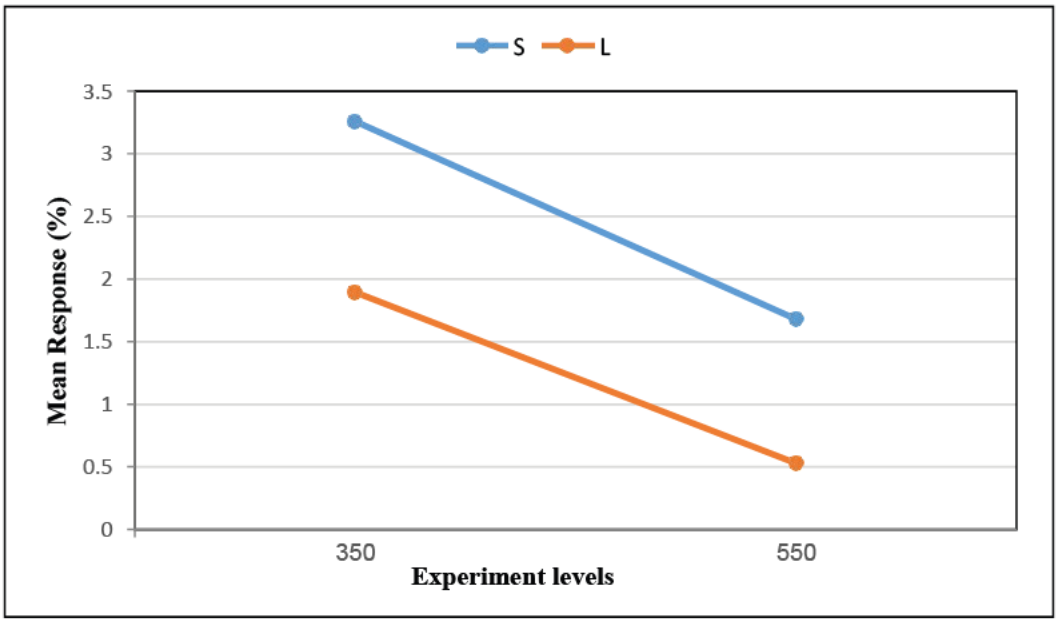

Figure 6.32 Interaction curve of temperature and sorbent size with respect to the mean response

From the above results for this specific set of experiment, a regression model was created that could be used to predict the sulphur sorption capacity at any temperature and sorbent size during desulphurisation. Since the interaction effect was so minimal the model would take the form of:

$$= \quad + \ _1 \ _1 + \ _2 \ _2 \qquad (6.6)$$

Where

Sorbent sulphur sorption capacity %

Average of all response at all levels

$_1$ A half of the main effect of temperature

$_2$ A half of the main effect of sorbent size

$_1$ Variable representing temperature

$_2$ Variable representing sorbent size

Where $_1$ and $_2$ are calculated by equations 5.5 and 5.6 given in section 5.2 of chapter 5. The final first order regression model is given by equation 6.7

$$y\ (Wt.\%) = 1.8413 - 0.7363x_1 - 0.6288\ x_2 \qquad (6.7)$$

To verify that the model fits the experimental data for this set of experiment, actual sulphur sorption capacity values obtained from the experiment were plotted against the predicted values (Figure 6.33). Figure 6.33 shows the values lie along the line of best fit indicating that the model fits well the experimental data giving an R^2 of 0.9421.

Figure 6.34 show a contour plot under a three-dimensional surface response diagram of sulphur sorption capacity obtained from the first order regression model with reaction temperature and sorbent size as the regressors. From Figure 6.34 the plane obtained from the first-order model rises at low levels of temperature and sorbent size and vice versa. This indicates that to obtain a high sulphur sorption capacity using the low surface area sorbent at an average space velocity of $610h^{-1}$, the reaction temperature should be low (<350 ^{0}C) and the sorbent size small (<1.63mm). The sulphidation reactions of zinc oxide pellets with H_2S have a negative Gibbs free energy ($\Delta G = -91607.18 + 15.16T\ J/mol$) indicating that they are thermodynamically capable of lowering H_2S levels at even ambient temperatures (Alexander and Bruce, 2011). Sorbent size will only be limited with the pressure drop across the bed. Figure 6.34 can therefore be used to obtain the optimum conditions for desulphurisation with the low surface area sorbent at an average space velocity of $610h^{-1}$.

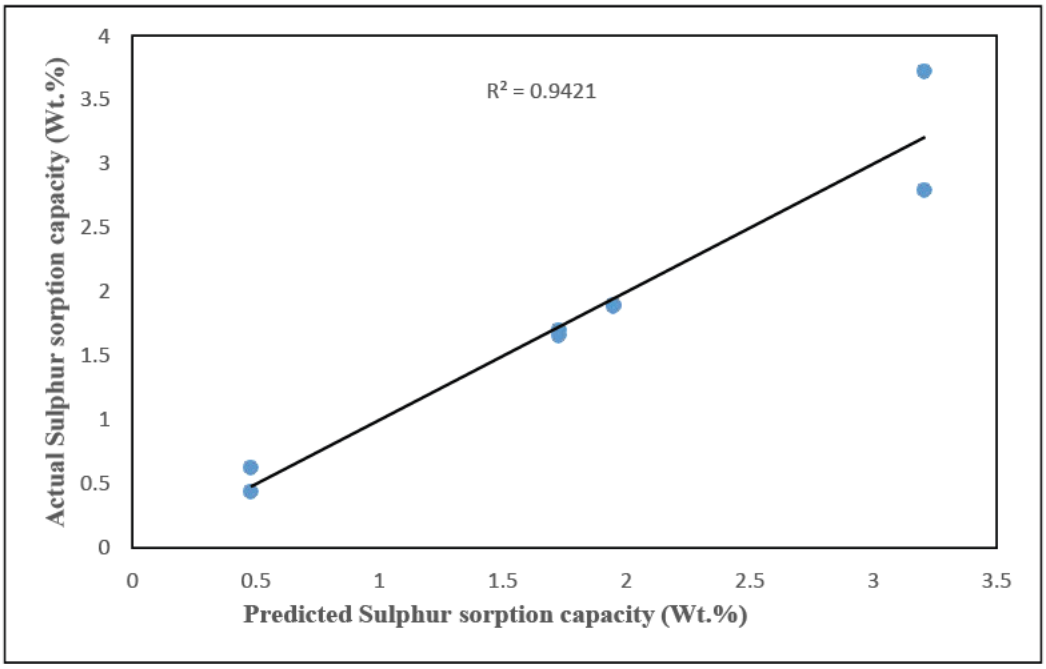

Figure 6.33 Parity plot of experimental data against predicted values of sulphur sorption capacity

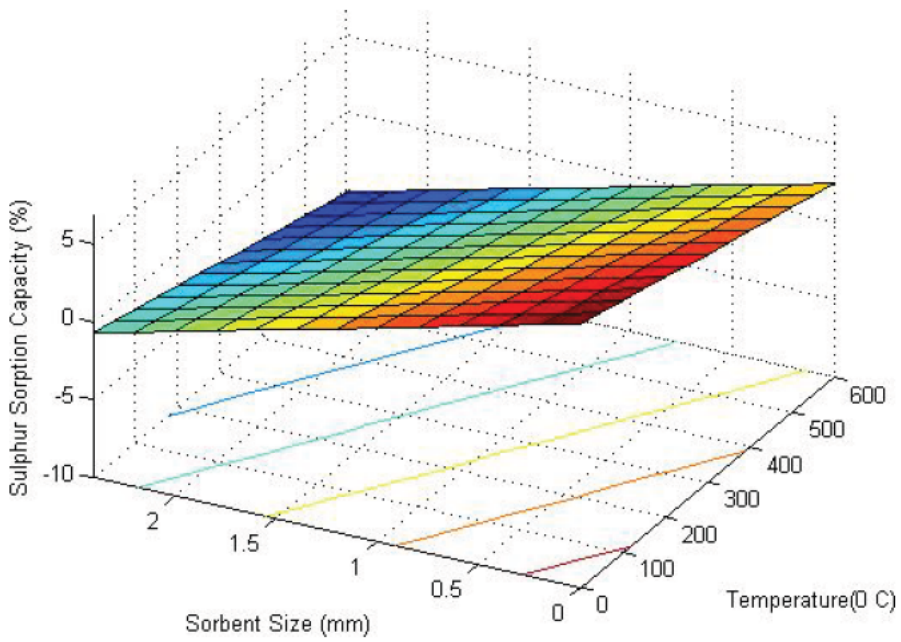

Figure 6.34 Surface and contour plot of the desulphurisation process using low surface area sorbent at low space velocities

6.4 Gas-Solid Reaction Modelling Results

The results of modelling for the desulphurisation process was limited to experiments performed using the low surface area sorbent at an average space velocity of 610h^{-1}. The fixed bed model outlined in section 4.2.3 adopted from Hepworth et al., (1997) was used in this study. It described the sulphidation process according to the shrinking core model. It was assumed that the process is isothermal. This assumption was verified experimentally from the reaction temperature profiles during desulphurisation given in Appendix C. The particle size of the zinc oxide was assumed to remain the same. This assumption was also verified by the physical appearance of the sorbent after the desulphurisation process which was similar to the initial fresh sorbent. The particle was also assumed to be non-porous. The adsorption isotherms (Figure 6.9 and 6.10) obtained from the BET analysis of the low surface area sorbents describes characteristics of non-porous and macro porous sorbent. As was mentioned before the pore sizes were in the range of macro porous materials (> 50nm). Research has shown that the shrinking core model does not describe well the sulphidation of porous material because it does not put into consideration the structural properties of the solid. Therefore for the shrinking core model to work for a macro porous material the global rate has to be controlled by the transport resistances that is mass transfer from the bulk gas to the surface of the pellet and diffusion through the porous product layer only and not the chemical reaction (Jothimurugesan and Harrison, 1990). For this to happen the chemical reaction rate must be very high so that the porous product layer would have been formed. Using this criterion the third term in the overall rate of the desulphurisation process can be dropped out during modelling since the reaction rate constant would be very high and its effect on Equation 4.45 (global rate of reaction) would be very negligible.

$$= \frac{3(1-\varepsilon)C_{Ab}}{}\left[\frac{1}{} + \frac{R}{}\left((1-X)^{-1/3} - 1\right) + \frac{1}{k(1-X)^{2/3}}\right]^{-1} \qquad (4.45)$$

The mass transfer coefficient and the effective diffusivity coefficient were taken from literature correlations and are thus approximate values. This has some limitations on the final model results because they are being used in situations which are far from which they were developed. Table 6.12 gives details of all the parameters used during the packed bed modelling.

Table 6.12 Model parameter values for packed bed sulphidation test

Parameter	Units	Run 1	Run 2	Run 3	Run 4	Source
	-	0.373	0.373	0.373	0.373	Calculated
	cm	0.815	0.102	0.0815	0.102	Measured
	cm/min	240	240	240	240	Jothimurugesan & Harrison,(1990)
	cm^2/min	6.4	6.4	6.4	6.4	Jothimurugesan & Harrison,(1990)
	cm	5.12	5.83	5.12	5.83	Measured
	cm/min	58.02	54.39	48.99	61.55	Calculated

The final packed bed model equations in terms of dimensionless parameters; Equation 4.46 and 4.47 were solved numerically using Euler's method at the initial boundary conditions given by Equations 4.48 and 4.49.

$$\frac{\partial C^\star}{\partial z^\star} = \frac{-r_A L}{0} \qquad (4.46)$$

$$\frac{}{\partial t^\star} = \frac{}{C_{A0} u} \qquad (4.47)$$

$$C^\star = 1 \; at \; z^\star = 0 \; at \; all \; t^\star \qquad (4.48)$$

$$X = 0 \; at \;\; t^\star = 0 \; at \; all \;\; z^\star \qquad (4.49)$$

The predicted breakthrough curves which were matched with the experimental breakthrough curves at the given conditions in Table 6.12 for each individual run are shown in Figure 6.36, 6.37, 6.38 and 6.39.

In all results none of the experimental breakthrough curves matched well with the predicted ones. Although at the initial stages of the process there was good agreement the reason that could only explain these are factors that could affect the movement of H_2S into the bulk of the sorbent. This

could be because of the other factors that affected the desulphurisation process as was discussed in section 6.2.5. These factors include effect of the CO in the syngas to the desulphurisation process resulting in the reduction of H_2S to COS which cannot be absorbed by zinc oxide pellets and therefore no reactant to absorb. The other and most influential factor with regard to transport resistances would be the deposition of carbon onto the surface of the sorbent, blocking the pores and therefore interfering with the mass transfer of the bulk gas to the surface of the particle. If there is no reactant penetrating the surface, the porous product layer would not be formed and consequently affecting the diffusion through the product layer resulting in short breakthrough times. In addition to this the reason could also be the use of external mass transfer and diffusion coefficients which do not match with this studies experimental condition.

The predicted breakthrough curves for run 1, 2 and 3 as described in Table 6.7 (SPLT, BPLT and SPHT respectively) support the experimental data with regard to the high sulphur sorption capacities. This is shown from the breakthrough points of the model breakthrough curve. The dimensionless time is a ratio of any time during desulphurisation over the theoretical time for complete sulphidation. Therefore it gives the conversion in terms of time. For run 1, the dimensionless time at breakthrough point was 0.62 which indicates a 62% conversion. For run 2 and 3 were 0.52 and 0.42 indicating 52 and 42 % conversions respectively. From the experimental results in order of increasing the sorbent sulphur sorption capacity run 4< run3<run 2< run 1 which matches well with the predicted values except for run 4. In conclusion the shrinking core model can be used to describe sulphidation of porous material only if the transport resistances control the global rate of reaction.

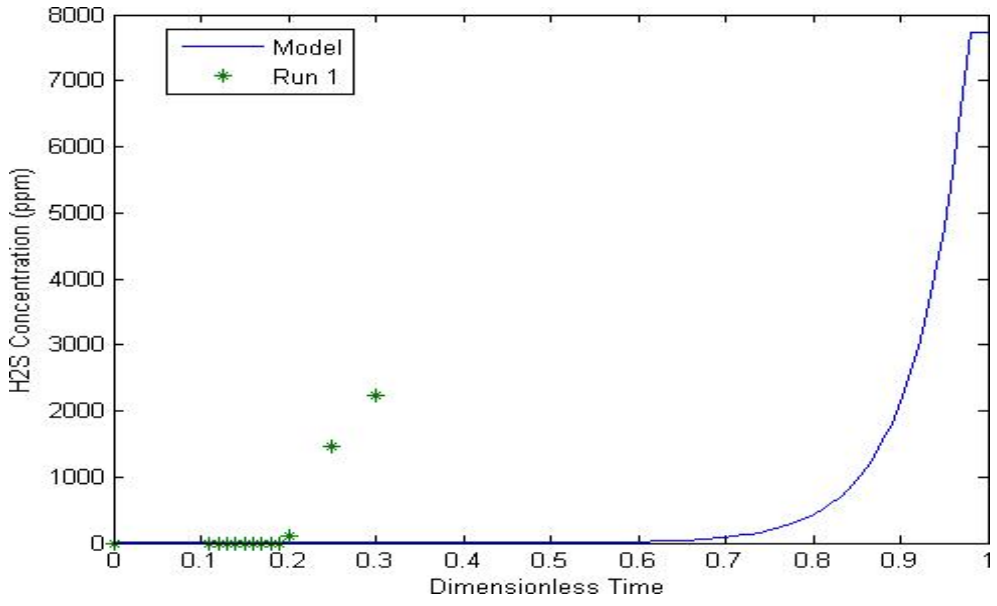

Figure 6.35 Predicted (-) and Experimental (*) breakthrough curves for small particles at low temperature run using the low surface area sorbent at 680h^{-1}

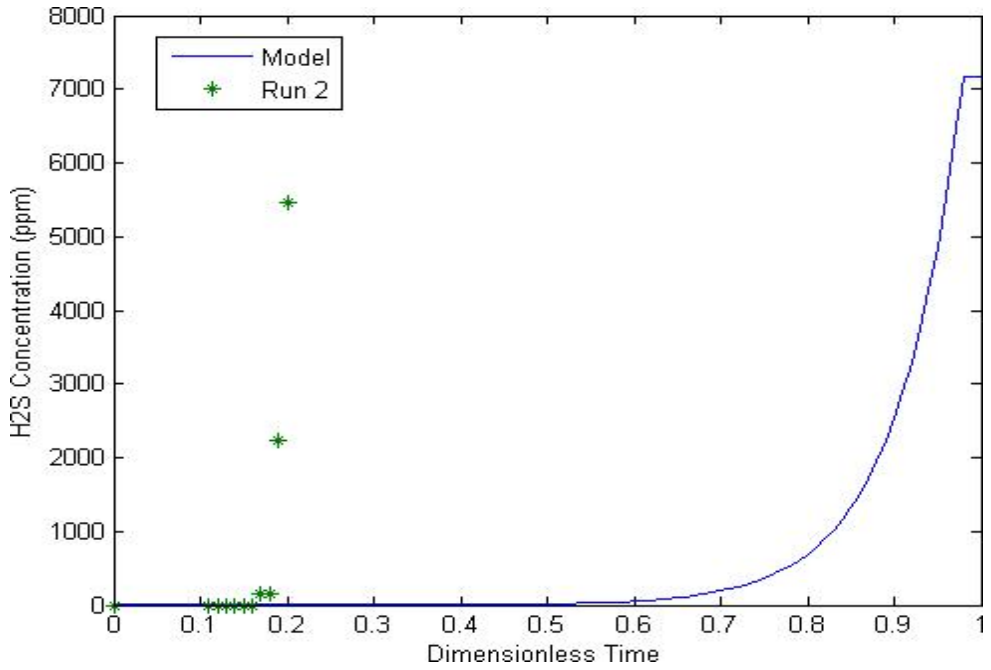

Figure 6.36 Predicted (-) and Experimental (*) breakthrough curves for large particles at low temperatures run using the low surface area sorbent at 560.14h^{-1}

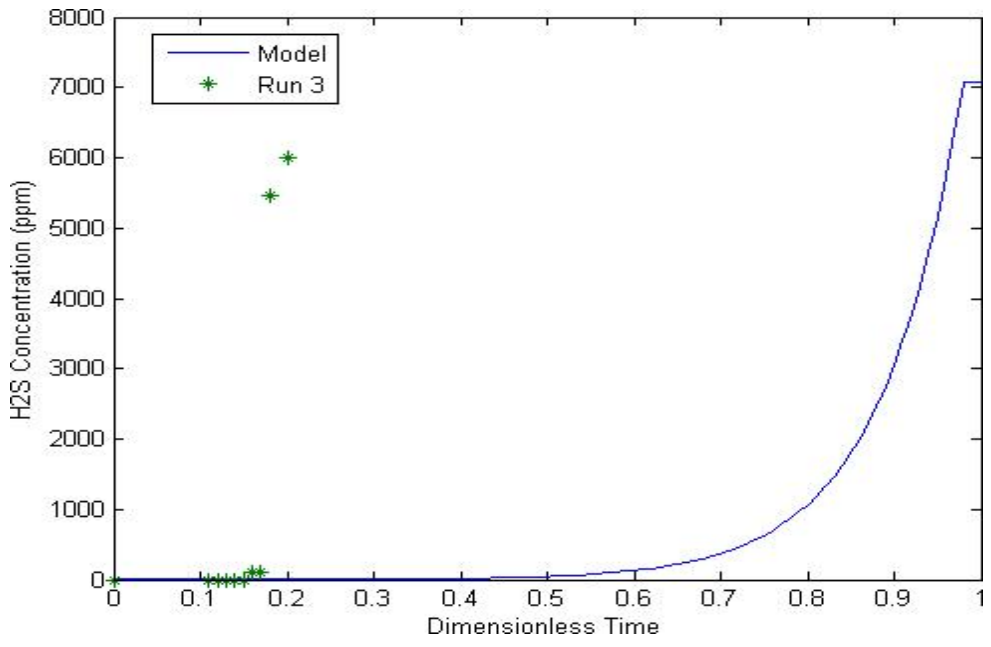

Figure 6.37 Predicted (-) and Experimental (*) breakthrough curves for small particles at high temperature run using the low surface area sorbent at 574.28h^{-1}

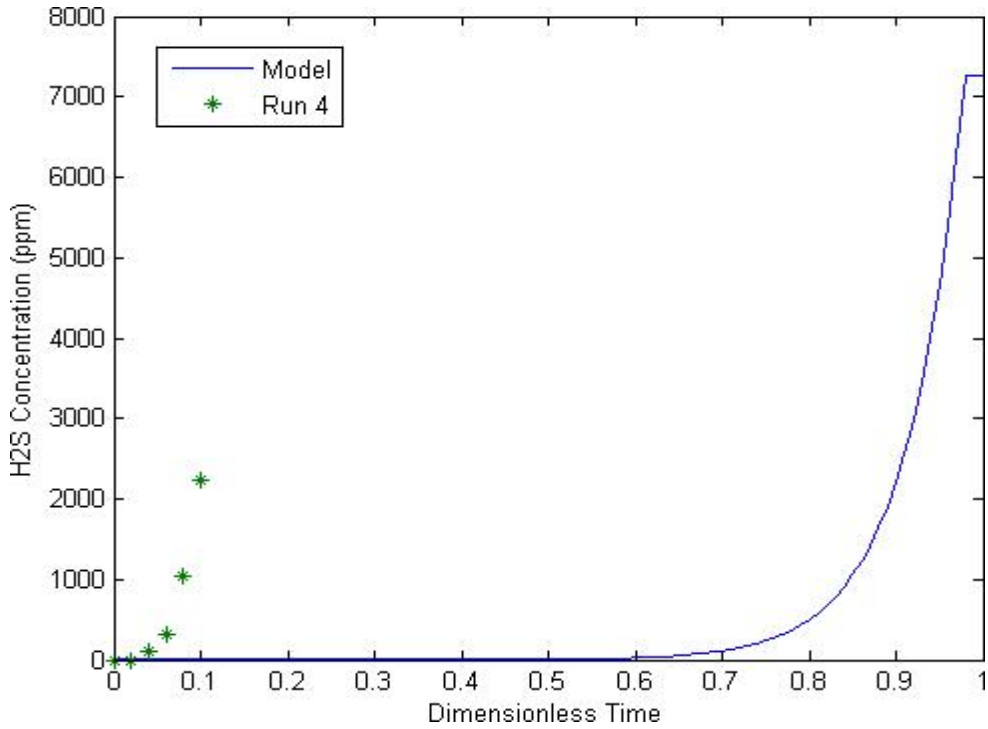

Figure 6.38 Predicted (-) and Experimental (*) breakthrough curves for large particles at high temperature run using the low surface area sorbent at 633.89h^{-1}

Chapter 7

CONCLUSION AND RECOMMENDATION

Production of syngas containing H_2S using a fuel mixture of 86% methanol and 14 % 2-propanethiol at 830 ^{0}C at atmospheric pressure was achieved. The use of liquid fuels to produce syngas containing H_2S has not been implemented elsewhere. This prevented the use of many gas cylinders and flow controllers to simulate syngas for hot gas desulphurisation studies. Preliminary experiments worked with liquid fuel flow of 0.108cm^3/s at an oxygen flow of 4.867cm^3/s. This resulted in production of 0.5-1 mole % H_2S. This fuel flow gave rise to a low sulphur sorption capacity during desulphurisation and was lowered to 0.042cm^3/s at an oxygen flow of 4.867cm^3/s. The low fuel flow resulted in production of 1-1.5 mole % H_2S. In both cases the H_2S concentrations were consistent within the range. The composition of syngas produced was analysed using GC fitted with a TCD detector. The experimental composition was compared to the results of simulation performed in ASPEN plus for equilibrium prediction of syngas composition during gasification. Good agreement between the concentration of H_2, CO and CH_4 was achieved. The rest of the components; H_2S, CO_2 and H_2O were not in agreement with the predicted compositions. The gasification process produced a H_2/CO ratio of 1.97:1 as was expected. For future studies it is recommended to have several sampling points on the gasifier to exactly establish the position at which the equilibrium syngas components are formed along the gasifier. This would verify the assumption that they are formed within seconds.

A 2*2 factorial design was adopted in the desulphurisation process where, sorbent particle size, and reaction temperature were varied at high and low levels using varied sorbent surface area and space velocity. The variation was to study the effect of all this factors towards the desulphurisation ability of zinc oxide pellets packed in a fixed bed reactor and observe if there was any interaction between the factors. Low sulphur sorption capacities were obtained at high space velocity on average of 3430h^{-1} (1.03-0.21 Wt. %) and sorbent surface area on average of 25m^2/g (1.07-0.047 Wt. %). The best results were obtained using low surface area sorbent (5.3m^2/g) at space velocity on average of 610h^{-1} (3.71-0.4 Wt. %) . This gave a conversion of 20%. In future work it is recommended to synthesize a high surface area zinc oxide pellets from precipitation methods and add precursors that would enhance the absorption of COS to further study the effect of sorbent surface area. In addition the online GC can be fitted with two detectors in series, to analyse both sulphur compounds and the other components of the syngas at the same time. This would explain better the effect of the syngas composition on the desulphurisation process. To prevent any chances of channelling in the packed bed it is recommended to place the packed bed in a vertical position.

Statistical analysis performed showed that there was no interaction between temperature and sorbent particle sizes. Variance analysis verified that low temperature had a higher effect to the sulphur sorption capacity than the small sorbent size. The surface response diagram obtained from a first order regression model for this set of experiment showed that to achieve a high sulphur sorption capacity, temperature and sorbent size should be kept at their low levels (<350 ^{0}C and <1.63mm).

Finally a packed bed model based on the shrinking core model was used to describe the desulphurisation process. There was no good agreement between the experimental and predicted breakthrough curve. Despite this the predicted conversion followed the same trend as the experimental data except at reactions using large particles at high temperature. To further clarify the assumption that transport resistances are rate controlling in porous pellets it is recommended that measures to prevent occurrence of these resistances should be put in place during experimentation. Alternatively the grain model could be adopted since it caters for porous materials with structural changes.

References

Alexander, S., and Bruce, J.T., (2011). Characterization of active sites, determination of mechanisms of H_2S, COS, and CS_2 sorption and regeneration of ZnO low-temperature sorbent: past, current and perspectives. *Phys.Chem. Phys.Chem*, **13**, 3197-3209

Altafini, C.R., Wander, P.R., and Barreto, R.M., (2003). prediction of the working parameters of a wood waste gasifier through an equilibrium model. *Energy conversion and management*.44:2763-2777

Artos, V., Benito, Y., Garcia, P., and Otero-Ruiz, J., (1995). Design of a Hot Gas desulphurisation plant, *Coal Science and Technology*, **24:**1879-1882

Botha F.M., (2010). Production and High temperature Treatment of Syngas, MSc Dissertation, University of Kwazulu Natal, South Africa

Buragohain, B., Mahanta, P., and Moholkav, V.S., (2010). Thermodynamic optimization of biomass gasification for decentralized power generation and Fischer-Tropsch synthesis. *Energy*, 35:2557-2579

Bambang, S.R., (2013). The assessment of syngas utilization by Fischer-Tropsch synthesis in the slurry- bed reactor using Co/SiO_2 catalyst, *International Journal of Engineering and Applied Sciences*, 4:1

Bolis, V., Bice, F., and Elio, G., (1989). Effect of form on the surface reactivity of differently prepared zinc oxides. *J.Chem,Soc., Faraday Trans. I*, 85(4), 855-867

Chiche, D., Diverch, C., Lucquin, A-C., Porcheron, F., and Defoort, F., (2013). Synthesis gas purification, *OGST Journal*, 68:4, 621-783

Christopher, H., and Maarten Van der Burgt., (2008). *Gasification*, 2nd Edition, Gulf professional publishing, UK

Chunshen, C., Gordon, X. Jamie, H., Evans, J., Yong, W., (2003). Kinetic studies of methanol steam reforming over Pd/ZnO catalyst using a microchannel reactor, *Journal of Applied catalysis*, **262(19-29)**

Colin, F.P., (2003). *The Essences of Chromatography*. Elsevier

Corrie, L.C., and Kenneth J.K., (2001). Unique Chemical Reactivities of nanocrystalline metal oxides toward Hydrogen Sulfide. *Chem. Material*, 14: 1806-1811

Davidson O, Winkler H, Kenny A, Prasad G, Sparks D, Howells M, Alfstad T, Mwakasonda S, Cowan B and Visagie E, (2006). Energy policies for sustainable development in South Africa: Options for the future, Cape Town, Energy Research Centre. [Online], Available from<http:// www.erc.uct.ac.za/publications/Energy%20policies%20for%20SD.pdf>[accessed on 17th July 2014]

Department of Energy (DOE) Republic of South Africa, (2013). Renewable Energy, South Africa. [Online] Available from<http://www.energy.gov.za/files/renewables_frame.html> [Accessed on 20th July 2014]

Department of Environmental Affairs (DEA), (2013). Highveld priority area air quality managementexecutivesummary.[Online]Availablefrom.<http://www.airqualitylekgotla.co.za/assets/hpa-aqmp-executive-summary---with-coverpage.pdf> [Accessed on 20th July 2014]

Doraiswamy .L.K and Sharma M.M., (1984). *Heterogeneous reactions: Analysis, examples and reactor design. Volume I: Gas-solid and solid-solid reactions*, John Wiley & Sons, New York

Dushyant, S., Spivey, J.J. & David, A.B., (2011). *Fuel Cells: Technologies for fuel processing*, Elsevier Science

Edouard, H., Bernard, C., Robert, D., Catherine, L.,Renaud, C., and Vasile, H., (2013). A highly efficient process for transforming methly mercaptan into hydrocarbons and H_2S on solid acid catalysts, *Applied Catalysis B: Environmental*, **134-135**:344-348

Everett, C.E., and Monaco, S.J., (1994). Data summary for M-W Kellog Zsorb sorbent tests. CRADA 92-008 Final report, US department of Energy, DOE/METC-96/1034

.

Everrentt, D.H., (1972). Manual of symbols and terminology for physicochemical quantities and units. Appendix II: Definations, terminology and symbols on colloidal and surface chemistry, Part 1: Colloid and surface chemistry. *Pure Applied Chemistry*, 31:577-638

Frank, B., Jentoft, F.C., Soerijanto, H., krohnert, J., Scholgl, R. and Schumacker, R., (2007). Steam reforming of methanol over copper-containing catalysts: Influence of support material on microkinetics, *Journal of catalysis*, **246(1),** 177

Ghencio, A.F., (2002). Review of fuel processing catalysts for hydrogen production in PEM fuel cell systems, *Curr Opin Solid St M*, **6:389(99)**

Gibson, J.B., and Harrison, P.D., (1980). The reaction between Hydrogen sulfide and sphereical pellets of zinc oxide. *Industrial Engineering Chem. Process Des.Dev*, 19:231-237

Gupta, R., Gangwal, S.K., and Jain S.C., (1992).Preprint of paper for publication in Energy and Fuels

Heesink, A.B.M., Prins, W., and Van Swaaij, W.P.M., (1993). A grain size distribution model for non-catalytic gas-solid reactions, *The Chemical Engineering Journal*, 53:25-37

Hepworth, M.T., Berns, J.J., Sadecki, K.A., (1997). Kinetics of Mn-Based sorbents for hot coal gasdesulphurisation.[Online]Availablefrom.http://www.fischer-tropsch.org/DOE/DOE_reports/94212/94212-11.pdf> [Accessed on 12th October 2014]

Hohn, K. L., & Lin, Y.-C., (2009). Catalytic partial oxidation of methanol and ethanol for hydrogen generation. *ChemSusChem*, *2*(10), 927–40. doi:10.1002/cssc.200900104

Holladay, J.D., Wang, Y. & Jones, E., (2004). Review of developments in portable hydrogen production using micro reactor technology. *Chemical Review*. **104:4767**

Horazak DA, Newby RA, Smeltzer EE, Slimane RB, Vann Bush P, Aderhold Jr JL and Bryan BG., (2005). Novel gas cleaning/ conditioning for integrated gasification combined cycle.Volume I - Conceptual commercial evaluation, Final Report, DOE Award Number: DE-AC26-99FT40674

Horn, R., Williams, K.A., Degenstein, N.S. & Schmidt, L.D., (2006). Syngas by catalytic partial oxidation of methane on rhodium: mechanistic conclusions from spatially resolved measurements and numerical simulation. *Journal of Catalysis*. **242:92**

Huiling F, Yanxu L, Chunhu L, Hanxian G and Kechang X., (2002). The apparent kinetics of H2S removal by zinc oxide in the presence of hydrogen, *Fuel*, **81**, 91-96

Jain, P., Mayank, B., Mark, S., and Junghuan, Y., (2014). Regenerable Oxide -Base sorbent. US Patent No 2014127106A1

James, G. Speight., (2011). Handbook of industrial Hydrocarbon processes, Elsevier Inc, 281-323 doi:10.1016/B978-0-7506-8632-7.10008-8

Jeffrey Phillips, (2006). Different type of gasifiers and their intergration with gas turbines, Gas TurbineHandbook[online]availablefrom<http://www.netl.doe.gov/File%20Library/Research/Coal/energy%20systems/turbines/handbook/1-2-1.pdf> [Accessed on 14th July 2014]

Johan, A., Magali, B., and Jose, L.G.F., (2003). Production of hydrogen from methanol over binary Cu/ZnO catalysts: Part II. Catalytic activity and reaction pathways, *Applied Catalysis A: General*, **253,** 213-223

Jothimurugesan K and Harrison D.P., (1990). Reaction between H2S and zinc oxide-titanium oxide sorbents. 2. Single-Pellet Sulfidation Modeling, *Industrial and Engineering Chemistry Research*, **29 (7),** 1167-1172

Ke, L., Chunsan, S. & Subramani, V., (2010). *Hydrogen and syngas production and purification technologies*, New Jersey, USA: John Wiley & Sons Publication

Keith, L.H. & Yu Chuan Lin., (2009). Catalytic partial oxidation of methanol and ethanol for hydrogen generation. *Chemsuschem* **2:927-940**

Klobes, P., meyer, K., and Munro, R.G., (2006). *Porosity and specific surface area measurements for solid materials*. US department of Commerce, technology Administration, National Institute of Standards and Technology

Koga, H., Fukahori, S., Kitaoka, T., Tomoda, A., Suzuki, R., & Wariishi, H., (2006). Autothermal reforming of methanol using paper-like Cu/ZnO catalyst composites prepared by a papermaking technique. *Applied Catalysis A: General*, *309*(2), 263–269. doi:10.1016/j.apcata.2006.05.014

Kohl A and Riesenfeld F., (1979). *Gas Purification*, 3rd edition, Gulf Publishing Company, Houston, Texas

Lattner, J. R., & Harold, M. P., (2007). Autothermal reforming of methanol: Experiments and modeling. *Catalysis Today*, *120*(1), 78–89. doi:10.1016/j.cattod.2006.07.005

Levenspiel O., (1979). *Chemical Reactor Omnibook*, OSU Book Stores

Levenspiel O., (1999). *Chemical Reaction Engineering*, 3rd edition, John Wiley & Sons, New York

Lew S, Sarofim AF and Flytzani-Stephanopoulos M., (1992 a). Sulfidation of Zinc Titanate and Zinc Oxide Solids, *Industrial and Engineering Chemistry Research*, **31 (8),** 1890-1899

Lew S, Sarofim AF and Flytzani-Stephanopoulos M., (1992 b). Modeling of the sulfidation of zinc-titanium oxide sorbents with hydrogen sulfide, *American Institute of Chemical Engineers Journal*, **38 (8),** 1161-1169

Li Y, Guo H, Li C and Zhang S., (1997). A Study on the Apparent Kinetics of H2S Removal Using a ZnO-MnO Desulfurizer, *Industrial and Engineering Chemistry Research*, **36 (9),** 3982-3987

Li, L., and King, D., (2006). H2S removal with ZnO during fuel processing for PEM fuel cell applications. *Catalysis Today*. 116:537-41

Li, X., Grace,J.R., Watkinson, A.P., Lim, C.J., and Ergundenier, A., (2001). Equilibrium modelling of gasification : a free energy minimisation approach and its application to a circulating fluidized bed coal gasifier, Fuel, 80:195-207

Li, Y., Zhang, S., Guo, H., and Zhong, B., (1997). Application of the shrinking core model to the kinetics of ZnO desulphurisation. *Chinese Journal of Chemical Engineering*, **5(4**):296-303

Lyubovisky, M., Roychoudhury, S. & La Pierre, R., (2005). Catalytic partial oxidation of methane to syngas at elevated pressures. *Catalysis letters*. **99:113**

.

Mahin Rameshni, P.E., (2000). State of the art in Gas treating, [Online] Available from <http://www.coltena.com/CSG/Hydrocarbons/Speciality capabilities/Documents/State of-the-art-in-Gas-Treating.pdf> [Accessed on 17th September 2014]

Maria, P., Joan, C.B., and Alberto, C., (2010) Review and analysis of biomass gasification models, *Renewables and Sustainable energy reviews*.14(9):2841-2851

Mary H. and Alison H., (2007) Clean Energy and Development for South Africa: Background Data, Report 1 of 3, Energy Research Centre UCT South Africa. [Online] Available from

<http://www.eri.uct.ac.za/Research/publications/07Haw-Hughes%20clean%20energy%20& %20development%20- %20.pdf?> [Accessed 16th July 2014]

Maciejewski, M., and Oswald, H.R., (1985). Morphological observation on the Thermal decomposition of Calcium Carbonate. *Thermochim Acta*, 85(1):39-42

Moezzi, A., Andrew, M.M., and Michael, B.C., (2012). Zinc oxide particles synthesis, properties and applications, *Chemical Engineering Journal*, 185-186 (1-22)

Montgomery, D.C., Raymond, H.M., and Christine, M.A-C., (2012). *Response Surface Methodology: Process and Product Optimisation using Designed Experiments*. 3rd Edition, WILEY Publication

National Energy Technology Laboratory (NETL)., (2013 b). Gasification cleaning and Conditioning, Department of energy USA. [Online] Available from <http://www.netl.doe.gov/technologies/coal power/gasification/gas-clean/index.html> [Accessed on 15th September 2014]

National Energy Technology Laboratory (NETL)., (2013 a). Introduction to Gasification, DepartmentofEnergy,USA.[Online Available from:http://www.netl.doe.gov/research/coal/energy-systems/gasification/gasifipedia/intro-to-gasification [Accessed on 10th July 2014]

Nick, K., Simbeck, D.R., and Wilhem, D.S., (2002). Process screening analysis of alternative gas treating and sulphur removal for gasification. SFA Pacific,Inc. Mountain View, CA

Nikoo, M.K., and Amin, N.A.S., (2010). Thermodynamic analysis of carbon dioxide reforming of methane in view of solid carbon formation. *Fuel processing Technology*, 92:687-691

Niksiar, A., and Rahimi, A., (2009). A study on deviation of non-catalytic gas-solid reaction models due to heat effects and changing of solid structure. *Powder technology*, 193:101-109

Novochinskii, I.I., Song, C., Ma, X., Liu, X., Shore, L., Lampert, J., and Farrauto, R.J., (2004). Low temperature H2S removal from steam-containing gas mixtures with ZnO for fuel cell application, 1. Zno particles and extrudates, *Energy Fuels*, 18:576

Osman K, Coquelet C, Ramjugernath D., (2013). Review of carbon dioxide capture and storage with relevance to the South African power sector. South Africa Journal of Science 2014; 10 (5/6), Art. #2013-0188

Palo, D.R., Dagle, R.A. & Holladay, J.D., (2007). Methanol steam reforming for hydrogen production. *Chemical reviews*. **107(10):3992**

Perry HP and Green DW (editors), (1999). *Perry's Handbook of Chemical Engineering*, 7th edition, McGraw Hill, New York

Prevost X., and Msibi L., (2005). Coal SAMI (South Africa's Mineral Industry) 2004 – 2005, DME Raal JD and Mühlbauer AL (1998). *Phase Equilibriua; Measurement and Computation*, Taylor and Francis, Bristol, Pennsylvania

Ranade MG and Evans J.W., (1980). Reaction between a gas and a solid in a nonisothermal packed bed- simulation and experiments, I*ndustrial and Engineering Chemistry Process Design and Development*, **19 (1),** 118-123

Rezaiyan J and Cheremisinoff N.P., (2005). *Gasification Technologies*, Taylor and Francis Group, Boca Raton, Florida

Ronald, W.B., 2010, Gasification processes, Old and New: A basic review of the major technologies, *Energies*, 3:216-240

Rostrup-Nielsen, J. & Lars, J.C., (2011). *Concepts in syngas manufacture*, London: World scientific publishing Co

Samson, M.A., Shaharin, S.A., and Suzana, Y., (2011). A simulation study of downdraft gasification of oil-palm fronds using ASPEN PLUS. *Journal of Applied Sciences II*. 11:1913-1920

Sánchez-Hervás JM, Otero J and Ruiz E., (2005). A study on sulphidation and regeneration of Z-Sorb III sorbent for H2S removal from simulated ELCOGAS IGCC syngas, *Chemical Engineering Science*, **60**, 2977 – 2989

Santosh, K. Gangwal, (2011). *Desulfurization for Fuel cells*, Copyright, Elsevier

Seader JD and Henley EJ., (2006). *Separation Process Principles*, 2nd edition, John Wiley & Sons, New York

Shangguan J., Yousheng, Z., Huiling, F., Litong, L., Fang, S., and Maoqian, M., (2011). Desulfurization behaviour of zinc oxide sorbent modified by the combination of Al_2O_3 and K_2CO_3. *Fuel*, **108**:80-84

Shen, J., and Smith, J.M., (1965). Diffusional effects in gas-solid reactions. *I & EC Fundamentals*, 4:293-301

Siddle, A., pointon, K.D., Judd, R.W., and Jones, S.L., (2003). Fuel processing for fuel cells- A status review and assessment of prospects. *A report of Advantica Ltd*. ETSU F/03/00252/Rep.URN 031644

Sing, K.W.S., Everret, D.H., Haul, R.A., Moscou, L., Pierotti, R.A., Rouquerol, J., and Siemieniewska, T., (1984). Reporting physisorption data for gas/Solid systems with special reference to the determination of surface area and porosity, *Pure and Applied Chemistr*y.603-619

Siriwardane, R.S., and Cicero, D.G., (2000). Durable zinc-oxide containing regenerable desulphurisation sorbents for both low and high temperature applications. Proceedings of AICHE Spring national Meeting. High temperature gas cleaning (gases and particles), session 7F004

Smith, J.M., Van Ness, H.C., and Abbott, M.M., (2001). *Introduction to Chemical Engineering Thermodynamics*, 6th Edition, McGraw- Hill, Singapore

Snavely. K., and Subramaniam, B., (1998). Thermal conductivity detector analysis of hydrogen using helium as carrier gas and Hysep D column, *Journal of chromatography science*, 36

Sotirchos, S.V., and Krishan, S.V., (1993). A variable diffusivity shrinking core model and its application to the direct sulfation of limestone. *The Canadian Journal of Chemical Engineering*, 71:734-745

Spath, P.L., and Dayton, D.C., (2003). Technical and Economic assessment of synthesis gas to fuels and chemicals with emphasis on the potential for Biomass-Derived syngas, Technical report National Renewable Energy Laboratory. USA

Subramani, V., Suzuki, K. & Osaki, T., (2006). Selective production of hydrogen by partial oxidation of methanol over catalyst derived from CuZnAl-layered double hydroxides. *Catalysis letters*. **10-1999**(62):159-167

Szekely J, Evans JW and Sohn HY., (1976). *Gas-solid reactions*, Academic Press, New York

Thompson, C.J., Meyer, R.A., and Ball, J.S., (1951). Thermal decomposition of sulphur compounds. I. 2-methly-2-propanethiol. [Online] Available from <http://pubs.acs.org/doi/pdf/10.1021/ja01133a019> [Accessed on 21st January 2014]

Trim,D.L., and Onsan, Z.I.,(2001). Onboard fuel conversion for hydrogen-fuel-cell-driven vehicles, *Cat Rev Scie Eng*, **43:31(84)**

Trunschke, A., (2013). Surface area and pore size determination. Heterogenous Catalysis Research

Turton R, Berry DA, Gardner TH and Miltz A., (2004). Evaluation of Zinc Oxide Sorbents in a Pilot-Scale Transport Reactor: Sulfidation Kinetics and Reactor Modeling, *Industrial and Engineering Chemistry Research*, **43 (5),** 1235-1243

Valco Instruments Co. Inc., (2009). Sample injection with a 6 port valve [online]. Available from: http://www.vici.com/support/app/app11.php, [Accessed 5th December 2013]

Victor S. Robinson, (1978). Method for preparing particulate zinc oxide shapes of high surface area and improved strength, U.S Patent No 4071609. [online] Available from < www.google.com/patents/US4071609> [Accessed on 4th December 2013]

Westmoreland PR and Harrison D.P., (1976). Evaluation of candidate solids for high-temperature desulfurization of low-Btu gases, *Environmental Science & Technology*, **10 (7)**, 659-661

Westmoreland PR, Gibson JB and Harrison D.P., (1977). Comparative Kinetics of High-Temperature Reaction between H2S and Selected Metal Oxides, *Environmental Science & Technology*, **11 (5)**, 488-491

Woods MC, Gangwal SK, Jothimurugesan K and Harrison D.P., (1990). Reaction between H2S and zinc oxide-titanium oxide sorbents. 1. Single-pellet kinetic studies, *Industrial and Engineering Chemistry Research*, **29 (7)**, 1160-1167

World nuclear organization, (2014). Nuclear power in South, South Africa. [Online] Available from < http://www.world-nuclear.org/info/country-profiles/countries-o-s/south-africa/> [Accessed on 16th July 2014]

Xin, M., Liwei, P., Na, L., Chunxi, Z., Shiying, L., Guanquan, S., and Shudong, W., (2007). *International Journal of Hydrogen Energy*, **32:3327**-3334

Yagi, S., and Kunii, D., (1955). Studies on combustion of carbon particles in flames and fluidized beds, Proceedings 5th Int. Symp. on combustion

Yong Zhang., (2004). Models of High Temperature Desulphurisation using Zinc Based sorbents. MSc Dissertation, West Virginia University, USA

Yu-Chuan, Lin, (2006). Methanol: *A chemical probe and Hydrogen source by catalytic partial oxidation*, a dissertation, Kansas State University, U.S.A

Yumura M and Furimsky E., (1985). Comparison of CaO, ZnO, and Fe2O3 as H2S adsorbents at High Temperatures, *Industrial and Engineering Chemistry Research*, **24 (4)**, 1165-1168

Yunhan, X., Zhen, L., Wang, B., Lifeng, Z., and Jingling, C., (2012).Thermodynamic performance Assessment of IGCC power plants with various syngas clean-up processes, *J.Therm. Sci.* **21:5**, 391-404.

Zainal, Z.A., Ali, R., lean, C.H., and Seetharamu, K.N., (2001). Prediction of performance of a downdraft gasifier using equilibrium modelling for different biomass materials. *Energy conservation and Management*, 42:1499-1515

Appendix A- Calibration Graphs and Standard Tables

A1.Calibration Graphs

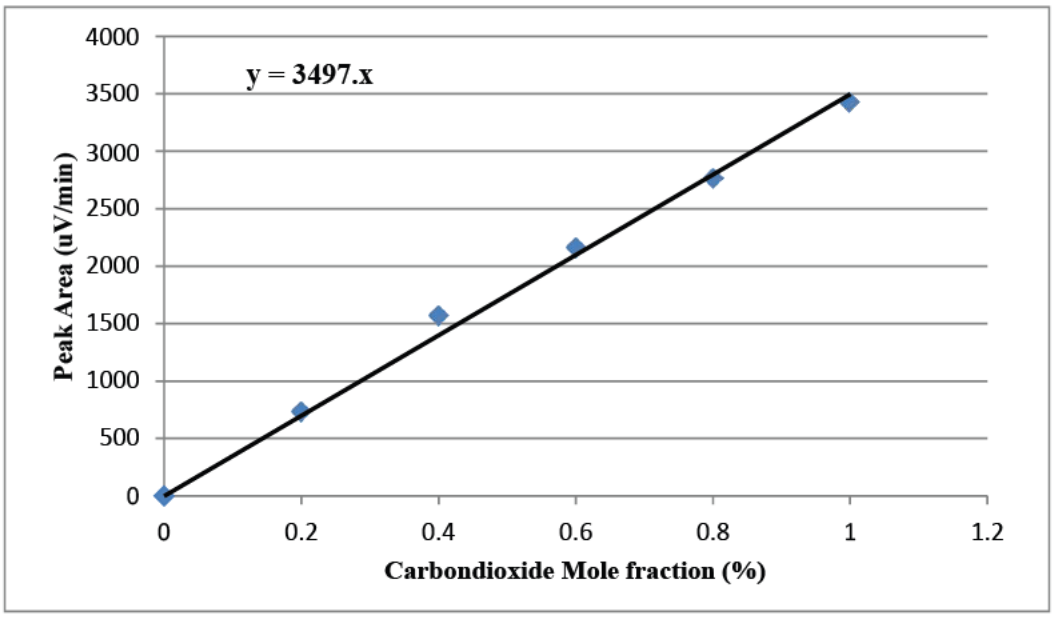

Figure A. 1 Graph showing the response of CO_2 gas when varying volumes representing the specific mole fractions of CO_2 are injected in GC with TCD

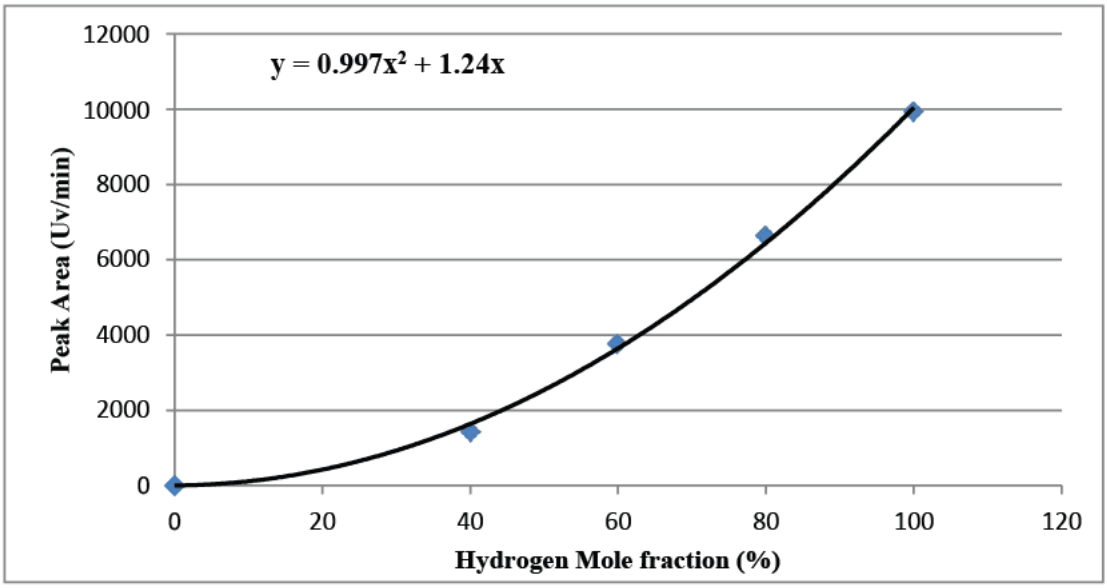

Figure A. 2 Graph showing the response of H_2 gas when varying volumes representing the specific mole fractions of H_2 are injected in GC with TCD

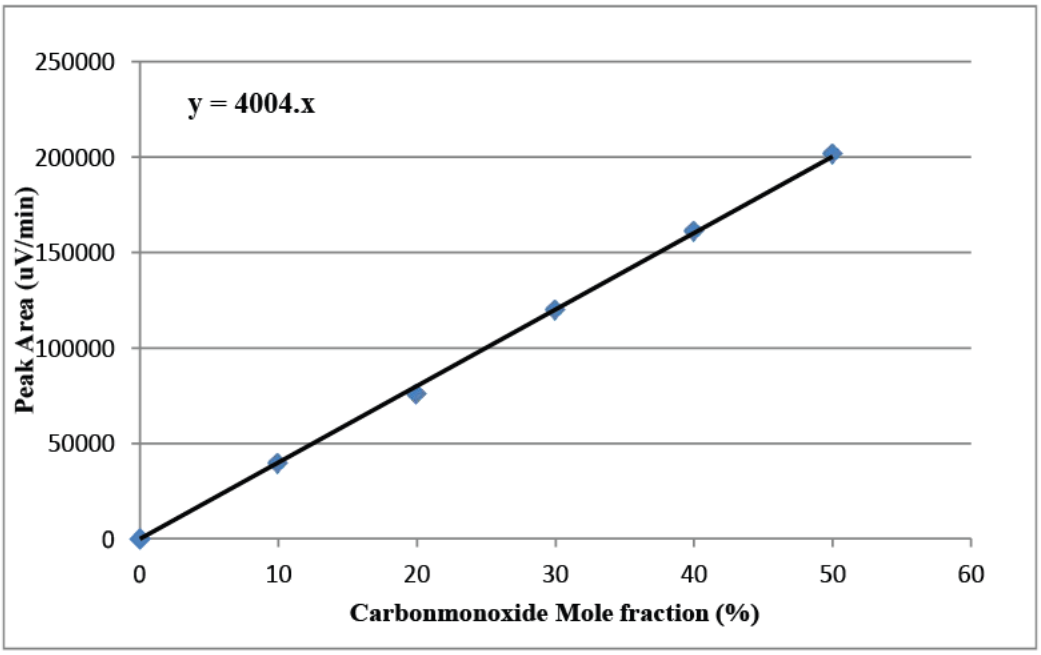

Figure A. 3 Graph showing the response of CO gas when varying volumes representing the specific mole fractions of CO are injected in GC with TCD

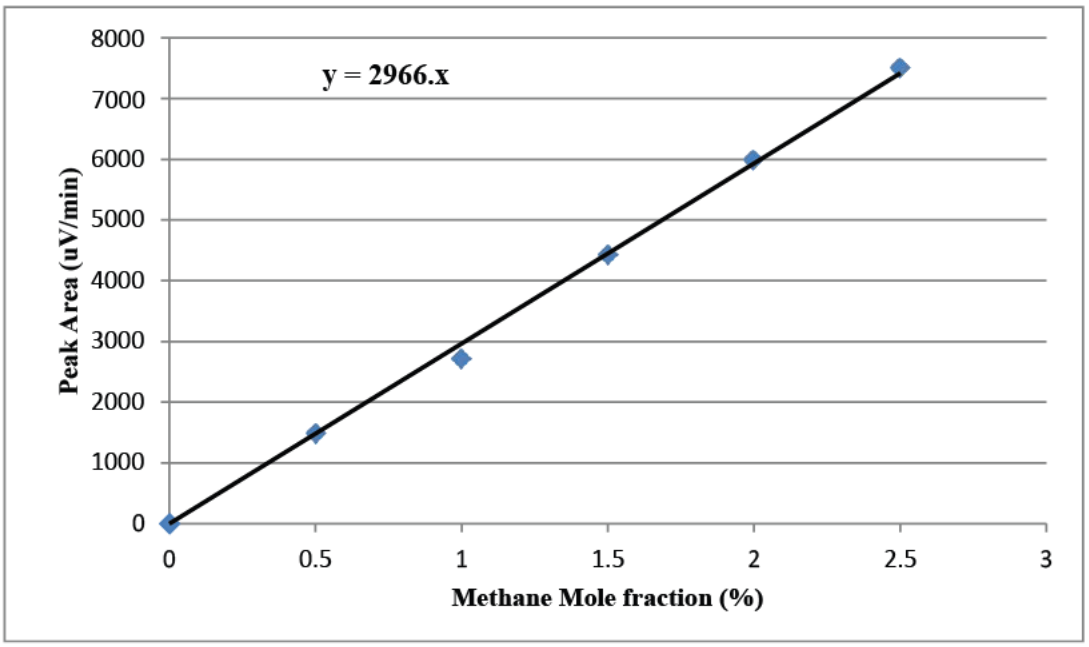

Figure A. 4 Graph showing the response of CH_4 gas when varying volumes representing the specific mole fractions of CH_4 are injected in GC with TCD

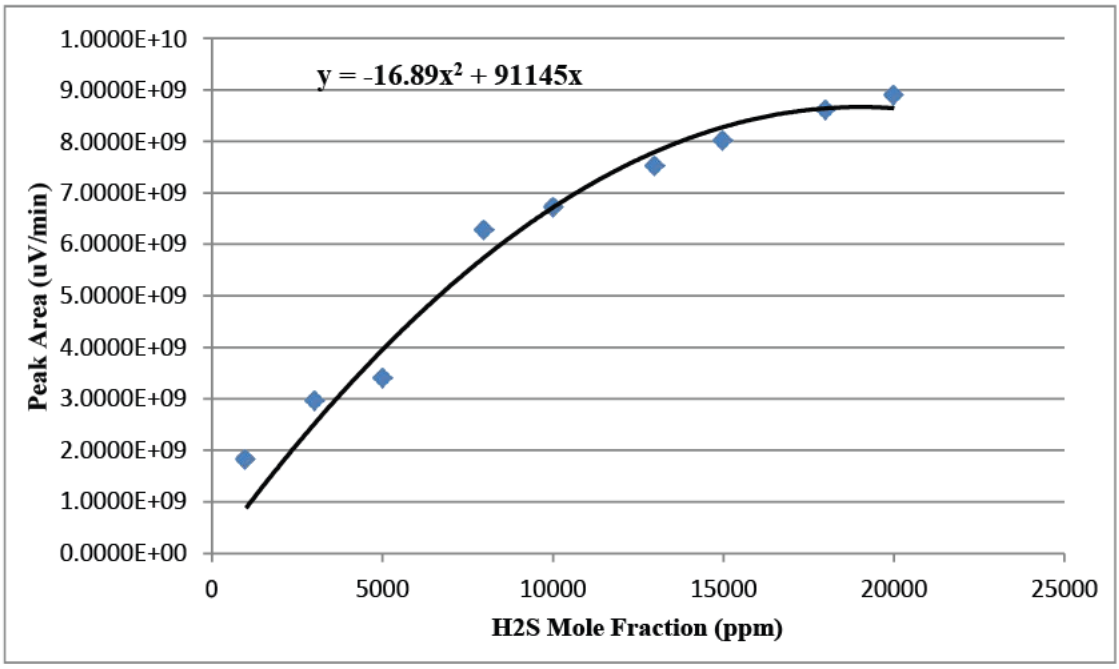

Figure A. 5 Graph showing the response of H_2S when varying volumes representing the mole fractions of H_2S is injected in the GC with FPD

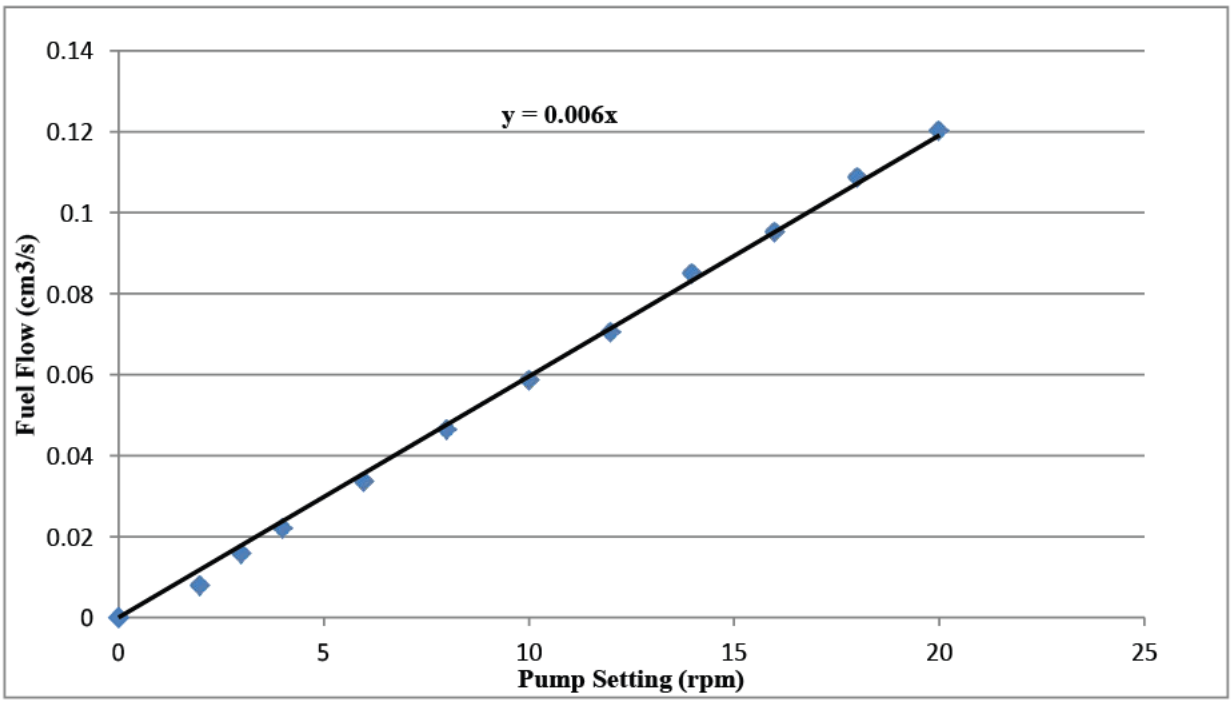

Figure A.6 Graph showing the peristaltic pump setting and the corresponding Fuel flow rate

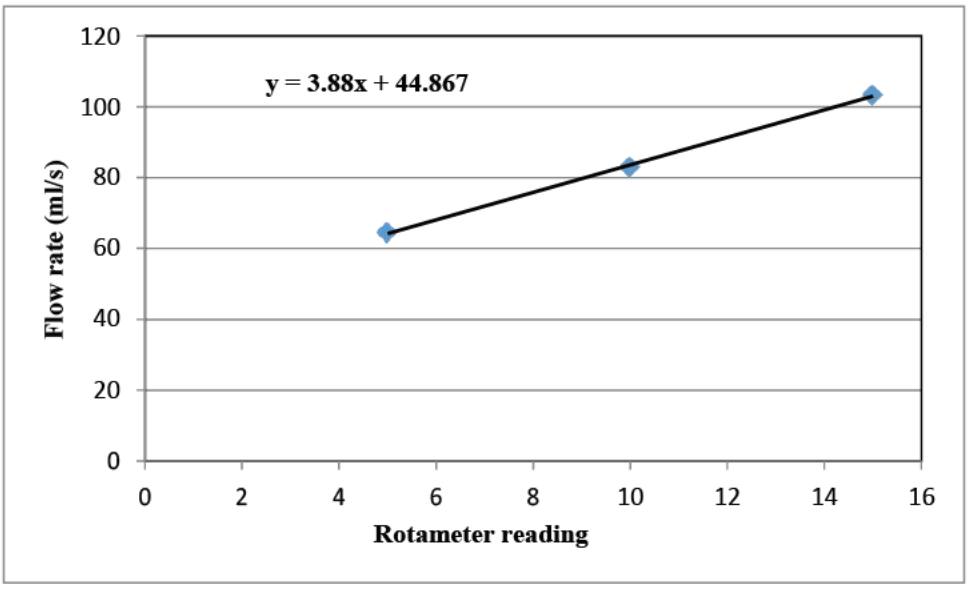

Figure A. 7 CO_2 Gas Rotameter calibration curve

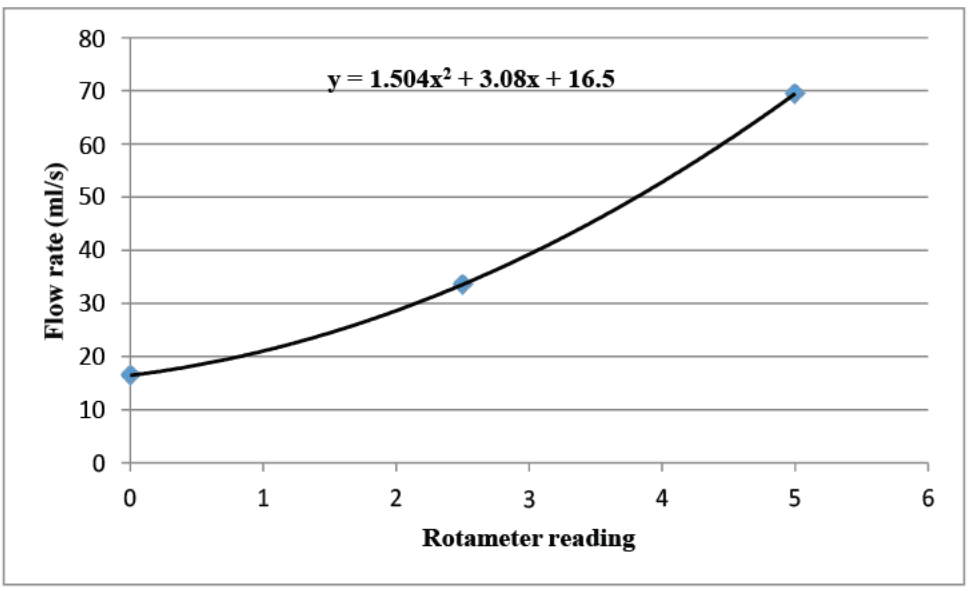

Figure A. 8 Compressed Air Rotameter calibration curve

A2. Calibration Standards Table

Table A. 1 CH_4 calibration standards

Sample	% Mole Fraction	Exact Moles (µmoles)	*Volume injected (µl)
1	0	0.0000	0
2	0.5	0.2037	5
3	1	0.4075	10
4	1.5	0.6112	15
5	2	0.8149	20
6	2.5	1.0186	25

* Value rounded off to accommodate syringe calibrations

Table A. 2 CO calibration standards

Sample	% Mole Fraction	Exact Moles (µmoles)	*Volume injected (ml)
1	0	0.0000	0
2	10	4.0599	0.1
3	20	8.1199	0.2
4	30	12.1798	0.3
5	40	16.2398	0.4
6	50	20.2997	0.5

* Value rounded off to accommodate syringe calibrations

Table A. 3 CO_2 calibration standards

Sample	% Mole Fraction	Exact Moles (µmoles)	*Volume injected (µl)
1	0	0.0000	0
2	0.2	0.08134	2
3	0.4	0.16268	4
4	0.6	0.24403	6
5	0.8	0.3254	8
6	1.0	0.4067	10

* Value rounded off to accommodate syringe calibrations

Table A. 4 H_2S calibration standards

Sample	Mole Fraction (ppm)	Exact Moles (µmoles)	*Volume injected (µl)
1	0	0	0
2	100	0.082	2
3	500	0.409	10
4	1000	0.817	20
5	1500	1.226	30
6	2000	1.635	40
7	2500	2.043	50
8	3000	2.452	60
9	3500	2.861	70
10	4000	3.269	80

Sample	Mole Fraction (ppm)	Exact Moles (µmoles)	*Volume injected (µl)
11	4500	3.678	90
12	5000	4.087	100
13	5500	4.495	110
14	6000	4.904	120
15	6500	5.313	130
16	7000	5.721	140
17	7500	6.130	150
18	8000	6.539	160
19	8500	6.947	170
20	9000	7.356	180
21	9500	7.765	190
22	10000	8.173	200
23	10500	8.582	210
24	11000	8.991	220
25	11500	9.399	230
26	12000	9.808	240
27	13000	10.625	260
28	14000	11.442	280
29	15000	12.260	300

* Value rounded off to accommodate syringe calibrations

Appendix B – Sample Calculations and Equations

B.1 Pressure Drop calculation

The pressure drop across the desulphurization reactor bed was calculated using equation B.1, the Ergun equation.

$$\frac{\Delta P}{} = \frac{150\mu(1-\varepsilon)^2 u_0}{3\ 2} + \frac{1.75(1-\varepsilon)\rho u_0^2}{3} \qquad (.1)$$

Where:

ΔP	Pressure drop across the bed	Pa
	Length of the packed bed	m
	Fluid viscosity	Pa.s
	Bed porosity	-
0	Fluid superficial velocity	m/s
	Particle diameter	m
	Density of fluid	kg/m^3

Length of the packed bed was calculated by equation B.2 for both large and small particles:

$$= \frac{4}{2} \qquad (.2)$$

Where:

	Mass of sorbent used	kg
	Sorbent bulk density	kg/m^3
	Desulphurization reactor diameter	m

Bed porosity was calculated from the correlation shown by equation B.3 for both large and small particles.

$$\varepsilon = 0.373 + 0.917\exp(-0.824\, D_R/d_p) \qquad (B.3)$$

Fluid superficial velocity was calculated by dividing syngas volumetric flow rate with the cross-sectional area of the desulphurization reactor. Particle diameters and their respective bulk densities were determined from the procedure given in section 5.3.2. Fluid viscosity and density were obtained from Perry and Green (1999) for gas mixtures similar to syngas.

Table B. 1 Parameters and their values for pressure drop calculations

Parameter	**Units**	**Large Particles**	**Small particles**
	m	0.0270	0.0270
	m	0.0021	0.00163
	-	0.3730	0.3730
	Kg/m^3	899.4	1023.54
	Kg	0.03	0.03
	m	0.0583	0.0512
0	m/s	0.00906	0.01207
	Pa. s	1.5866E-5	1.5866E-5
	Kg/m^3	1.1752	1.1752
ΔP	**Pa**	**0.028**	**0.264**

B.2 Sulphur sorption capacity calculation Equations

To measure the sorbent utilization in the reactor the sulphur sorption (loading) capacity was calculated. First the actual sulphur captured by the sorbent until the exiting concentration of H_2S exceeds 100ppm was calculated by equation B.4:

$$_2 = \frac{[MW_{H2S} * P * Q * y_{H2S} * t_b]}{T * R_g} \qquad (.4)$$

2	Actual sulphur captured	g
2	Molecular weight of H_2S	g/mol
	Pressure at reaction conditions	bar
	Volumetric gas flow rate	L/min
2	Inlet H_2S mole fraction	-
	Breakthrough time	min
	Temperature at reaction conditions	K

	Universal gas constant	L.bar/K.mol

The sulphur sorption capacity is given by equation B.5:

$$S\,\% = \frac{m_{H2S}}{} * 100 \qquad (B.5)$$

%	Sulphur sorption capacity	%
2	Actual sulphur captured	g
	Initial mass of ZnO in bed	g

To use the above equations it is assumed that all the sulphur is absorbed by the sorbent and none leaves with the exiting gas (Sanchez-Hervas et al. 2005).

For complete sulphidation, the amount of sulphur captured in grams is given by equation B.6

$$= 0.195 \qquad (\ .6)$$

The theoretical breakthrough time is thus given by:

$$t_f = \frac{[MW_{H2S} * P * Q * y_{H2S}]}{T * R_g} \qquad (\ .7)$$

Appendix C – Desulphurisation Temperature Profiles

C.1 High surface area at low flow rate

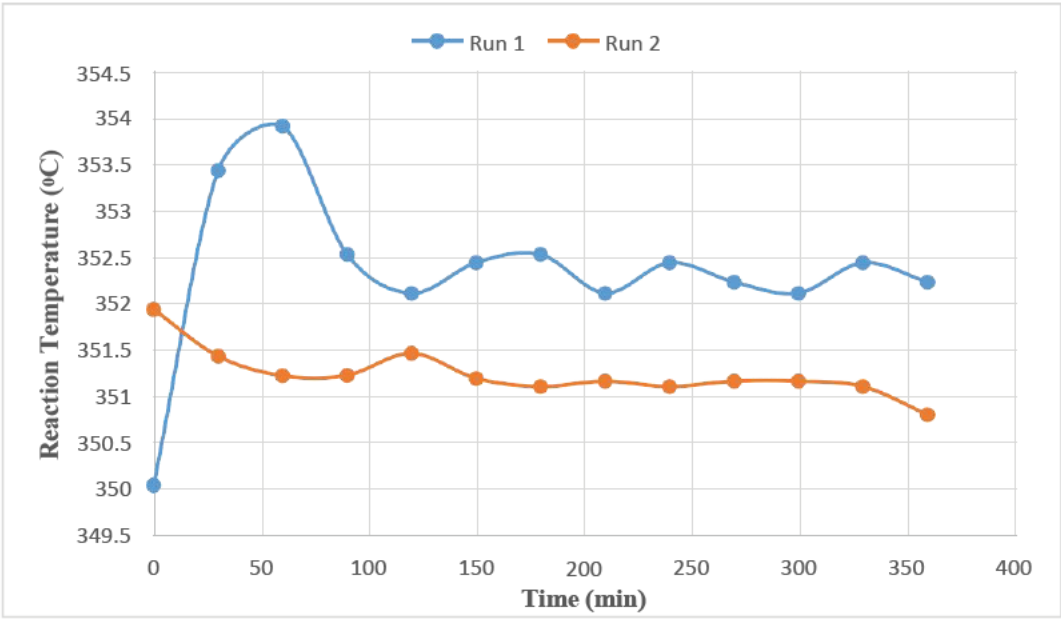

Figure C. 1 Reaction temperature profile at 350 ^{0}C, of increased surface area sorbent Run 1- small particles and Run 2- large particles at 780 and 530 h^{-1} space velocity respectively

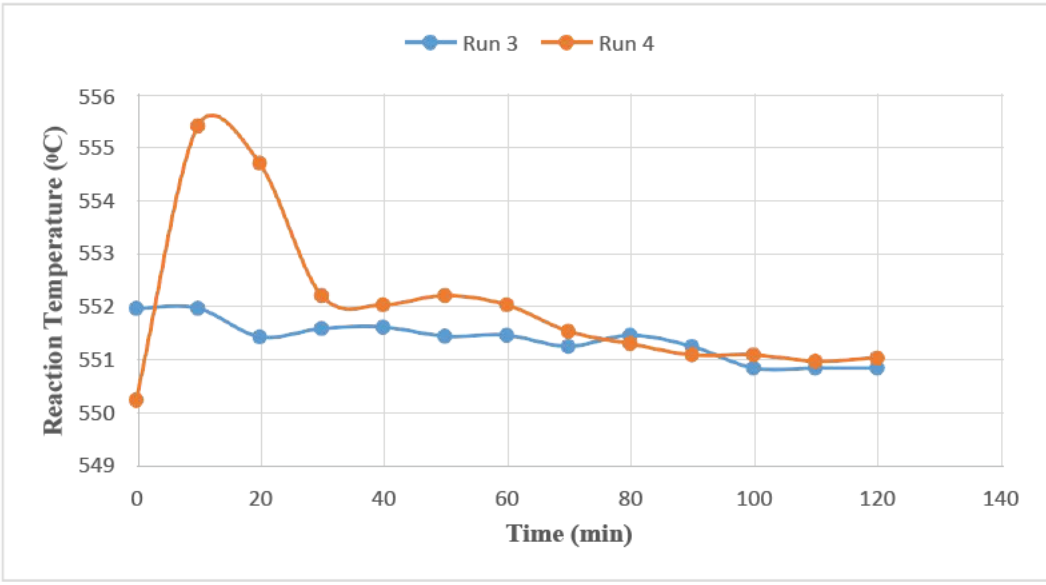

Figure C. 2 Reaction temperature profile at 550 ^{0}C, of increased surface area sorbent Run 3- small particles and Run 4- large particles at 640 and 460 h^{-1} space velocity respectively

C.2 Low surface area at low flow rate

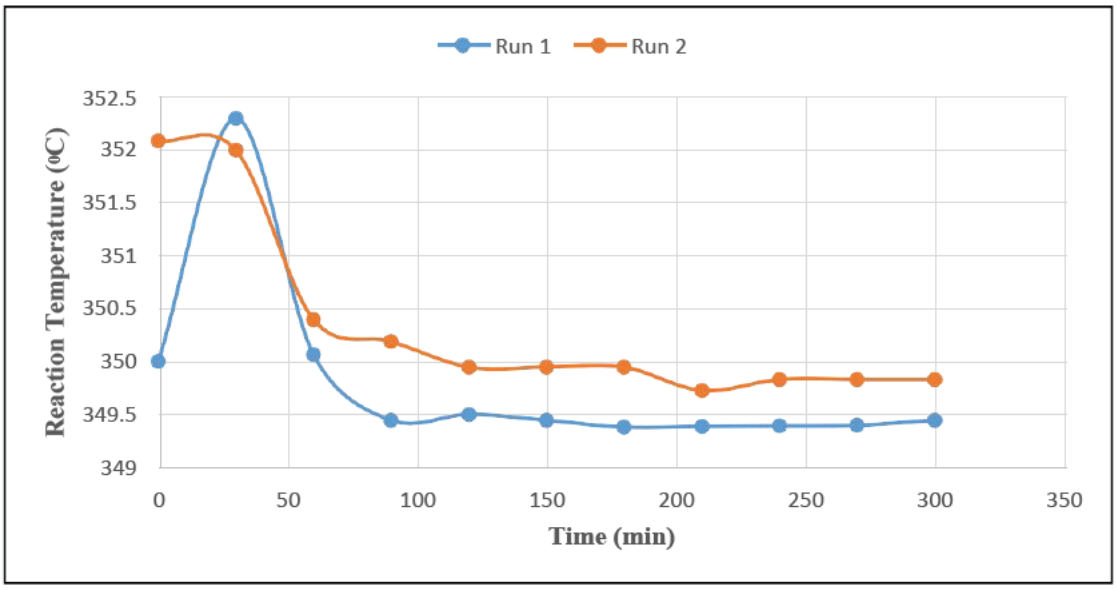

Figure C. 3 Reaction temperature profile at 350 ^{0}C, of low surface area sorbent Run 1-small particles and Run 2- large particles at 680 and 560 h^{-1} space velocity respectively

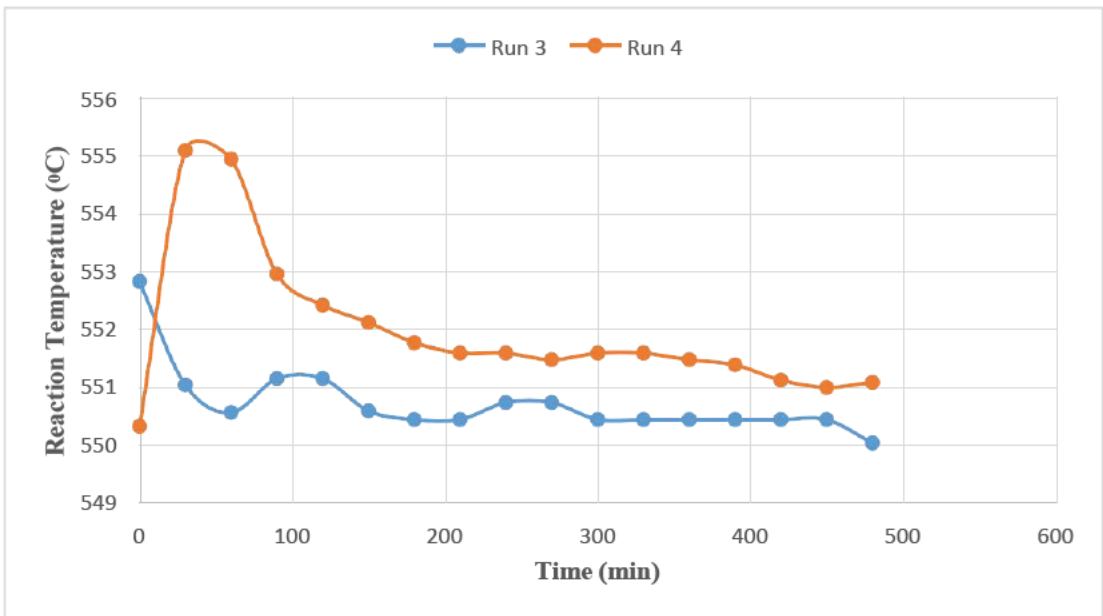

Figure C. 4 Reaction temperature profile at 550 ^{0}C, of low surface area sorbent Run 3-small particles and Run 4- large particles at 575 and 635 h^{-1} space velocity respectively

C.3 Low surface area at High flow rate

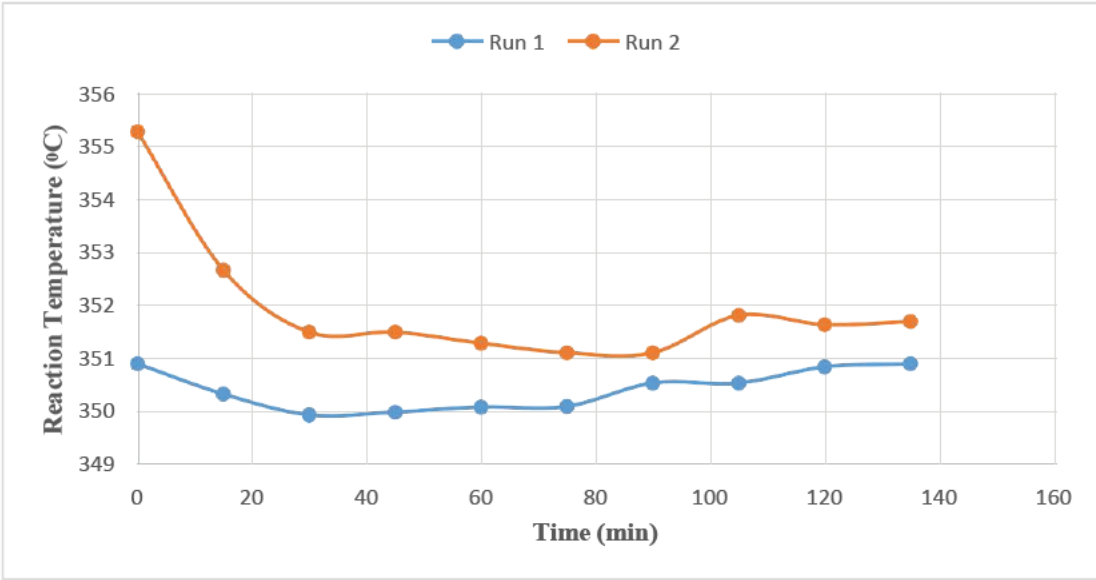

Figure C. 5 Reaction temperature profile at 350 ^{0}C, of low surface area sorbent Run 1-small particles and Run 2- large particles at 3310 and 2630 h^{-1} space velocity respectively

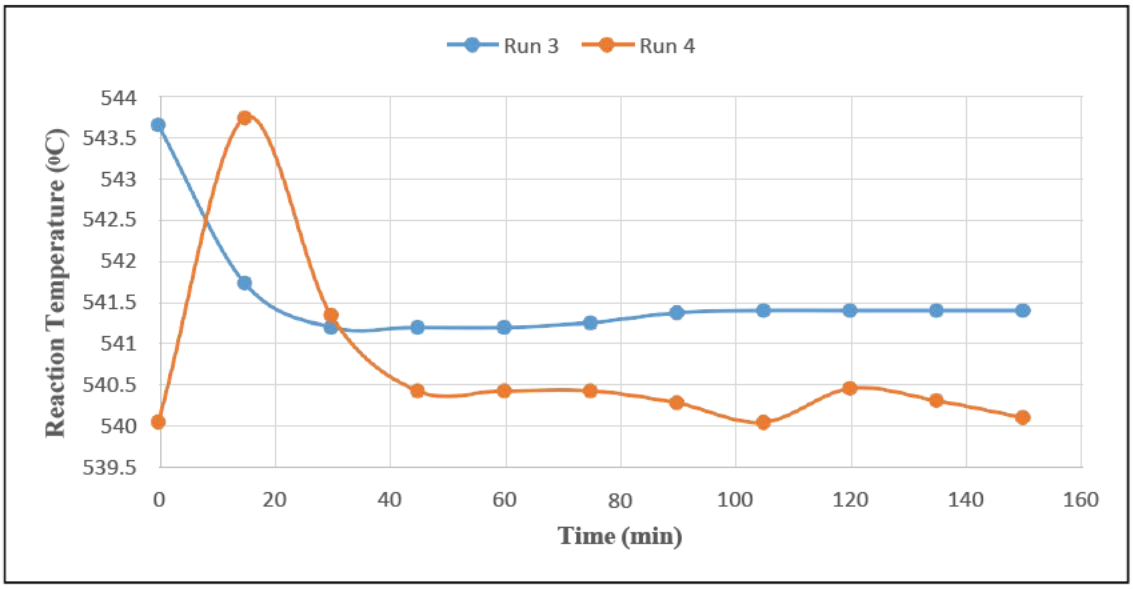

Figure C. 6 Reaction temperature profile at 550 ^{0}C, of low surface area sorbent Run 3-small particles and Run 4- large particles at 4010 and 3300 h^{-1} space velocity respectively